Studies on Staged Pyrolysis of Biomass for Production of Chemicals and Metallurgical Coke

魏, 富

出版情報：Kyushu University, 2022, 博士（工学）, 課程博士
バージョン：
権利関係：

Studies on Staged Pyrolysis of Biomass for Production of Chemicals and Metallurgical Coke

By

Fu Wei

Department of Applied Science for Electronics and Materials

Interdisciplinary Graduate School of Engineering Sciences

Kyushu University, Japan

2022

Contents

Thesis Summary

The world currently faces the challenge of reducing its reliance on fossil fuels and achieving a sustainable supply of renewable energy. The full development and utilization of lignocellulosic biomass, the only recyclable carbon source, is an important strategy for producing chemicals and liquid fuels to solve energy shortages and reduce CO_2 emissions. Pyrolysis of lignocellulosic biomass, which can convert biomass into a series of high value-added products, especially pyrolytic volatiles containing a variety of condensable fine chemicals and non-condensable high calorific value gas products, is one of the most promising biomass utilization technologies. However, due to the influence of various factors such as the overlapping pyrolysis temperature of the components and the difference in reaction conditions, the products from direct pyrolysis have the defects of complex composition, low selectivity of valuable compounds, and poor stability, which make them unable to be directly utilized. Although certain kinds of high value-added compounds can be enriched by catalytic reforming volatiles by selecting suitable catalysts, most of the researches on this catalytic reforming focus on a single target product, and there are few reports on the co-production of multiple target products. This way of consuming the catalyst not only requires a large investment, but also causes the waste of the high value-added component resources of the bio-oil itself. Therefore, suitable pretreatment methods or the combination of different techniques to enrich high value-added compounds are necessary.

Considering the differences in decomposition temperatures and chemical structures of each component, in order to achieve efficient conversion of different biomass components, this thesis

innovatively proposes the staged pyrolytic conversion strategy to obtain multi-target products. The brief summary of each chapter of this thesis is as follows:

Chapter 1 presents the background, motivation, objective and outline of this work.

Chapter 2 explores the chemical and thermal characteristics of torrefaction and *in-situ* pyrolytic reforming of the volatiles through torrefaction-*in situ* pyrolytic reforming. Also, in order to explore the influence of alkali and alkaline earth metallic species, the effects of water washing on the above described characteristics of the torrefaction and pyrolytic reforming is also reported. The results showed that torrefaction and *in-situ* pyrolytic reforming both successfully can conserve the chemical energy of biomass with relatively small heat requirements. *in-situ* pyrolytic reforming can convert the chemical energy of bio-oil to that of CO/H_2-rich syngas with higher LHV of 17–18 MJ/Nm^3-dry, which was represented by those of CO and CH_4, C_2H_4, and H_2. The pyrolytic reforming can convert at most 90 wt% of the bio-oil from the torrefaction at 300 °C into gas, while selective removal of the heavier components was difficult only by the vapor-phase reforming.

Chapter 3 innovatively proposes and discusses in detail the staged pyrolysis of acid-loaded biomass for the co-production of chemicals and metallurgical coke. Wood biomass loaded with H_2SO_4 or H_3PO_4 was selected to produce levoglucosan and levoglucosenone during torrefaction. The obtained char after water washing was further pelletized and then carbonized to produce the coke. The product distribution of pellet carbonization was also analyzed. The results shows that loading acids, especially H_2SO_4, that are equal to or slightly less than the metals inherent in the biomass can produce more sugars at lower temperatures torrefaction. The maximum total yield of anhydrosugars from wood reached 12.1 wt% and 10.3 wt% after loading with suitable H_2SO_4 and H_3PO_4, respectively. The resulting char can be further prepared into high-strength

metallurgical coke. In comparison with the direct carbonization of cedar, the staged conversion promoted strength enhancement of metallurgical coke. More importantly, unlike H_3PO_4 loading which increased the coke yield, H_2SO_4 loading further promoted the improvement of coke strength. The resulting coke had a much higher strength (24.2 MPa) than that of coke prepared directly from cedar (9.0 MPa). At the same time, the staged pyrolysis also promoted the formation of phenols because the obtained char was rich in lignin, although the yield was slightly low. Most notably was that the staged conversion loading of H_2SO_4 and H_3PO_4 achieved the valorization of cedar in total yields of 45.7 and 49.2 wt% for anhydrosugars, phenols, gas, and strong coke, respectively.

Chapter 4 develops a staged steam treatment progress to enrich the high value-added chemicals in the extracts such as terpenoids and coniferyl aldehyde. The results showed that the formation of coniferyl aldehyde was mainly produced from the binding sites of lignin and hemicellulose, not lignin. Steam treatment can promote the production of coniferyl aldehyde, especially at higher water-to-biomass ratio. The staged steam treatment can further improve the selectivity of coniferyl aldehyde in the extracts at 220 °C, and directly extract the natural component terpenoids below 160 °C.

Chapter 5 summarizes the findings described in previous chapters.

Chapter 1 General Introduction

1.1 Background

Energy is the foundation and driving force of human civilization and progress. The development of the world economy is highly dependent on the stable supply of energy. According to the BP Statistical Review of World Energy 2021 [1], global primary energy consumption in 2020 decreased by 4.5%, which was the first decline in energy consumption since 2009. And the carbon emissions from energy use also decreased by 6.3%. Among them, the growth of energy consumption was mainly renewable energy of 9.7% and hydropower of 1.0%. Oil still accounts for the largest proportion of 31.2% in the primary energy consumption of current human society. Coal, the second largest fuel, accounts for 27.2%, and gas and renewable energy rise to 24.7% and 5.7%, respectively. It is worth noting that the proportion of renewable energy has now exceeded that of nuclear energy in the primary energy consumption. According to the prediction, the proportion of renewable energy can exceed that of coal and natural gas by 2030, and even surpass that of oil by 2050, becoming the largest category of energy consumption.

Furthermore, the extensive use of energy, especially fossil fuels, inevitably has an important impact on the environment. It will produce a large amount of toxic and harmful gases, such as CO_2, NO_x, SO_x, etc, causing serious problems such as urban air pollution, greenhouse effect, and acid rain [2,3]. What is more serious is that human beings' high dependence on fossil fuels will inevitably accelerate the depletion of fossil fuels, resulting in an increasingly tense relationship between energy supply and demand. Therefore, effective measures such as improving the energy structure system, updating energy utilization technology, improving energy utilization rate, or

developing clean and renewable alternative energy are important guarantees for the sustainable and rapid development of the world economy today [4].

In recent years, the development and utilization of clean and environmentally friendly renewable energy, mainly including solar energy, ocean energy, biomass energy, wind energy, water energy, hydrogen energy and geothermal energy, have attracted extensive attention in the world [5]. In short, solar energy refers to its thermal radiation energy. There are three ways to use: photoelectric conversion, photothermal conversion and photochemical conversion. Ocean energy includes tidal energy, wave energy, salt difference energy, ocean current energy and temperature difference energy that can be used for power generation. Similarly, wind energy and hydropower can be converted into other forms of energy such as electric energy by using their own kinetic energy. However, such energy is often restricted by many factors, such as season, day and night, climate, geographical latitude, altitude and other natural conditions. Geothermal energy is also a kind of abundant energy, which will not generate greenhouse gases during the utilization process. However, due to the immature application technology at this stage, it will lead to serious secondary heat pollution. Hydrogen energy has the characteristics of high calorific value, good combustion performance, and non-polluting products, and is widely used in chemical synthesis, fuel cells, food processing and other fields. But so far, the production of hydrogen mainly comes from the gasification or reforming of coal, oil and natural gas, resulting in a large consumption of fossil fuels. Moreover, the storage of hydrogen is also an urgent problem to be solved in the process of its large-scale utilization.

Compared with other renewable energy sources, biomass energy is the only carbon source that can be recycled and regenerated. It is the fourth largest energy after coal, oil and natural gas, and plays an important role in the entire energy system. It can prepare a variety of high value-added

chemicals and fuel energy such as solid fuel, gas, and liquid fuel, and can completely replace fossil energy in the future [6-8]. Biomass energy can not only obtain energy through direct combustion, but also be transformed into a variety of chemical products and other forms of energy through thermochemical and biochemical. Its rich resources and strong renewable characteristics are conducive to improving the environment and sustainable development [9,10]. Therefore, strengthening the development and utilization of biomass energy is bound to become an inevitable trend in the development of energy strategies of all countries in the world.

1.2 Biomass and its utilization

Biomass generally refers to all organisms formed directly or indirectly through photosynthesis. It is generally divided into the plant and non-plant biomass. The former mainly includes agricultural wastes (straw, shell and straw), forestry wastes (wood, sawdust and bark) and energy crops. The latter includes organic components in livestock manure, sludge, wastewater and municipal waste, etc. Lignocellulose biomass has received the most attention in the process of biomass energy utilization because of its most content, the most extensive sources and the lowest cost. Generally, lignocellulose biomass is mainly composed of 30-55 wt% cellulose, 15-40 wt% hemicellulose and 10-40 wt% lignin [11].

The development and utilization technologies of biomass mainly include three categories: physical, bio-chemical and thermal-chemical conversion technologies [12]. Through these conversion technologies, it will be converted into clean high-grade gas or liquid fuel that can be used as an alternative energy for fossil fuels in power, transportation, urban gas and other aspects. As shown in **Figure 1-1**, the ways of biomass conversion mainly include: pelletization/briquetting,

direct combustion, gasification, hydrothermal, pyrolysis, anaerobic digestion, hydrolysis fermentation and other technologies.

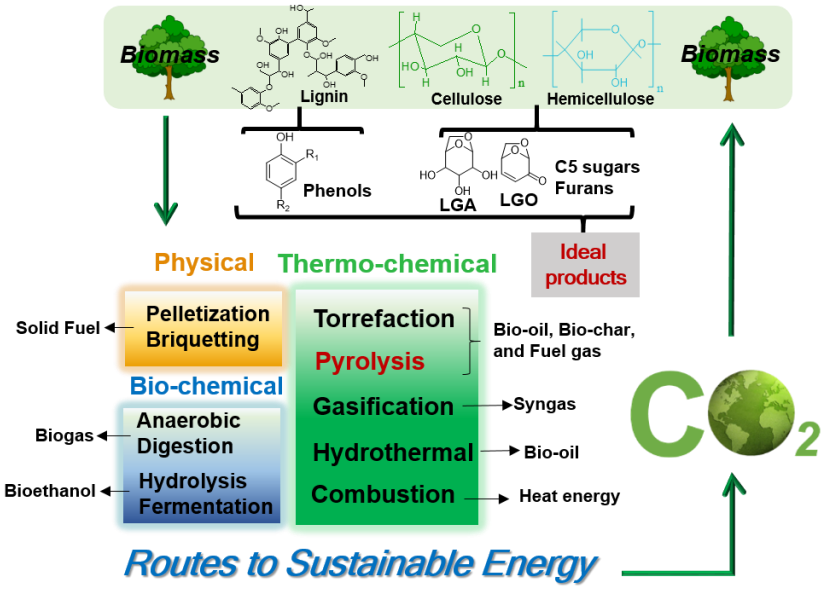

Figure 1-1 Biomass utilization technology.

1.2.1 Physical and bio-chemical conversion

Physical conversion technology mainly refers to biomass solid briquetting technology. That is, biomass with large particles and irregular shape is first crushed to a certain particle size, and then extruded into a certain shape under high pressure to produce solid fuel. It solves the problems of different shapes of biomass, small and loose bulk density, inconvenient transportation and storage, and improves the thermal efficiency of biomass. But it mainly uses its compact physical structure to convert it into materials for use in life and industry, and it is difficult to convert biomass into renewable products that can replace petroleum-based products.

Bio-chemical conversion technology refers to the use of microorganisms to degrade biomass into small molecular compounds under certain conditions. It mainly includes two technologies: anaerobic digestion mainly used to produce biogas and hydrolysis fermentation mainly used to produce ethanol liquid fuel.

1.2.2 Thermal-chemical conversion technologies

Biomass thermochemical conversion technology is an important part of biomass energy conversion, and it is also the most researched technology at present. It mainly includes direct combustion, gasification, liquefaction (hydrothermal upgrading) and pyrolysis [13,14]. The purpose is to convert biomass into gas, solid and liquid fuels and other chemical products.

Direct combustion

Direct combustion is the simplest biomass thermochemical utilization technology, which refers to the process that biomass is burned in the air and then converted into heat or electricity by different equipment (such as stoves, boilers, and turbine generators). However, due to the low energy density of raw biomass, it often leads to problems such as low calorific value and poor continuous heat production capacity, and is easy to cause heat loss and low energy utilization [15].

Gasification

Gasification refers to the process that biomass reacts with gasification agent to obtain small molecule combustible gas mixture at high temperature (700–900 °C). Common gasification agents are air, oxygen, carbon dioxide, water vapor, etc. Using different gasification agents, the gas composition of biomass gasification is also different. In general, the main gas products are CO, H_2,

CO_2 and CH_4 [16]. The obtained combustible gas can be directly burned or provide fuel for engines and boilers, and can also be used to further synthesize liquid fuels such as methanol and dimethyl ether and other chemical products through chemical methods.

Compared with the direct combustion, gasification has greatly improved the energy conversion efficiency. However, gasification also has its own limitations, mainly because a large amount of tar is produced in the gasification process. At present, there is no mature method to treat tar, which limits the utilization of gas [17].

Liquefaction

Liquefaction refers to the process of converting biomass into liquid fuel, which is generally divided into direct liquefaction and indirect liquefaction. Direct liquefaction is to directly convert solid biomass into liquid fuel by adding H_2, CO and their mixtures or with the help of suitable catalysts under atmospheric or high pressure and the presence of chemical liquefaction reagents. Indirect liquefaction is to convert biomass into mixed gases such as H_2, CO, and then regulate the C/H ratio according to the characteristics of the target product. Finally, they are synthesized into methanol, ethanol, aromatic compounds and other chemical raw materials with the help of catalysts. Liquefaction can convert refractory biomass waste into liquid bio-oil, and also produce high-grade liquid fuels and high-value chemical products through reprocessing [18].

Pyrolysis

Pyrolysis refers to the process of thermal degradation of biomass at high temperature under the condition of no oxygen or lack of oxygen to obtain liquid bio-oil, solid product (char), and gas [19,20]. Bio-oil can be used as fuel or as a raw material for the synthesis of other high-value

chemical products after further processing. Gas can be used as fuel for power generation and heat supply, or for the production of syngas with high fuel value. As for char, it can be used as an adsorbent for the treatment of pollutants in wastewater because of its porous structure. It can also be used as a carrier material to support active components in the field of catalysis, or further processing to produce multifunctional carbon materials. Therefore, pyrolysis is generally considered to be the most promising conversion technology [21,22].

1.3 Objective of this study

In order to realize the efficient conversion of biomass, the main objective of this thesis is to explore the staged conversion to obtain multiple target products according to the different decomposition temperatures and chemical structures of each component. The ideal multistage thermal conversion is shown in **Figure 1-2**, in which the target products from different components can be selectively obtained through appropriate pretreatment or combined with different treatment methods at different stages.

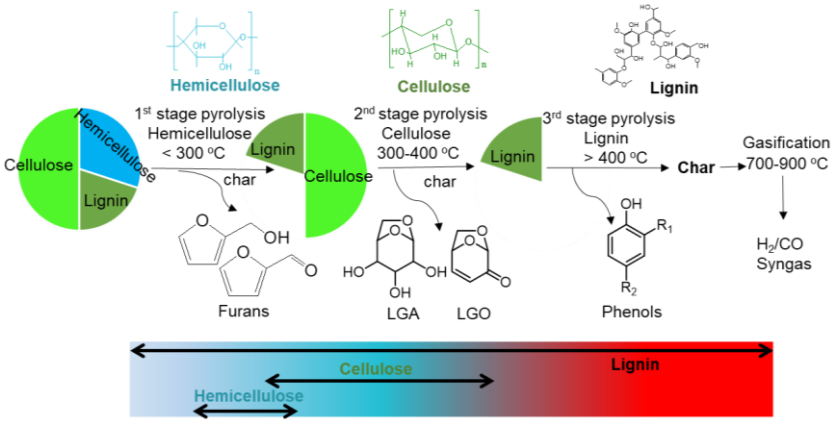

Figure 1-2 The ideal multistage thermal conversion of biomass.

However, considering the overlapping decomposition temperature of the components, the pyrolysis products are still complex and need to be further combined with other methods to obtain various target products. Therefore, based on the staged product characteristics, the research objectives are as follows:

1. Investigate the chemical and thermal characteristics of torrefaction and in-situ vapor-phase pyrolytic reforming of the volatiles in chapter 2 with a view to obtaining high-quality syngas.

2. Selectively produce target products such as anhydrosugars, phenols, gas, and strong coke from different components by staged pyrolytic conversion of acid-loaded biomass to achieve efficient utilization of biomass in chapter 3.

3. Enrich high value-added chemicals such as terpenoids and coniferyl aldehyde from the extracts through steam treatment in chapter 4.

1.4 Outline of this study

In chapter 1, the current energy structure, types of biomass resources, biomass conversion methods, and the main problems faced by pyrolysis are described.

In chapter 2, the product distribution and heat required for torrefaction of woody biomass at 250–350 °C and those for *in-situ* vapor-phase pyrolytic reforming of bio-oil at 500–800 °C were investigated in detail. In addition, the effects of water washing on the above described characteristics of the torrefaction and pyrolytic reforming were also investigated.

In chapter 3, a scheme of staged pyrolysis was proposed to obtain valuable chemicals, such as anhydrosugars and phenols, and strong coke. First, cedar loaded with different concentrations of sulfuric acid and phosphoric acid were selected to explore the product distribution at 250–500 °C. The obtained char was further pelletized and then carbonized to produce the coke. Their

performances were evaluated in comparison with those prepared by torrefied raw cedar. The product distribution of pellet carbonization was also analyzed.

In chapter 4, the product composition and distribution of the extracts from cedar torrefaction under steam treatment at 130–250 °C were investigated, and also as the effects of water/biomass mass ratio. Furthermore, staged extraction was proposed for obtaining high selectivity of coniferyl aldehyde and terpenoids.

Chapter 5 described the general conclusion of this study.

1.5 References

[1] BP, Statistical review of world energy 2021, (2021).

[2] P.R. Bhoi, A.S. Ouedraogo, V. Soloiu, R. Quirino, Recent advances on catalysts for improving hydrocarbon compounds in bio-oil of biomass catalytic pyrolysis, Renewable Sustainable Energy Rev, 121, (2020) 109676.

[3] X. Hu, M. Gholizadeh, Biomass pyrolysis: A review of the process development and challenges from initial researches up to the commercialisation stage, J Energy Chem, 39, (2019) 109-143.

[4] W. Chen, M. Gong, K. Li, M. Xia, Z. Chen, H. Xiao, Y. Fang, Y. Chen, H. Yang, H. Chen, Insight into KOH activation mechanism during biomass pyrolysis: Chemical reactions between O-containing groups and KOH, Appl Energy, 278, (2020) 115730.

[5] T. Dickerson, J. Soria, Catalytic fast pyrolysis: A review, Energies, 6, (2013) 514-538.

[6] G. W. Huber, S. Iborra, A. Corma, Synthesis of transportation fuels from biomass: Chemistry, catalysts, and engineering, Chem Rev, 106, (2006,) 4044-4098.

[7] J.C. Serrano-Ruiz, J.A. Dumesic, Catalytic routes for the conversion of biomass into liquid hydrocarbon transportation fuels, Energy Environ Sci, 4, (2011) 83-99.

[8] S. Stephanidis, C. Nitsos, K. Kalogiannis, E.F. Iliopoulou, A.A. Lappas, Catalytic upgrading of lignocellulosic biomass pyrolysis vapours: Effect of hydrothermal pre-treatment of biomass, Catal Today, 167, (2011) 37-45.

[9] A. Galadima, O. Muraza, In situ fast pyrolysis of biomass with zeolite catalysts for bioaromatics/gasoline production: A review, Energy Convers Manage, 105, (2015) 338-354.

[10] M.I. Jahirul, M.G. Rasul, A.A. Chowdhury, N. Ashwath, Biofuels production through biomass pyrolysis—A technological review, Energies 5, (2012) 4952-5001.

[11] S. Wang, G. Dai, H. Yang, Z. Luo, Lignocellulosic biomass pyrolysis mechanism: A state-of-the-art review, Prog Energy Combust Sci, 62, (2017) 33-86.

[12] F.M. Demirbas, Biorefineries for biofuel upgrading: A critical review, Appl Energy, 86, (2009) S151-S161.

[13] M. Asadullah, A.M. Adi, N. Suhada, N.H. Malek, M.I. Saringat, A. Azdarpour, Optimization of palm kernel shell torrefaction to produce energy densified bio-coal, Energy Convers Manage, 88, (2014) 1086-1093.

[14] H.C. Ong, W.-H. Chen, A. Farooq, Y.Y. Gan, K.T. Lee, V. Ashokkumar, Catalytic thermochemical conversion of biomass for biofuel production: A comprehensive review, Renewable Sustainable Energy Rev, 113, (2019) 109266.

[15] D.O. Glushkov, G.S. Nyashina, R. Anand, P.A. Strizhak, Composition of gas produced from the direct combustion and pyrolysis of biomass, Process Saf Environ Prot, 156, (2021) 43-56.

[16] S. Pang, Advances in thermochemical conversion of woody biomass to energy, fuels and chemicals, Biotechnol Adv, 37, (2019) 589-597.

[17] V.S. Sikarwar, M. Zhao, P. Clough, J. Yao, X. Zhong, M.Z. Memon, N. Shah, E.J. Anthony, P.S. Fennell, An overview of advances in biomass gasification, Energy Environ Sci, 9, (2016) 2939-2977.

[18] A.R.K. Gollakota, N. Kishore, S. Gu, A review on hydrothermal liquefaction of biomass, Renewable Sustainable Energy Rev, 81, (2018) 1378-1392.

[19] M.B. M. Balat, E. Kirtay, H. Balat, Main routes for the thermo-conversion of biomass into fuels and chemicals. Part 1: Pyrolysis systems, Energy Convers Manage, 50, (2009) 3147-3157.

[20] A.V. Bridgwater, G.V.C. Peacocke, Fast pyrolysis processes for biomass, Renewable Sustainable Energy Rev, 4, (2000) 1-73.

[21] D. Mohan, C.U. Pittman Jr, P.H. Steele, Pyrolysis of wood/biomass for bio-oil: A critical review, Energy Fuels, 20, (2006) 848-889.

[22] R. Kumar, V. Strezov, H. Weldekidan, J. He, S. Singh, T. Kan, B. Dastjerdi, Lignocellulose biomass pyrolysis for bio-oil production: A review of biomass pre-treatment methods for production of drop-in fuels, Renewable Sustainable Energy Rev, 123, (2020) 109763.

Chapter 2 Torrefaction of Woody Biomass and *in-situ* Pyrolytic Reforming of Volatile Matter: Analyses of Products and Process Heat Demand

2.1 Introduction

Lignocellulosic biomass, the only renewable source of carbon, can be converted into fuels, chemicals, and materials through thermochemical and/or biochemical conversion [1,2]. Apart from the attractive physicochemical nature of biomass, its properties such as high O/C ratio, low calorific value, low volumetric energy density, and complex chemical compositions limit efficiency of conversion into final products [3,4]. It is often necessary to pretreat biomass before subsequent conversion for improving fuel properties. Torrefaction is an attention-drawing thermochemical process to improve some of the above-mentioned properties by altering the chemical composition and structure of biomass, and even enhance its properties to those equivalent to coal. Torrefaction is also a process to produce bio-oil and combustible gas, while with yields lower than those by pyrolysis operated at higher temperatures. Research efforts to date have been focused mainly on physicochemical properties of torrefied biomass relevant to processes such as pelletization, pyrolysis, combustion, and gasification [5-8], but ignoring the importance of volatile matter that accounts for 20–50 wt% or even more of dry biomass [9-11].

A general way of bio-oil utilization is to burn it together with non-condensable gas for supplying heat to endothermic torrefaction and/or drying. The effectiveness of this way is, however, limited because of low heating value of the volatile matter in form of vapor, in particular, for

torrefaction operated at lower temperatures [12,13]. It is also known that bio-oil from torrefaction contains several types of valuable chemicals such as acids, furans, and ketones [14-16]. Phenolic compounds and anhydrosugars are also involved in the bio-oil when the torrefaction temperature is relatively high [11,17].

Some recent studies focused on the biochemical conversion of torrefaction condensate into CH_4 via anaerobic digestion [18-20]. However, slow conversion exclusively of acids in the condensate limited its further application. Advanced approaches are therefore necessary to make better use of bio-oil as well as gases. An effective way of converting the bio-oil is reforming, *i.e.*, its *in-situ* conversion into syngas. Pyrolytic reforming without steam or CO_2 supply is attractive, because of high oxygen content of bio-oil and copresence of steam and CO_2 at substantial fractions in the vapor phase. The pyrolytic reforming is also expected to simplify the composition of the bio-oil although selective production of particular types of compounds would be difficult without catalysts. Some previous reports are available on the vapor-phase conversion at 600–800 °C of bio-oil from fast pyrolysis at around 500 °C [21,22], but none for bio-oil from torrefaction.

As outlined above, some different types of processes are applicable to the production of torrefied biomass, bio-oil, and/or syngas. The followings are just three examples, which are graphically shown in **Figure 2-1**.

- The entire portions of bio-oil and non-condensable gas are burned to supply heat to the torrefaction, biomass drying, and/or others. The torrefied biomass is the only product.
- The entire portion of gas and a portion of the bio-oil (if necessary) are burned to supply heat to the torrefaction and others. The products are torrefied biomass and bio-oil.
- The entire portion of gas and bio-oil is further converted into syngas completely or partially. A portion of syngas is burned for supplying heat to the reforming, torrefaction, and others.

Otherwise, heat (for example, joule heat from solar/wind power) is supplied externally. The products from this process are torrefied biomass, syngas, and/or bio-oil (secondary bio-oil from the reforming).

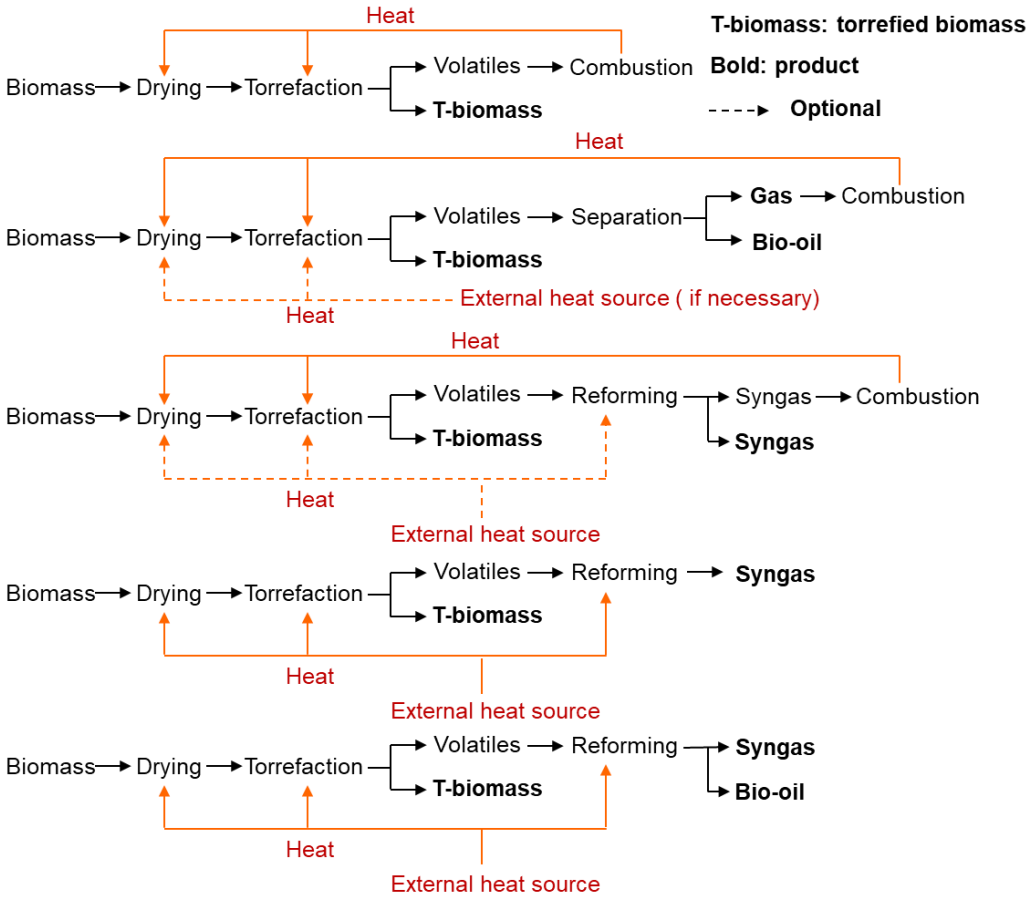

Figure 2-1 Some variety of torrefaction process.

Regardless of such types/modes of torrefaction, the heat required for the torrefaction and that for the reforming are essential for designing the process and estimating its thermal performance. Without saying, detailed compositions of bio-oil and gas, which are functions of operating variables, are necessary for the process design and optimization.

This work has been carried out to investigate the effects of torrefaction temperature on detailed product distribution and heat required for the torrefaction of woody biomass at temperature of 250–350 °C, and also those for *in-situ* vapor-phase pyrolytic reforming of bio-oil at 500–800 °C. This paper reports and analyzes the data and discusses the chemical and thermal characteristics of the torrefaction and pyrolytic reforming.

This work has another purpose to evaluate the impact of washing the biomass with water prior to the torrefaction. It is known that inherent alkali and alkaline earth metallic species (AAEMs) of biomass catalyze the pyrolysis and vapor-phase secondary reactions of bio-oil over char [14,23,24]. The washing is the cheapest way to reduce the content of AAEMs, which often cause problems in the further conversion of the torrefied biomass, though the reduction is less than washing with acidic water. This paper also reports the effects of this pretreatment on the above described characteristics of the torrefaction and pyrolytic reforming.

2.2 Experimental section

2.2.1 Materials

A type of chipped Japanese cedar was ground, sieved to sizes of 125–212 μm, dried at 105 °C for 12 h, and then used as the feedstock. The cedar was stirred in deionized water at ambient temperature for 24 h at a water/cedar mass ratio of 20. The treated cedar, which will be termed w-cedar, was dried in the same way as above. The cedar and w-cedar were subjected to ultimate analysis to determine the contents of C, H, and O. The contents of main inorganic species were measured by a sequence of low temperature combustion, acid digestion, and ion chromatography, the details of which were available elsewhere [25,26]. **Table 2-1** shows the elemental compositions

and calorific values of the samples. The higher heating values (HHVs) and standard enthalpies were calculated according to methods reported by Yang *et al*. [27].

Table 2-1 Properties of cedar and w-cedar.

Properties of the feedstock	cedar	w-cedar
Elemental composition and thermodynamic properties		
H/C atomic ratio	1.45	1.48
O/C atomic ratio	0.67	0.66
heating value, MJ-HHV kg-daf^{-1}	19.8	20.0
heating value, kJ-HHV mol-C^{-1}	477	479
standard enthalpy of formation (H_{biomass}), kJ mol-C^{-1}	–124	–126
Contents of AAEMs and ash (wt%-dry)		
Na	0.047	0.006
K	0.194	0.089
Ca	0.171	0.090
Mg	0.004	0.002
ash	0.92	0.49

2.2.2 Torrefaction and vapor-phase pyrolytic reforming

A home-made two-stage pyrolyzer was employed to investigate the characteristics of vapor-phase cracking of nascent volatiles from torrefaction. **Figure 2-2** schematically presents the experimental apparatus. About 1 g of the cedar or w-cedar, which had been wrapped in a sheet of SUS-316-made mesh (mesh opening; 106 μm), was quickly inserted into the first reactor that had been heated up to the prescribed temperature for torrefaction (T_{TR}). The time for heating the cedar or w-cedar was fixed at 40 min. The vapor of volatiles was continuously carried by steady flow of atmospheric N_2 (purity > 99.9999 vol%) at a rate of 200–400 ml-stp min^{-1} to the second reactor for the pyrolytic reforming at 500–800 °C and residence time of about 1 s. The volatile product was cooled to –70 °C in the condenser equipped with an aerosol filter, where the entire portions

of the organic compounds (except C_1–C_2 light hydrocarbons) and water were condensed. The non-condensable gases (inorganic gases and the above-mentioned hydrocarbons) were collected in the gasbag together with N_2.

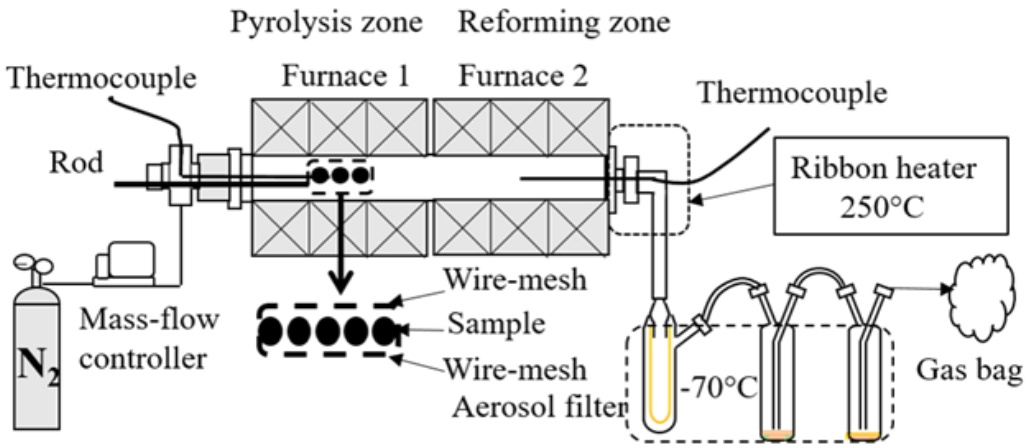

Figure 2-2 Schematic diagram of experimental apparatus.

Experimental runs were also performed without the second reactor for investigating the torrefaction exclusively at T_{TR} = 250–350 °C. The volatile products were collected in the same way as mentioned above. The total mass of the condensed products was measured. The heavier portion of the bio-oil was condensed between the second reactor and condenser, and it was collected and quantified by a sequence of dissolution into acetone and its rotary evaporation. The total product recovery was within a range of 95–99% of the dry mass of the feedstock. Through exhaustive examinations, it was concluded that the major portion of the apparent loss, 0.5–4.0%, was caused by moisture uptake by the feedstock until measurement of its mass and evaporation of the moisture in the first reactor in flowing N_2 before the torrefaction and collection of volatile matter. In other words, the mass of unrecovered products, if any, was negligible.

2.2.3 Product analyses

The non-condensable gas consisted mainly of CO, CO_2, H_2, CH_4, C_2H_4, and C_2H_6. These were quantified by gas chromatography (GC). An Agilent 490 Micro-gas chromatograph was used for the GC. The condensed liquid was recovered by dissolution in acetone. The solution was subjected to Karl Fischer titration with a Kyoto Electronics model (MKC-210), and the yield of pyrolytic water was determined. The bio-oil yield was given as the difference between the total mass of the condensed product and that of water. In this paper, the bio-oil was defined as the condensable organic matter. In other words, it involved no water.

It was confirmed in each run of torrefaction or torrefaction/pyrolytic reforming that a very small portion of the volatile product was converted to carbonaceous solid, i.e., soot that was deposited onto the reactor wall. The soot was quantified as its carbon by a general combination of combustion and GC analysis of CO and CO_2. The torrefied cedar (or w-cedar), which is hereafter referred to as char, was subjected to ultimate analysis for measuring C, H, and O contents. The overall elemental composition of the bio-oil was given by the difference in the amounts of C, H, and O between the three products (water, non-condensable gas, and char) and the feedstock.

Every bio-oil was analyzed by gas-chromatography/mass-spectrometry (GC/MS) with a PerkinElmer model (Clarus SQ8) to know the detailed composition, as reported elsewhere in detail [28]. The identified major compounds were quantified by using standard samples. For the compounds which could not be either purchased or provided by other researches, those were semi-quantified by assuming their GC/MS sensitivities were equivalent to those of the available standard compounds having the closest chemical structures. The yields of some particular types of compounds contained in the bio-oil, such as acetic acid, formic acid, and levoglucosan (LGA), were determined by high-performance liquid chromatography (HPLC) with photodiode array and

refractive index detectors in a Shimadzu LC-20 prominence system. A BioRad Aminex 87H column was used for acid separation. A mobile phase, 5 mM H_2SO_4 solution, was provided at a flow rate of 0.6 mL/min and 35 °C. LGA was separated in two SP0810 sugar columns connected in series at 80 °C using deionized water as the mobile phase at a flow rate of 0.6 mL/min.

Pyrolytic sugars in the bio-oil were detected and quantified in forms of monosaccharides (arabinose, xylose, mannose, galactose, and glucose). Briefly, the bio-oil sample was dried by rotary evaporation to remove the solvent (acetone), and then mixed with 20 mL of 4% H_2SO_4 solution. The mixture was heated at 121 °C for 1 h for the acid-catalyzed hydrolysis, cooled to ambient temperature, neutralized, and filtered. The resulting solution was then analyzed by HPLC. Among the monosaccharides, xylose and galactose were separated by two SP0810 sugar columns in series, while arabinose and glucose were separated by a BioRad Aminex 87H column. Mannose was separated by a NH2P-50 4E column at 50 °C. The mobile phase consisted of acetonitrile and aqueous solution of 0.25 M phosphoric acid (80:20, v:v), and it was delivered at a flow rate of 1 mL/min.

Thermogravimetric analysis (TGA) was carried out to evaluate the influence of water washing on the pyrolytic behavior of the cedar. About 5 mg of sample was heated from 30 to 800 °C at a rate of 10 °C min^{-1} under a steady flow of nitrogen at a rate of 100 mL-stp min^{-1}. As depicted in **Figure 2-3**, the washing with water resulted in a shift of the onset temperature for the pyrolytic mass release to the higher temperature side, and also more overall mass release at elevated temperature. These results were brought about by the removal of a substantial portion of AAEMs in the cedar by the washing, as shown in **Table 2-1**.

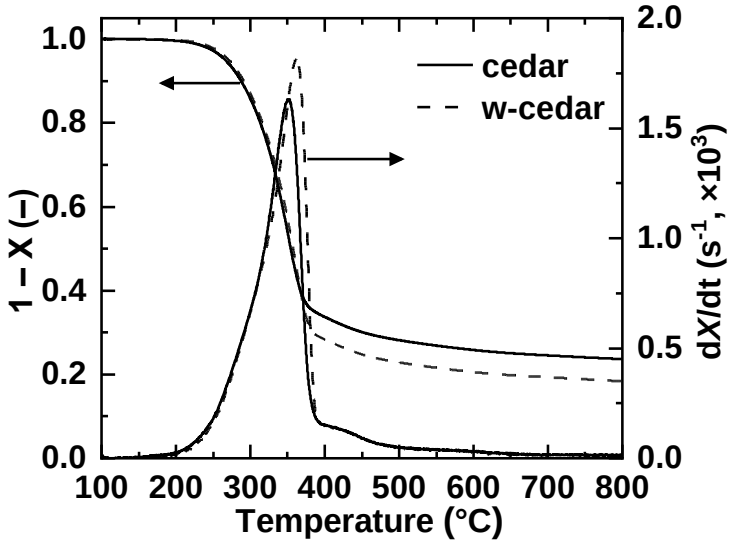

Figure 2-3 TGA of cedar and w-cedar.

2.2.4 Estimation of heat required for torrefaction and vapor-phase reforming

The heat required for torrefaction and that for the subsequent pyrolytic reforming, which were hereafter denoted by Q_{TR} and Q_{PYR}, respectively, were calculated by the following equations.

$$Q_{TR} = H_{char}(T_{TR}) + H_{bio\text{-}oil}(T_{TR}) + H_{water}(T_{TR}) + H_{gas}(T_{TR}) - H_{cedar}(25\ °C) \quad (1)$$

$$Q_{PYR} = \{H_{bio\text{-}oil}(T_{PYR}) + H_{water}(T_{PYR}) + H_{gas}(T_{PYR})\} - \{H_{bio\text{-}oil}(T_{TR}) + H_{water}(T_{TR}) + H_{gas}(T_{TR})\} \quad (2)$$

$$Q_{PYR} + Q_{TR} = H_{char}(T_{TR}) + H_{bio\text{-}oil}(T_{PYR}) + H_{water}(T_{PYR}) + H_{gas}(T_{PYR}) - H_{cedar}(25\ °C) \quad (3)$$

$H_i(T)$ indicated the enthalpy of product i at T. H_{water} was the enthalpy of not liquid water but water vapor. $H_{bio\text{-}oil}$ was the enthalpy of bio-oil in form of vapor. In the case of the conversion of the w-cedar, $H_{cedar}(25\ °C)$ can be just replaced by $H_{w\text{-}cedar}(25\ °C)$. Both equations assumed that the product, *i.e.*, char (torrefied cedar), bio-oil, water, and gas, exited the torrefier or reformer at T_{TR}

or T_{PYR}, respectively. H_{water} and H_{gas} were calculated from the yields of water and the gaseous compounds (H_2, CO, CO_2, CH_4, C_2H_4, and C_2H_6), and thermodynamic data of those compounds. $H_{bio\text{-}oil}$ was calculated according to Yang *et al*. [27], who developed a set of equations to estimate the enthalpy of bio-oil vapor as a function of temperature only from its overall C, H, and O contents. The H/C and O/C atomic ratios calculated by the GC/MS-detectable compounds were also used to estimate the enthalpy of bio-oil vapor for comparative studies. Yang *et al*. [27] also recommended to use average specific heat of char, ≈ 0.02 kJ mol-C^{-1}, over a temperature range from 300 to 800 °C. H_{char} was calculated by following this recommendation.

Differential scanning calorimetry (DSC) was often applied to the measurement of heat of thermochemical reactions. DSC was, however, inapplicable to investigate the enthalpy of volatile matter, which should be presented as a function of temperature. Similar limitations of DSC were claimed by Yang *et al.* [27].

2.3 Results and discussion

2.3.1 Torrefaction

Yields and compositions of torrefaction products

Figure 2-4 shows yields of the torrefaction products (char, gas, water, and bio-oil). The total product yields, except that from w-cedar at 350 °C, were in a range of 96.0–99.5 wt%. The loss in the product recovery, 0.5–4.0 wt%, was caused by the moisture that the feedstock adsorbed until weighing and released in the torrefier before heating, as explained in **Section 2.2.2**. Two important features were noted commonly for both feedstocks. First, the bio-oil yield reached substantial levels of 21–25 wt% at T_{TR} = 300 °C, and exceeded 30 wt% at 320 °C. Second, the gas consisted solely of CO and CO_2. It was also seen that the washing with water influenced the product yields.

The char yield from the w-cedar was greater than that from the cedar at $T_{TR} \leq 320$ °C, but smaller at $T_{TR} = 350$ °C. The trend at $T_{TR} \leq 320$ °C was attributed to acceleration of the pyrolysis by AAEMs [29]. The other trend at $T_{TR} > 320$ °C was, taken together with the bio-oil yield from the w-cedar (41 wt%) than that from the cedar (36 wt%), in agreement with the well-known suppression of cross-linking and enhancement of depolymerization by removal of AAEMs [14,30]. TGA was performed to examine the accelerated pyrolysis by AAEMs, and then it was confirmed as shown in **Figure 2-3**.

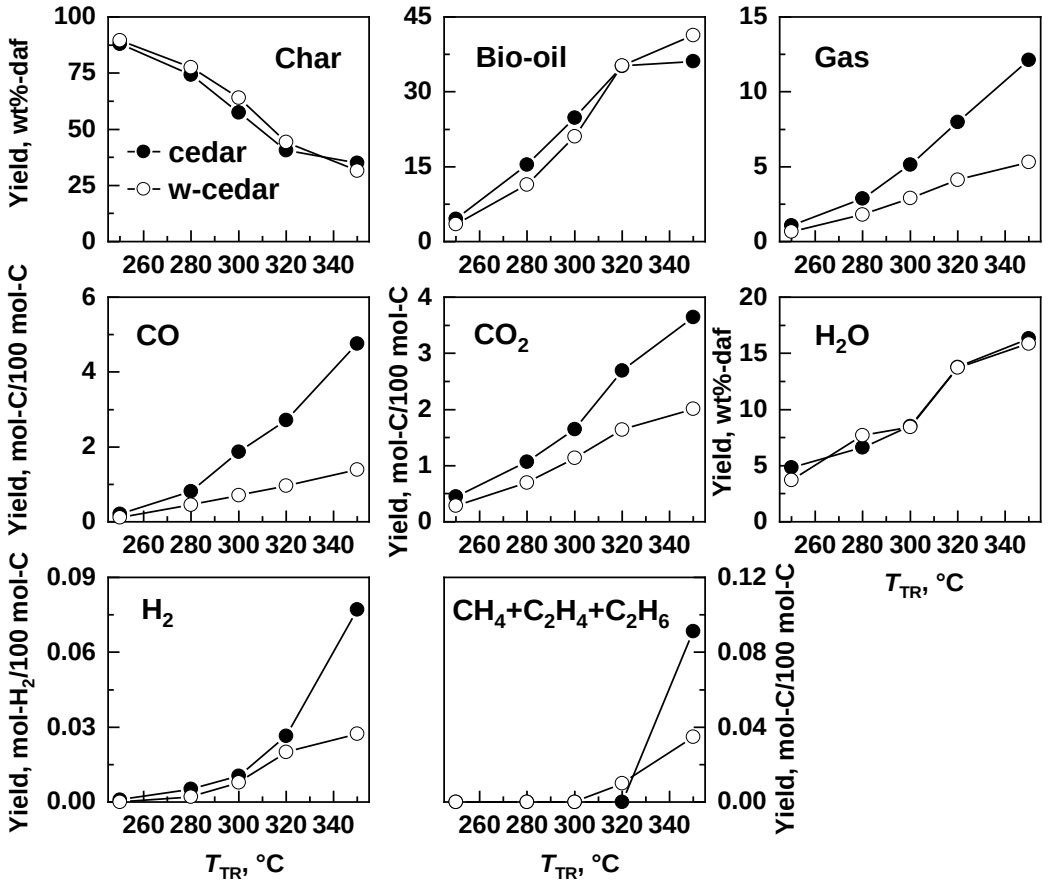

Figure 2-4 Yields of char, bio-oil, water, gas and individual gaseous products from torrefaction.

The torrefaction of the cedar gave clearly more CO_2 and CO than that of the w-cedar. This was due to suppression of cross-linking resulting from the washing with water that had removed 55% of the inherent AAEMs (on a mol-equivalent basis). It was believed that AAEMs catalyzed cleavage of etheric bonds and decomposition of C=O groups of hemicellulose, and also intraparticle secondary reactions of bio-oil leading to CO formation [15,31]. On the other hand, the removal of AAEMs caused no or very little reduction of water yield. The water-soluble AAEMs seemed to play no or very little role in dehydration condensation of hydroxylic and carboxylic groups [32].

Chemical composition of bio-oil from torrefaction

Figure 2-5 shows the major GC-detectable chemical components of bio-oil from the torrefaction. The GC-detectable compounds accounted for 32–40 wt% of the entire bio-oil. In other words, about 2/3 of the bio-oil was GC-undetectable high-molecular-mass compounds. The identified organic compounds were classified into ten different types, *i.e.*, acids, alcohols, ketones, aldehydes, phenolics, furans, esters, hydrocarbons, pyrans, and sugars. The figure plots the yields of the eight main types against T_{TR}. Detailed compounds involved in the individual types are listed in **Table 2-2**.

Table 2-2 Chemical compositions of bio-oil during torrefaction.

	T_{TR}, °C (cedar)					T_{TR}, °C (w-cedar)				
	250	280	300	320	350	250	280	300	320	350
Compound yield (wt%-daf-biomass)										
Furans	**0.102**	**0.569**	**1.405**	**2.063**	**2.286**	**0.083**	**0.5**	**1.18**	**2.49**	**2.802**
Furan	-	0.003	0.005	0.008	0.01	-	0.004	0.006	0.011	0.018
2,3-dihydrofuran	-	-	-	0.008	0.009	-	-	-	0.01	0.012
2-methylfuran	-	-	0.011	0.02	0.028	-	-	0.006	0.019	0.028
oxolan-2-ol	-	0.01	0.009	0.014	0.014	-	0.007	0.016	0.029	0.037
2-methyloxolan-2-ol	-	0.011	0.022	0.028	0.036	-	0.008	0.014	0.023	0.031
Furfural	0.015	0.046	0.101	0.136	0.166	0.023	0.051	0.104	0.179	0.23
2-furanmethanol	0.087	0.218	0.572	0.713	0.704	0.06	0.178	0.392	0.745	0.761
2-acetylfuran	-	-	-	0.028	0.039	-	-	-	0.026	0.031
3-furanmethanol	-	0.061	0.114	0.158	0.171	-	0.062	0.12	0.225	0.213
5-methyl furfural	-	-	-	0.038	0.06	-	-	-	0.051	0.088
γ-butyrolactone	-	0.032	0.056	0.083	0.116	-	0.016	0.027	0.056	0.068
2(5H)-furanone	-	0.09	0.249	0.398	0.427	-	0.076	0.197	0.429	0.501
5-methyl-2(5H)-furanone	-	-	-	0.035	0.041	-	-	-	0.039	0.055
methyl 3-furoate	-	-	-	0.047	0.050	-	-	-	0.038	0.06
3-hydroxyoxolan-2-one	-	0.04	0.089	0.113	0.146	-	0.038	0.091	0.15	0.189
5-(hydroxymethyl)oxolan-2-one	-	0.048	0.085	0.093	0.088	-	0.045	0.114	0.219	0.151
5-hydroxymethylfurfural	-	-	0.045	0.072	0.091	-	-	0.049	0.139	0.189
(S)-5-hydroxymethyldihydrofuran-2-one	-	-	0.028	0.044	0.057	-	-	0.012	0.035	0.059
dihydro-4-hydroxy-2(3H)-furanone	-	0.009	0.018	0.025	0.032	-	0.014	0.032	0.066	0.078
Ketones	**0.15**	**0.797**	**1.771**	**2.52**	**3.021**	**0.137**	**0.547**	**1.331**	**2.584**	**3.015**
2,3-butanedione	0.015	0.053	0.058	0.117	0.113	0.017	0.028	0.047	0.087	0.123
2-butanone	-	-	0.013	0.016	0.025	-	-	0.006	0.024	0.028
acetol	0.119	0.597	1.246	1.641	2.021	0.12	0.446	1.034	1.857	2.100
1-hydroxy-2-butanone	-	-	-	-	0.018	-	-	-	-	0.015
acetoxyacetone	-	-	0.013	0.023	0.027	-	-	0.013	0.021	0.027
2-methyl-2-cyclopenten-1-one	-	-	0.008	0.017	0.035	-	-	0.006	0.018	0.036
4-cyclopentene-1,3-dione	-	-	-	0.010	0.014	-	-	-	0.013	0.013

2-hydroxycyclopent-2-en-1-one	0.016	0.133	0.398	0.601	0.532	-	0.065	0.201	0.471	0.488
2-oxobutyl acetate	-	-	-	0.009	0.017	-	-	-	0.020	0.035
3-methylcyclopentane-1,2-dione	-	0.013	0.035	0.069	0.117	-	0.007	0.023	0.057	0.111
2,5-dimethylcyclohexanone	-	-	-	-	0.019	-	-	-	-	0.009
2-methylcyclohexane-1,3-dione	-	-	-	0.017	0.021	-	-	-	0.014	0.029
Phenolics	**0.123**	**0.417**	**0.629**	**0.880**	**1.349**	**0.087**	**0.332**	**0.640**	**0.990**	**1.369**
phenol	-	0.014	0.027	0.041	0.067	-	0.006	0.013	0.024	0.039
guaiacol	0.014	0.048	0.125	0.200	0.339	-	0.026	0.072	0.142	0.256
p-cresol	-	-	-	0.008	0.017	-	-	-	0.010	0.018
4-ethylguaiacol	-	-	0.021	0.028	0.052	-	-	0.017	0.028	0.044
creosol	-	0.024	0.042	0.077	0.146	-	0.02	0.046	0.096	0.187
4-vinylguaiacol	0.01	0.031	0.07	0.112	0.157	0.009	0.024	0.061	0.103	0.140
isoeugenol	0.016	0.052	0.084	0.114	0.168	0.013	0.018	0.107	0.155	0.193
2-methoxy-3-allylphenol	-	0.013	0.017	0.021	0.032	-	0.013	0.02	0.029	0.037
dihydroeugenol	-	0.023	0.028	0.045	0.058	-	0.02	0.031	0.060	0.069
vanillin	-	0.021	0.032	0.035	0.044	-	0.014	0.030	0.041	0.046
acetovanillone	-	0.028	0.031	0.038	0.051	-	0.02	0.030	0.041	0.051
guaiacylacetone	-	0.028	0.036	0.046	0.059	-	0.017	0.031	0.044	0.052
coniferyl alcohol	-	0.021	0.022	0.025	0.033	-	0.03	0.025	0.035	0.039
homovanillic acid	-	0.031	0.043	0.055	0.073	-	0.024	0.042	0.061	0.073
3-(4-hydroxy-3-methoxyphenyl)-2-propenal	0.045	0.08	0.048	0.033	0.052	0.031	0.098	0.114	0.120	0.123
isovanillin	0.02	-	-	-	-	0.018	-	-	-	-
p-hydroxybenzalacetone	0.017	-	-	-	-	0.016	-	-	-	-
Hydrocarbons	**0.035**	**0.014**	**0.016**	**0.017**	**0.022**	**0.019**	**0.012**	**0.015**	**0.016**	**0.019**
calamenene	-	0.008	0.008	0.008	0.01	-	0.005	0.005	0.005	0.005
3-ethyl-1,2,4,5-tetramethyl-benzene	-	0.006	0.008	0.009	0.012	-	0.007	0.010	0.011	0.014
(5α,9α,10ß)-Kaur-15-ene	0.006	-	-	-	-	0.003	-	-	-	-
muurolene	0.002	-	-	-	-	0.002	-	-	-	-
α-selinene	0.004	-	-	-	-	0.003	-	-	-	-
cadinene	0.004	-	-	-	-	0.002	-	-	-	-
calamenene	0.005	-	-	-	-	0.003	-	-	-	-

9,10-dehydroisolongifolene	0.002	-	-	-	-	0.001	-	-	-	-
azulol	0.012	-	-	-	-	0.005	-	-	-	-
Aldehydes	**0.009**	**0.059**	**0.171**	**0.311**	**0.437**	**0.015**	**0.051**	**0.142**	**0.371**	**0.519**
glycolaldehyde	-	0.047	0.075	0.109	0.123	-	0.048	0.089	0.168	0.170
butanedial	0.009	0.011	0.096	0.18	0.276	0.015	0.003	0.052	0.189	0.317
glutaraldehyde	-	-	-	0.022	0.038	-	-	-	0.014	0.032
Esters	**-**	**0.044**	**0.119**	**0.217**	**0.31**	**-**	**0.079**	**0.195**	**0.451**	**0.648**
allyl acetate	-	0.044	0.119	0.199	0.283	-	0.079	0.195	0.415	0.589
vinyl methacrylate	-	-	-	0.018	0.027	-	-	-	0.036	0.059
Alcohols	**0.016**	**0.05**	**0.106**	**0.155**	**0.216**	**0.011**	**0.065**	**0.139**	**0.260**	**0.340**
2-hydroxyethyl acetate	-	0.038	0.090	0.133	0.193	-	0.055	0.117	0.223	0.303
trans-1,2-cyclopentanediol	-	0.012	0.016	0.022	0.016	-	0.010	0.022	0.037	0.028
4-isopropylcyclohexanol	-	-	-	-	0.007	-	-	-	-	0.008
2,4-dimethylphenethyl alcohol	0.007	-	-	-	-	0.006	-	-	-	-
cubenol	0.009	-	-	-	-	0.005	-	-	-	-
Acids	**1.035**	**2.858**	**5.213**	**5.688**	**5.994**	**0.777**	**2.303**	**3.739**	**4.896**	**4.613**
formic acid	0.667	1.982	3.8	4.158	4.106	0.526	1.676	2.789	3.771	3.496
acetic acid	0.367	0.876	1.413	1.531	1.888	0.251	0.627	0.951	1.125	1.116
Pyrans	**-**	**-**	**0.01**	**0.022**	**0.029**	**-**	**-**	**0.012**	**0.032**	**0.054**
tetrahydro-2H-pyran-2-one	-	-	0.01	0.022	0.029	-	-	0.012	0.032	0.054
Sugars	**-**	**0.035**	**0.176**	**0.565**	**0.696**	**-**	**0.066**	**0.197**	**0.928**	**1.133**
2,3-anhydro-D-mannosan	-	-	-	0.019	0.031	-	-	-	0.016	0.042
1,4:3,6-dianhydro-α-d-glucopyranose	-	-	0.016	0.059	0.069	-	-	0.008	0.046	0.077
levoglucosan	-	0.015	0.128	0.458	0.565	-	0.027	0.145	0.823	0.974
DL-arabinose	-	0.02	0.031	0.029	0.031	-	0.039	0.044	0.042	0.039
Total mass fractions (%-bio-oil)	**32.8**	**31.5**	**38.8**	**35.4**	**39.6**	**32.5**	**34.7**	**36.1**	**37**	**35.1**

The yields of all the compound types, except acids from the w-cedar, increased monotonously with T_{TR}. Amongst the ten compound types, the acids were the most abundant in the bio-oil, and represented by acetic and formic acids, which were formed by the decomposition of O-acetyl and of glucuronic acid groups [33,34]. The mass fraction of those two acids was as high as 70% in mass of the total GC-detected compounds at T_{TR} = 250 °C, but decreased monotonously to 30–40% with increasing T_{TR} due to more extensive increase in the yields of other types. The removal of AAEMs seemed to decrease the acid yield due to loss of catalysis of AAEMs in reactions such as ring fission and fragmentation of carbohydrate units [33,35].

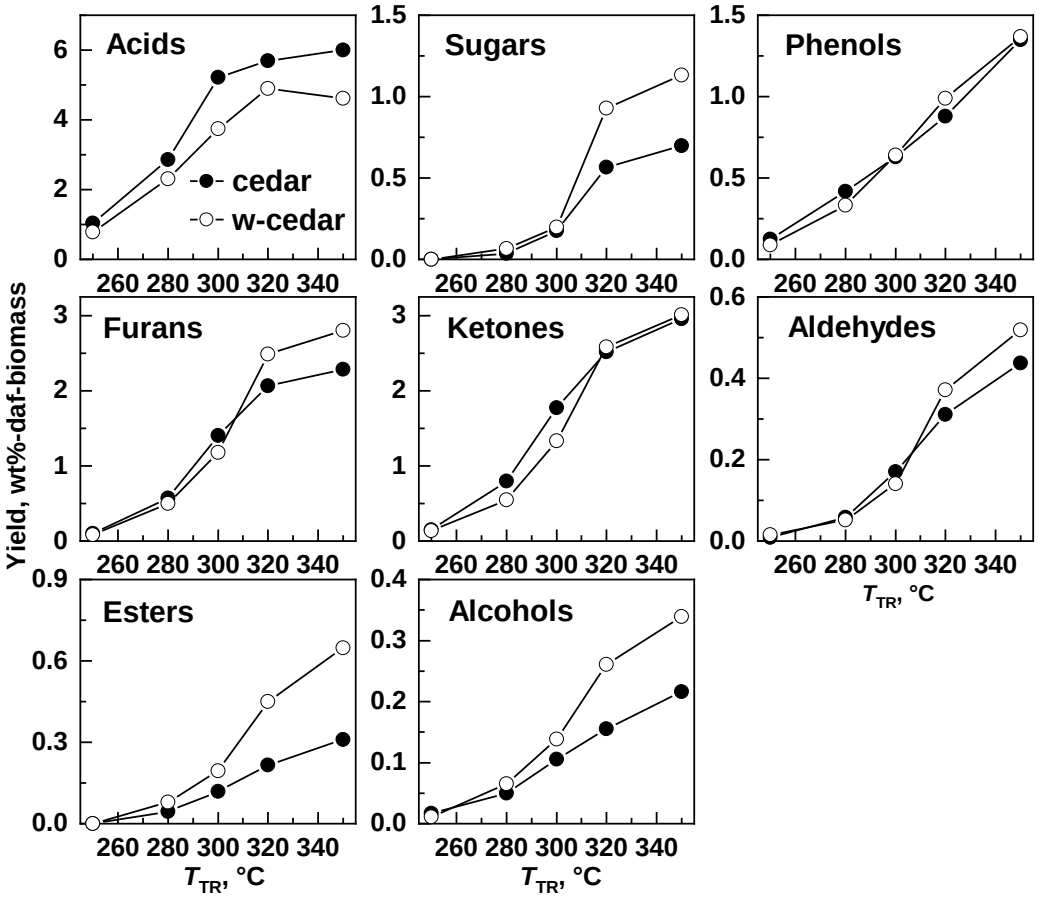

Figure 2-5 Composition of GC-detectable portion of bio-oil from torrefaction.

The formation of phenols and sugars (mainly consisting of LGA) at 250–280 °C indicated the pyrolysis of lignin and cellulose at such low temperatures. Their yields were as low as 0.3–0.4 wt% and < 0.1 wt%, respectively. Furans and ketones were products from depolymerization, dehydration, and cyclization of carbohydrate units [36,37]. The yields of furans and ketones were greater by factors of 10–40 than that of sugars at 250–280 °C. This strongly suggested that furans and ketones were formed mainly from hemicellulose. The total yield of furans and ketones increased greatly at T_{TR} > 280 °C and then reached 5.2–5.8 wt% at 350 °C. It was believed that the cellulose pyrolysis led to the formation of furans and ketones, together with LGA, of that yield increased steeply at T_{TR} > 300 °C.

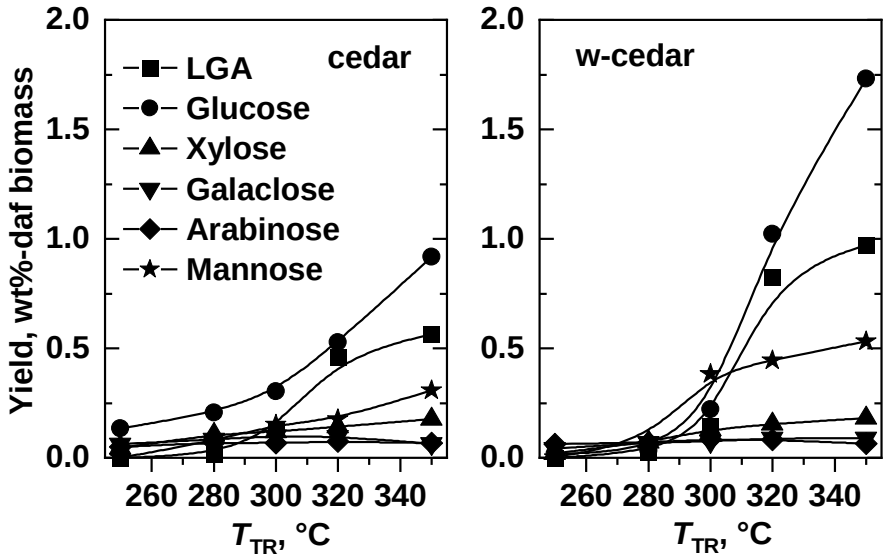

Figure 2-6 Yields of mono-sugars from acid hydrolysis of bio-oil together with LGA yield from torrefaction.

The conversion of cellulose and hemicellulose was investigated in more detail by quantifying the sugar units of oligo-sugars involved in the bio-oil by hydrolysis. The result was shown in

Figure 2-6. At T_{TR} > 300 °C, precursors of glucose and the other C5/C6 mono-sugars were more abundant in the w-cedar bio-oil than that from the cedar. This was a result of suppressed depolymerization by main chains breaking of the carbohydrates by AAEMs. The glucose yield (after the hydrolysis) was always greater than that of LGA from the torrefaction, while the LGA/glucose ratio was 0.47–0.96 on a molar basis at $T_{TR} \geq 300$ °C. Thus, the C6 sugar oligomers and other LGA precursors were at most as abundant as LGA [38]. The total yield of mannose, galactose, xylose, and arabinose increased with T_{TR} and reached 0.7–0.9 wt% at 300 °C. This indicated some abundance and thermal stability of 'hydrolyzable' oligo-anhydrosugars [33,39,40]. On the other hand, only two anhydrosugar monomers, 2,3-anhydro-D-mannosan and DL-arabinose, were found in the bio-oil with yields much smaller than 0.1 wt%. No mono-anhydrosugars such as xylosan, mannosan, and galactosan were detected in the bio-oil. Thus, mono-anhydrosugars other than LGA were hardly formed under the present conditions of torrefaction.

2.3.2 Fate of chemical energy of cedar and heat required for torrefaction

Figure 2-7 shows the chemical energies of char, bio-oil, gas, and the total of them. Every chemical energy was given as HHV. **Table 2-3** summarizes the properties of bio-oil and char such as the overall H/C and O/C atomic ratios, which were necessary for calculating their chemical energies, $H_{bio\text{-}oil}(T_{TR})$, and $H_{char}(T_{TR})$. In the calculation of the chemical energies, the char, gas, and bio-oil yields were corrected so that their total was 100 wt%-dry-feedstock. This was reasonable because the loss in the product recovery was negligible, as stated above. The overall fates of the chemical energies of the cedar and w-cedar were similar to each other. The chemical energies of the char and bio-oil decreased and increased monotonously with T_{TR}, respectively, and became

equivalent to each other at T_{TR} = 350 °C. Thus, the bio-oil was not a byproduct anymore. The chemical energy of the gas, which was represented by that of CO, was much smaller than the others.

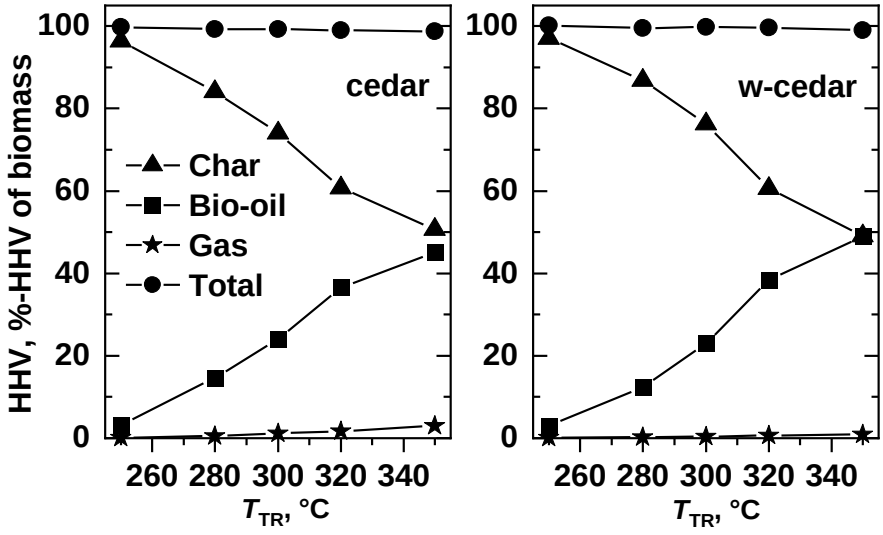

Figure 2-7 Chemical energies of products. Total: sum of chemical energies of char, bio-oil, and gas.

Table 2-3 Properties of chars and bio-oils for torrefaction.

	T_{TR}, °C (cedar)					T_{TR}, °C (w-cedar)				
	250	280	300	320	350	250	280	300	320	350
Properties of chars										
H/C atomic ratio	1.37	1.23	1.03	0.82	0.69	1.37	1.30	1.17	0.96	0.71
O/C atomic ratio	0.57	0.52	0.41	0.26	0.25	0.59	0.54	0.49	0.34	0.23
heating value, MJ-HHV (kg-daf)$^{-1}$	21.3	22.2	24.5	28.9	28.5	21.0	22.0	22.9	26.5	29.2
heating value, kJ-HHV (mol-C)$^{-1}$	481	480	481	489	474	480	482	480	487	479
standard enthalpy of formation $\Delta H_f°_{char}$, kJ mol-C^{-1} [a)]	−108	−90	−61	−22	−18	−109	−97	−81	−44	−15
Properties of bio-oils										
H/C atomic ratio	0.72	1.66	1.91	1.65	1.62	1.68	1.22	1.58	1.41	1.44
O/C atomic ratio	0.93	0.75	0.81	0.69	0.50	0.85	0.57	0.64	0.60	0.57
standard enthalpy of formation $\Delta H_f°_{bio\text{-}oil}$, kJ/mol-C [a)]	−101	−149	−172	−134	−93	−174	−93	−120	−107	−100
$R_{\Delta H,bio\text{-}oil}$ [b)]	0.69	0.81	0.88	0.79	0.75	0.84	0.68	0.76	0.72	0.72
Heat required for torrefaction										
MJ/kg-daf-biomass	0.2	0.3	0.3	0.5	0.6	0.2	0.4	0.5	0.7	0.8
%-HHV-daf-biomass	1.0	1.4	1.8	2.8	3.2	1.2	1.9	2.6	3.4	4.0
Properties of bio-oils from GC/MS-detectable compounds										
H/C atomic ratio	1.71	1.69	1.67	1.62	1.61	1.72	1.69	1.65	1.60	1.57
O/C atomic ratio	1.00	0.96	0.93	0.85	0.79	1.02	0.98	0.89	0.79	0.73
standard enthalpy of formation $\Delta H_f°_{bio\text{-}oil}$, kJ/mol-C [a)]	−218	−207	−196	−171	−157	−225	−210	−184	−157	−141
$R_{\Delta H,bio\text{-}oil}$ [b)]	0.91	0.89	0.87	0.83	0.81	0.92	0.89	0.85	0.81	0.78

a) $\Delta H_f°_{char}$ and $\Delta H_f°_{bio\text{-}oil}$ were calculated according to Yang *et al*. b) $R_{\Delta H,bio\text{-}oil}$ is an essential parameter for calculating the enthalpy of bio-oil vapor as a function of temperature, and is a function of H/C and O/C ratios of the bio-oil.

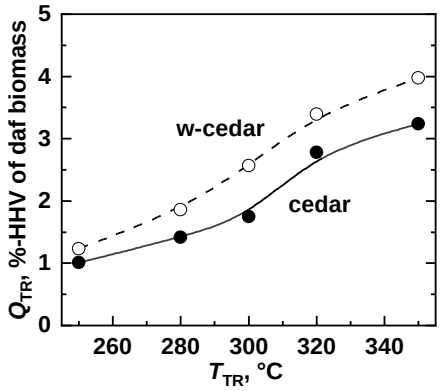

Figure 2-8 Q_{TR} for cedar or w-cedar as a function of T_{TR}.

Figure 2-8 compares Q_{TR} between the cedar and w-cedar. It was noted that the total chemical energy of the products was almost equivalent to that of the feedstock (i.e., cedar or w-cedar). This was reasonable in consideration that the torrefaction was a weakly endothermic process. Q_{TR} was as small as 1.0–3.2%-HHV-daf-cedar or 1.2–4.0%-HHV-daf-w-cedar. These ranges were reasonable if compared with heat demands of pyrolysis [27,41]. Taken together with the data shown in **Figure 2-7**, it was clearly said that combustion of only the gas cannot supply sufficient quantity of heat to the torrefaction, but that of a small portion of the bio-oil was enough to drive the torrefaction. In other words, combustion of the entire portion of the volatiles was unreasonable. It also seemed that combustion of a certain portion of the bio-oil can supply heat not only to the torrefaction but also to drying. Here was assumed that the moisture content of the feedstock was 25 wt%-wet (≈ 0.33 kg-water/kg-daf-cedar), and the latent heat of the moisture was 0.81 MJ/kg-daf-cedar. This latent heat, in the case of torrefaction at T_{TR} = 300 °C, was only 18% of the chemical energy of the bio-oil. **Figure 2-8** also shows that Q_{TR} for the w-cedar was systematically greater than that for the cedar, and the difference was about 0.57%-HHV-daf-cedar in average. A

large portion of such difference was explained by that the standard enthalpy of formation between the cedar and w-cedar, which was about 0.50%-HHV-daf-cedar.

2.3.3 Pyrolytic reforming

Overall product distribution and gas composition

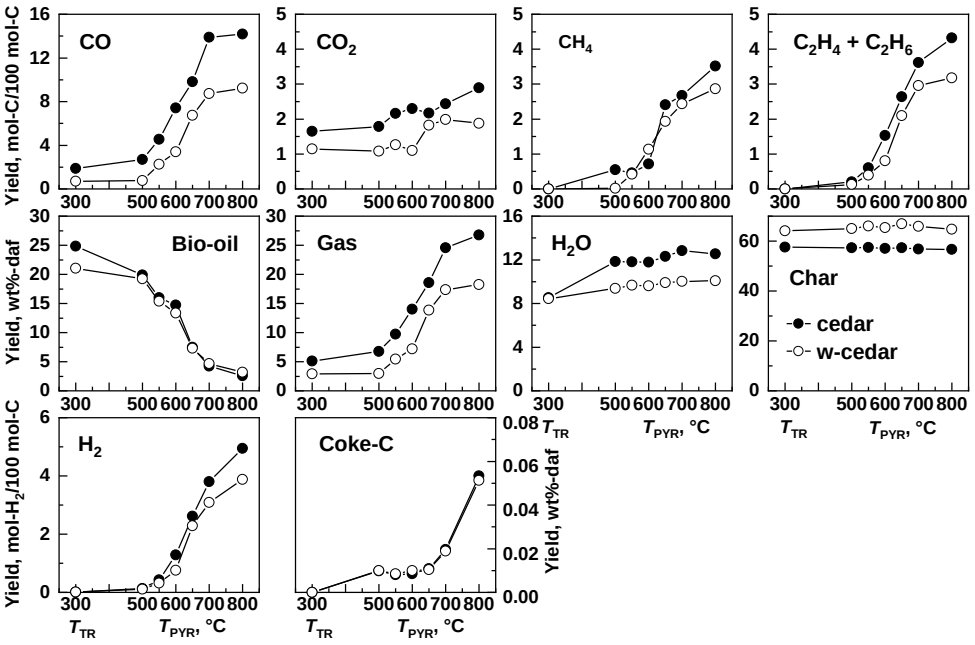

Figure 2-9 Yields of char, bio-oil, pyrolytic water, and gas products during vapor-phase pyrolytic reforming.

Figure 2-9 presents the product yields from the pyrolytic reforming of the volatiles formed in the torrefaction at T_{TR} = 300 °C. The reforming changed only the composition of the volatiles, while the char yield remained unchanged within experimental errors with standard deviations of 0.3 wt%-daf-cedar and 0.7 wt%-daf-w-cedar. The pyrolytic reforming was, as expected, featured by significant increase and decrease in the gas and bio-oil yields, respectively. The maximum reduction of the bio-oil was as much as 90% at T_{PYR} = 800 °C. The total yield of C-containing

gases and H_2, on C and molar bases, respectively, increased monotonously with T_{PYR}, and was greater than that from the torrefaction at 300 °C by factors of 7.9 and 10.5 for the cedar and w-cedar, respectively. Such significant increase was contributed largely by those of CO, H_2, and C_1–C_2 hydrocarbons. These gases were produced mainly by thermal decomposition of O-containing compounds (sugars, ethers, alcohols, ketones, aldehydes, and phenols), dehydrogenation (associated with unsaturated C=C bond formation, aromatization, and aromatic-ring condensation), and C-C/C-O bond cleavage leading to dealkylation, respectively [42-46].

The CO_2 yield increased but less significantly than CO and H_2. The increment, at most 1 mol/kg-daf, was greater than that of acetic acids (≈ 0.3 mol/kg-daf) as a major CO_2 precursor formed in the torrefaction and additionally in reforming. The formic acid was more abundant in the bio-oil than acetic acid, but it was not necessarily an important precursor of CO_2 [45,47]. Presence of other types of acids or others in the bio-oil was suggested.

The H_2O yield increased by 3.3 and 1.7 mol/kg-daf at 300–500 °C for the cedar and w-cedar respectively, and slightly at higher T_{PYR}. Such increase in the H_2O yield would arise from intra-molecular dehydration between hydroxylic groups. The H/C and O/C ratios of the bio-oil from the cedar torrefaction at T_{TR} = 300 °C were 1.91 and 0.81, respectively, and higher than the corresponding ratios for the w-cedar, 1.58 and 0.64. Combined with that the total bio-oil yield from the cedar was greater than that from the w-cedar at T_{TR} = 300 °C, it was believed that the bio-oil from the cedar contained more hydroxylic groups as H_2O precursors than the w-cedar. Vapor-phase steam reforming was expected initially, but no evidence of its occurrence such as the decrease in the H_2O yield was obtained.

It was also found that a very small portion of the volatiles was converted into coke that was defined as the carbonaceous deposits on the reactor wall. The coke yield increased with T_{PYR}, but

at most 0.05 wt%-daf for both the cedar and w-cedar. A photograph of coke deposited on the reactor wall is available in **Figure 2-10.**

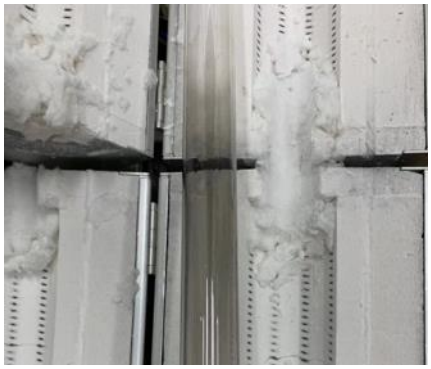

Figure 2-10 A photograph of the reaction tube after secondary vapor-phase reforming at 800 °C.

Quality of gas as fuel

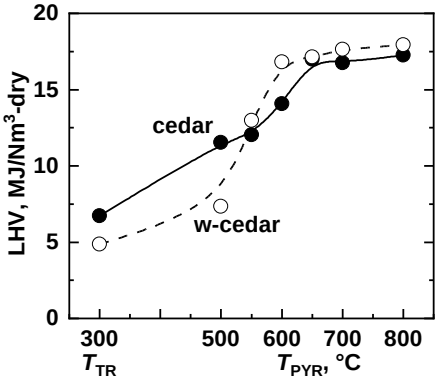

Figure 2-11 Lower calorific value of gas from cedar or w-cedar as a function of T_{PYR}.

The total lower heating values (LHVs) of the gas are plotted against T_{PYR} in **Figure 2-11**. At $T_{PYR} \geq 650$ °C, the LHVs were 17–18 MJ/Nm^3-dry, and greater than those from the torrefaction by factors of 2.6–3.7. The LHV for the w-cedar increased greatly at T_{PYR} = 500–650 °C. This was due to significant bio-oil conversion into gas in the same range of T_{PYT}. The LHV increased further

but slightly at T_{PYR} > 650 °C, where the yields of H_2, CO, and light hydrocarbons increased without changing the molar composition largely.

Chemical compositions of bio-oil from pyrolytic reforming

Figure 2-12 provides changes in the yields of the individual GC-quantified components of the bio-oil with T_{PYR}. Detailed product compositions are summarized in **Table 2-4**. The total mass fractions of the GC-detectable compounds in the bio-oils from 36–39% of the entire bio-oils from the torrefaction at T_{TR} = 300 °C. Those fractions varied with T_{PYR} over ranges of 29–72% with no clear trends. Considering that the GC-undetectable portion was the heavier portion of the bio-oil, the pyrolytic reforming was effective for conversion of the bio-oil but not for selective conversion of the heavier portion.

All the component yields changed with T_{PYR}, but with more or less different trends. In the following, behaviors of the components with maximum yields over 1 wt%-daf, *i.e.*, those of phenols, aromatic hydrocarbons and sugars are reported and discussed individually.

Aromatic hydrocarbons

The aromatic hydrocarbons were absent in the bio-oil from the torrefaction, and formed exclusively by the pyrolytic reforming. For both the cedar and w-cedar and at T_{PYR} = 700–800 °C, the abundances of aromatics with different ring numbers were in the order of mono-aromatics > di-aromatics (naphthalenes, indenes, biphenyls, and fluorenes) > tri-aromatics (acenaphthylenes, anthracenes, and phenanthrenes) > tetra-aromatics (pyrenes, detected only at T_{PYR} = 800 °C). The influence of the AAEMs removal, if any, seemed to be insignificant.

Table 2-4 Chemical compositions of bio-oil during pyrolytic reforming.

	T_{PYR}, °C (cedar)						T_{PYR}, °C (w-cedar)					
	500	550	600	650	700	800	500	550	600	650	700	800
Compound yield (wt%-daf-biomass)												
Furans	**1.809**	**1.934**	**1.350**	**0.521**	**0.139**	**0.016**	**1.317**	**1.578**	**0.768**	**0.343**	**0.144**	**0.015**
furan	0.016	0.028	0.042	0.035	0.021	0.005	0.016	0.023	0.034	0.030	0.017	0.005
2,3-dihydrofuran	0.019	0.072	0.087	0.035	0.009	-	0.015	0.050	0.051	0.022	0.012	-
2-methylfuran	0.019	0.025	0.029	0.016	-	-	0.020	0.024	0.018	0.017	-	-
tetrahydro-furan	0.061	0.036	-	-	-	-	0.012	0.011	-	-	-	-
oxolan-2-ol	0.036	0.207	0.365	0.125	-	-	0.021	0.120	0.143	0.055	-	-
2-methyloxolan-2-ol	0.035	0.068	0.053	-	-	-	0.016	0.040	0.026	-	-	-
furfural	0.127	0.129	0.116	0.074	-	-	0.107	0.114	0.071	0.044	-	-
2-furanmethanol	0.581	0.494	0.346	0.142	-	-	0.373	0.358	0.203	0.093	-	-
2-acetylfuran	0.022	0.035	-	-	-	-	0.015	0.022	-	-	-	-
3-furanmethanol	0.101	-	-	-	-	-	0.091	-	-	-	-	-
γ-butyrolactone	0.077	0.108	0.104	-	-	-	0.040	0.079	0.049	-	-	-
2(5H)-furanone	0.239	0.204	0.096	-	-	-	0.168	0.128	0.071	-	-	-
3-hydroxyoxolan-2-one	0.093	0.075	0.021	-	-	-	0.093	0.101	0.009	-	-	-
5-(hydroxymethyl)oxolan-2-one	0.235	0.291	-	-	-	-	0.166	0.261	-	-	-	-
2-methylbenzofuran-5-ol	0.023	0.032	0.025	-	-	-	0.022	0.050	0.027	-	-	-
2,3-dihydrobenzofuran	0.021	0.038	0.065	0.093	0.109	-	0.017	0.056	0.064	0.080	0.115	-
5-hydroxymethylfurfural	0.055	0.033	-	-	-	-	0.069	0.060	-	-	-	-
(S)-5-hydroxymethyldihydrofuran-2-one	0.029	0.036	-	-	-	-	0.021	0.028	-	-	-	-
dihydro-4-hydroxy-2(3H)-furanone	0.018	0.022	-	-	-	-	0.034	0.051	-	-	-	-
dibenzofuran	-	-	-	-	-	0.011	-	-	-	-	-	0.010
Ketones	**2.102**	**2.118**	**1.713**	**0.759**	**0.022**	**-**	**1.491**	**1.616**	**1.032**	**0.516**	**0.015**	**-**
3-buten-2-one	0.010	0.033	0.035	0.020	-	-	0.012	0.027	0.025	0.021	-	-

2,3-butanedione	0.091	0.070	0.024	-	-	-	0.074	0.081	0.024	-	-	-
2-butanone	0.095	0.053	0.017	-	-	-	0.011	0.014	0.017	-	-	-
acetol	1.384	1.435	1.236	0.686	-	-	1.099	1.144	0.757	0.470	-	-
acetoin	0.014	0.026	0.032	-	-	-	0.010	0.025	0.026	-	-	-
acetoxyacetone	0.024	0.017	0.016	-	-	-	0.022	0.021	0.009	-	-	-
2-cyclopentenone	-	-	-	-	0.017	-	-	-	-	-	0.011	-
2-methyl-2-cyclopenten-1-one	0.017	0.022	0.022	0.013	0.005	-	0.011	0.019	0.011	0.008	0.004	-
2-hydroxycyclopent-2-en-1-one	0.405	0.396	0.267	0.039	-	-	0.221	0.226	0.121	0.016	-	-
3-methylcyclopentane-1,2-dione	0.042	0.039	0.014	-	-	-	0.021	0.032	0.007	-	-	-
2,5-dimethylcyclohexanone	0.012	0.013	0.030	-	-	-	0.003	0.008	0.021	-	-	-
2-(2-butynyl)cyclohexanone	0.008	0.013	0.017	-	-	-	0.006	0.018	0.014	-	-	-
Phenolics	**0.412**	**0.240**	**0.310**	**0.450**	**0.400**	**0.082**	**0.350**	**0.221**	**0.230**	**0.303**	**0.275**	**0.086**
salicylaldehyde	0.014	0.014	0.013	-	-	-	0.006	0.013	0.014	-	-	-
phenol	0.037	0.052	0.087	0.152	0.246	0.082	0.016	0.045	0.057	0.095	0.159	0.086
guaiacol	0.065	0.022	0.028	-	-	-	0.042	0.017	0.015	-	-	-
o-cresol	0.007	0.012	0.025	0.044	0.044	-	0.004	0.015	0.022	0.031	0.032	-
p-cresol	0.007	0.013	0.026	0.061	-	-	0.007	0.016	0.020	0.033	-	-
m-cresol	-	-	0.022	0.039	-	-	-	-	0.020	0.031	-	-
3-ethylphenol	0.024	0.008	0.011	0.017	0.009	-	0.027	0.008	0.008	0.013	0.009	-
2,3-xylenol	-	0.005	0.006	0.012	0.006	-	-	0.005	0.006	0.009	0.004	-
4-ethylphenol	0.003	0.009	0.015	0.027	0.005	-	0.003	0.013	0.014	0.020	0.005	-
5-ethyl-*m*-cresol	-	0.007	-	-	-	-	-	0.006	-	-	-	-
4-ethyl-*o*-cresol	-	-	-	0.005	-	-	-	-	-	0.005	-	-
4-ethylguaiacol	0.020	-	-	-	-	-	0.015	-	-	-	-	-
2,5-xylenol	-	-	0.023	0.024	0.023	-	-	-	0.014	0.017	0.015	-
4-vinylguaiacol	0.038	0.013	0.010	-	-	-	0.042	0.010	0.007	-	-	-
m-eugenol	0.013	-	-	-	-	-	0.013	-	-	-	-	-
isoeugenol	0.042	0.012	-	-	-	-	0.052	0.008	-	-	-	-
2-isopropoxyphenol	-	0.011	0.014	0.016	0.020	-	-	0.007	0.009	0.012	0.012	-

2-allylphenol	-	0.027	0.017	0.012	0.010	-	-	0.031	0.015	0.010	0.009	-
dihydroeugenol	0.032	-	-	-	-	-	0.028	-	-	-	-	-
vanillin	0.031	0.013	-	-	-	-	0.025	0.010	-	-	-	-
thymol	-	-	0.011	-	-	-	-	-	0.008	-	-	-
3-methylcatechol	-	-	-	0.014	-	-	-	-	-	0.007	-	-
1-naphthalenol	-	-	-	0.007	0.007	-	-	-	-	0.006	0.007	-
2-naphthalenol	-	-	-	0.012	0.012	-	-	-	-	0.010	0.012	-
2-methyl-1-naphthol	-	-	-	0.006	-	-	-	-	-	0.003	-	-
euresol	-	-	-	-	0.016	-	-	-	-	-	0.011	-
acetovanillone	0.031	0.020	-	-	-	-	0.026	0.016	-	-	-	-
guaiacylacetone	0.026	-	-	-	-	-	0.021	-	-	-	-	-
coniferyl alcohol	0.019	-	-	-	-	-	0.021	-	-	-	-	-
Hydrocarbons	**0.038**	**0.049**	**0.090**	**0.386**	**0.899**	**0.718**	**0.020**	**0.044**	**0.065**	**0.314**	**0.648**	**0.830**
5-methylcyclopentadiene	-	-	0.005	0.045	0.017	-	-	-	0.005	0.040	0.022	-
benzene	0.005	0.010	0.035	0.124	0.322	0.275	0.002	0.013	0.028	0.099	0.275	0.335
toluene	0.014	0.017	0.023	0.037	0.097	0.049	0.006	0.013	0.015	0.047	0.061	0.041
ethylbenzene	-	-	-	0.008	0.009	-	-	-	-	0.009	0.009	-
p-xylene	-	-	-	0.008	0.014	-	-	-	-	0.009	0.009	-
o-xylene	-	-	0.004	0.005	0.007	0.004	-	-	0.003	0.005	0.005	0.004
phenylethyne	-	-	-	-	0.006	0.004	-	-	-	-	0.005	0.004
styrene	-	-	0.006	0.010	0.030	0.015	-	-	0.004	0.012	0.020	0.012
3-ethyltoluene	-	-	-	-	0.005	-	-	-	-	-	0.004	-
1,2,4-trimethylbenzene	-	-	-	0.003	0.003	-	-	-	-	0.003	0.003	-
2-methylstyrene	-	-	-	0.007	0.009	-	-	-	-	0.005	0.005	-
indene	-	-	-	0.023	0.046	0.015	-	-	-	0.015	0.021	0.015
3-methylindene	-	-	-	0.023	0.024	-	-	-	-	0.013	0.013	-
1-methyl-4-(1-propyn-1-yl)-benzene	-	-	-	0.007	-	-	-	-	-	0.004	-	-
naphthalene	-	-	-	-	0.088	0.061	-	-	-	-	0.049	0.056
2-methylnaphthalene	-	-	0.007	0.015	0.023	0.012	-	-	0.005	0.007	0.011	0.010
1-methylnaphthalene	-	-	-	0.015	0.018	0.008	-	-	-	0.009	0.010	0.008
1,3-dimethyl-naphthalene	-	-	-	-	-	0.006	-	-	-	-	-	0.005

1,8-dimethyl-naphthalene	-	-	-	-	-	-	-	-	-	-	-	0.006
biphenyl	-	-	-	-	-	0.027	-	-	-	-	-	0.029
1-ethyl-naphthalene	-	-	-	0.004	0.003	-	-	-	-	0.003	0.003	-
2,6-dimethyl-naphthalene	-	0.008	0.009	0.020	0.020	-	-	0.005	0.005	0.011	0.014	-
2-vinylnaphthalene	-	-	-	0.009	0.015	0.008	-	-	-	0.006	0.012	0.008
acenaphthylene	-	-	-	0.017	0.045	0.086	-	-	-	0.012	0.029	0.091
1-allylnaphthalene	-	-	-	-	0.004	-	-	-	-	-	0.004	-
2,3,5-trimethylnaphthalene	-	-	-	0.003	-	-	-	-	-	0.003	-	-
1H-phenalene	-	-	-	-	0.006	0.004	-	-	-	-	0.005	0.004
fluorene	-	-	-	-	0.041	0.010	-	-	-	-	0.027	0.052
1-methylfluorene	-	-	-	-	-	0.006	-	-	-	-	-	0.006
2-methylfluorene	-	-	-	-	-	0.004	-	-	-	-	-	0.004
9-methylidenefluorene	-	-	-	-	0.016	0.045	-	-	-	-	0.010	0.049
anthracene	-	-	-	-	0.007	0.020	-	-	-	-	0.005	0.024
1,9-dihydropyrene	-	-	-	-	-	0.002	-	-	-	-	-	0.003
2-methylanthracene	-	-	-	-	0.005	0.004	-	-	-	-	0.004	0.004
4-methylphenanthrene	-	-	-	-	0.016	0.011	-	-	-	-	0.011	0.010
fluoranthene	-	-	-	-	-	0.013	-	-	-	-	-	0.017
pyrene	-	-	-	-	-	0.027	-	-	-	-	-	0.031
calamenene	0.012	-	-	-	-	-	0.006	-	-	-	-	-
guaiazulene	-	0.014	-	-	-	-	-	0.013	-	-	-	-
(5α,9α,10ß)-kaur-15-ene	0.007	-	-	-	-	-	0.006	-	-	-	-	-
Aldehydes	**0.160**	**0.182**	**0.111**	**0.029**	**-**	**-**	**0.093**	**0.142**	**0.063**	**0.035**	**-**	**-**
glycolaldehyde	0.077	0.079	0.055	0.015	-	-	0.052	0.070	0.041	0.024	-	-
butanedial	0.084	0.103	0.057	-	-	-	0.041	0.071	0.022	-	-	-
cinnamaldehyde	-	-	-	0.014	-	-	-	-	-	0.011	-	-
Esters	**0.130**	**0.097**	**0.030**	**0.008**	**-**	**-**	**0.143**	**0.169**	**0.041**	**0.010**	**-**	**-**
isopropenyl acetate	-	-	-	0.008	-	-	-	-	-	0.010	-	-
allyl acetate	0.130	0.097	0.030	-	-	-	0.143	0.169	0.041	-	-	-
Alcohols	**0.108**	**0.115**	**0.116**	**0.012**	**0.012**	**-**	**0.106**	**0.159**	**0.099**	**0.011**	**0.011**	**-**

2-propen-1-ol	-	0.016	0.050	-	-	-	-	0.013	0.036	-	-	-
2-hydroxyethyl acetate	0.108	0.099	0.066	-	-	-	0.106	0.146	0.063	-	-	-
1H-indenol	-	-	-	0.012	0.012	-	-	-	-	0.011	0.011	-
Acids	**3.759**	**4.623**	**2.456**	**1.947**	**1.581**	**-**	**2.638**	**3.380**	**1.523**	**1.080**	**0.750**	**-**
formic acid	2.499	3.019	0.882	0.490	0.288	-	1.896	2.327	0.761	0.252	0.191	-
acetic acid	1.260	1.604	1.573	1.457	1.293	-	0.742	1.052	0.763	0.828	0.559	-
Sugars	**0.175**	**0.145**	**0.111**	**0.008**	**-**	**-**	**0.197**	**0.144**	**0.103**	**0.012**	**-**	**-**
DL-arabinose	0.019	-	-	-	-	-	0.024	-	-	-	-	-
levoglucosan	0.155	0.145	0.111	0.008	-	-	0.173	0.144	0.103	0.012	-	-
Total mass fractions (%-bio-oil)	**43.8**	**59.5**	**42.7**	**55.0**	**71.8**	**31.5**	**33.1**	**48.5**	**29.4**	**35.8**	**39.7**	**29.4**

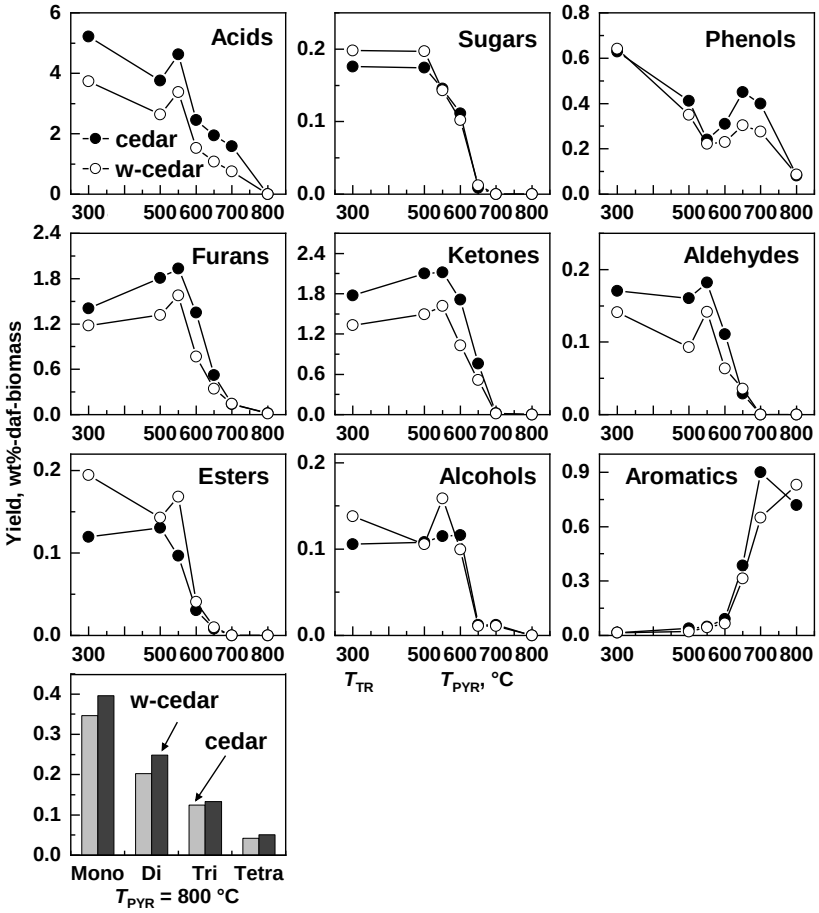

Figure 2-12 Composition of GC-detectable portion of bio-oil from pyrolytic reforming. Mono; mono-aromatics, Di; di-aromatics, Tri; tri-aromatics, Tetra; tetra-aromatics.

Sugars

The most important and common behavior was complete conversion at T_{PYR} = 700 or 800 °C into gas, or otherwise, aromatic hydrocarbons. The sugars yield remained unchanged at T_{PYR} = 300–500 °C, and then decreased at higher T_{PYR} reaching zero at 700 °C. The little change in the sugar yield at 300–500 °C was a result of the slight increase in the LGA yield and decrease in those of other more labile sugars. The total yield of acid-hydrolyzable sugars was measured by the same method as the bio-oil from the torrefaction. The results are shown in **Figure 2-13**. Glucose

represented LGA and its precursor (anhydrosugar oligomers), while the others are C5 or C6 anhydrosugar oligomers that were hydrolyzed to the corresponding mono-sugars. The anhydrosugar oligomers survived in the gas phase at $T_{PYR} < 600$ or 650 °C, but were decomposed completely at higher T_{PYR}. Here is considered the behaviors of LGA and its precursors both of that were hydrolyzed to glucose. **Figure 2-14** plots their yields against T_{PYR}. The slight decrease and increase in the precursor and LGA yields, respectively, at $T_{PYR} \leq 500$ °C supported the precursor to LGA conversion. Such conversion was not necessarily supported at higher T_{PYR} where their yields decreased at similar rates. A simple kinetic simulation showed that such a trend occurred only if the conversion of LGA was more rapid than that of the precursor, as shown in **Figure 2-15**. More rapid decomposition of monomer than oligomer was implausible, and it was therefore concluded that the anhydrosugar oligomers were, if any, hardly converted to LGA at $T_{PYR} > 500$ °C. It was rather believed that LGA was a source of CO and light hydrocarbon gases via intermediates such as aldehydes, ketones, and alcohols [44,46].

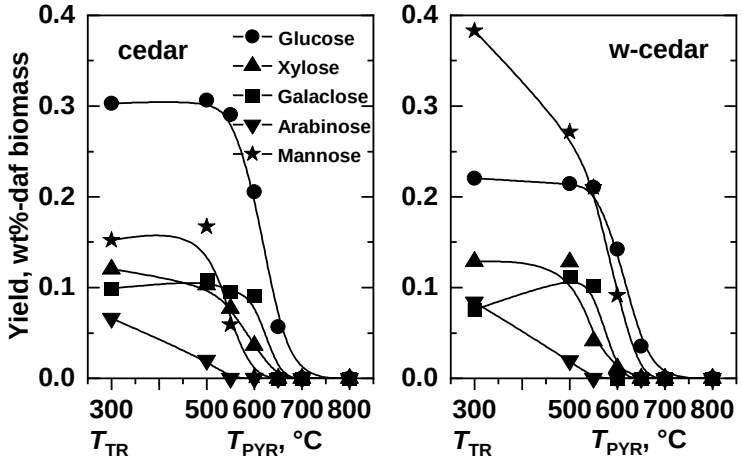

Figure 2-13 Yields of acid-hydrolyzable sugars in the bio-oil from the pyrolytic reforming.

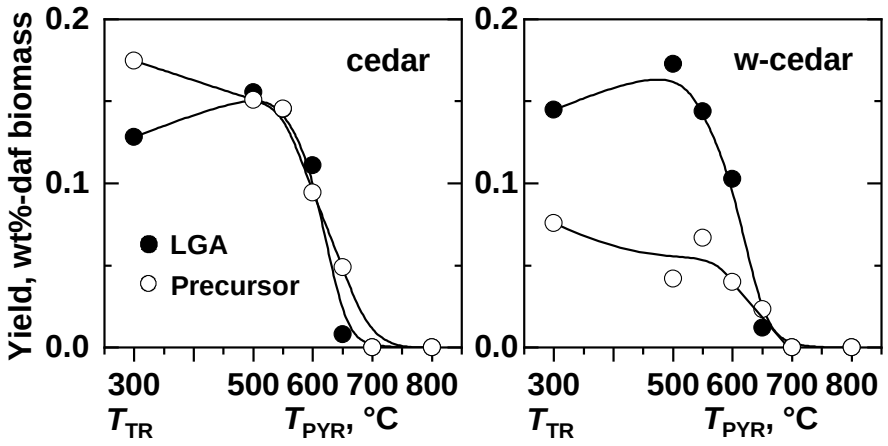

Figure 2-14 Effects of T_{PYR} on yields of LGA and its precursor (anhydrosugar oligomers).

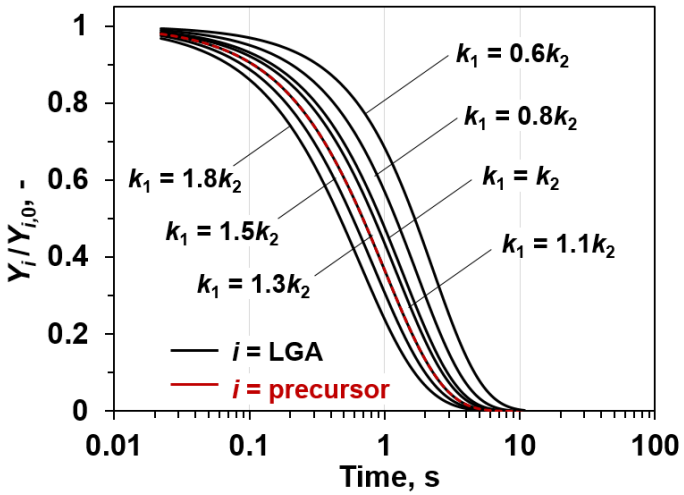

Figure 2-15 A kinetic simulation for the conversion of LGA and precursor. k_1: first-order rate constant for the conversion of LGA precursor to LGA. k_2: first-order rate constant for the conversion of LGA. k_1 was assumed to be 1 s^{-1}. $Y_{i,0}$: yield of i before conversion.

Furans and ketones

The furans yield increased at $T_{PYR} \leq 550$ °C, and decreased at higher T_{PYR}. It was believed that furans were formed from hemicellulose-derived anhydrosugar oligomers and also pyran ring derivatives [33,39], and decomposed into CO, formic acid, and other light gases [45,47]. The

yields of major compounds such as oxolan-2-ol, furfural, γ-butyrolactone, and 5-(hydroxymethyl)oxolan-2-one changed in manners very similar to that of the total furans. Some types of furans such as 2-furanmethanol, 3-furanmethanol, and 2(5H)-furanone decreased monotonously with T_{PYR} due to lower thermal stabilities. Ketones were as abundant as the furans, and this was partly attributed to the presence of their common precursors. The ketones yield increased at $T_{PYR} \leq 550$ °C, and decreased at higher T_{PYR} more quickly than the furans. Acetol and 2-hydroxycyclopent-2-en-1-one were the major compounds of this component. Decomposition of these major ketones and the others formed CO, H_2, and other light gases [43].

Acids

The acid component was the most abundant in the bio-oil vapor before the reforming. The common trend for its yield was the monotonous decrease with T_{PYR} except that at 550 °C. A slight increase in the yield at 550 °C was attributed to the decomposition of precursors such as anhydrosugars [36,40]. This component was represented by only two compounds, *i.e.*, acetic and formic acids. Acetic acid was relatively stable, and its yield slowly decreased at $T_{PYR} \leq 700$ °C, while decomposed into gases completely at 800 °C. According to a previous study [48], the first-order rate constant of gas phase decomposition of acetic acid was *ca.* 0.1 s^{-1} at 800 °C. This allowed to estimate the conversion for 1 s, which was as small as 10%. The measured conversion of acetic acid was much greater. This was probably due to the presence of active species such as radicals. Thus, the co-existence of more labile components enhanced the decomposition of acetic acid. The main fates of acetic acid were probably CO_2 and CH_4, but also CH_2CO (ethenone) and H_2O [42,48]. It was believed that formic acid mainly was converted mainly into CO and H_2O [45,47].

Phenols

The phenols yield changed with T_{PYR} in a complex manner, i.e., decreased at $T_{PYR} \leq 550$ °C, increased at 550–650 °C, and again decreased at ≥ 700 °C. The total yield was the highest without reforming, and this was primarily due to the decomposition of thermally labile guaiacols. For example, creosol (2-methoxy-4-methylphenol), homovanillic acid ((4-hydroxy-3-methoxyphenyl)-acetic acid), and trans-coniferyl alcohol (3-(4-hydroxy-3-methoxyphenyl)-2-propenal) were involved in the bio-oil at T_{TR} = 300 °C, but not at all after the reforming. On the other hand, phenol, cresols, xylenols, some other alkylated phenols, and naphthalenols were formed exclusively by the reforming. The net increase in their yields caused the above described increase in the total yield at 550–650 °C. It was believed that not only the guaiacols but also lignin oligomers, which were undetectable by the GC/MS, behaved as precursors of phenol and alkylated phenols [49]. Decomposition of phenol was important as a reaction to form CO, benzene and cyclopentadiene [50]. Cyclopentadiene is an important precursor of benzene, indene, naphthalene, and even more-condensed aromatics [51].

2.3.4 Estimation of heat required for pyrolytic reforming

Figure 2-16a shows the heat required for the pyrolytic reforming, Q_{PYR}, as a function of T_{PYR}. Q_{PYR} increased monotonously with T_{PYR} over the entire range. Q_{PYR} at 800 °C, where about 90% of the initial bio-oil was converted into gas, was 5.8% and 4.6% of HHV of the cedar and w-cedar, respectively. The slope drawn for the cedar was greater by a factor of 1.2 than that for the w-cedar. This was straightforwardly explained by that the bio-oil yield from the cedar at T_{TR} = 300 °C was about 1.2 times that from the w-cedar. **Figure 2-16b** plots Q_{PYR} against the degree of conversion of the bio-oil by the reforming, which was defined by the difference in the bio-oil yield between

the torrefaction at T_{TR} = 300 °C and reforming at T_{PYR}. Q_{PYR} was a non-linear function of the degree of conversion, but hardly influenced by the AAMEs removal. This non-linearity was reasonable because major types of reactions depended on the chemical composition of bio-oil that varied with the progress of reforming.

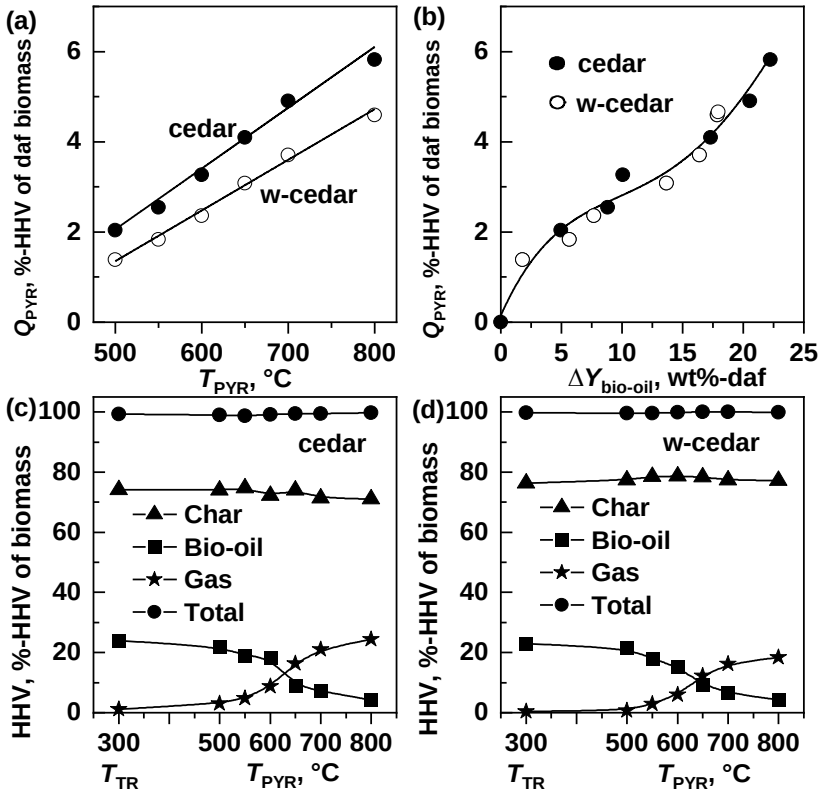

Figure 2-16 (a) Heat required for the pyrolytic reforming of bio-oil from the torrefaction at T_{TR} = 300 °C. (b) Q_{PYR} as a function of the degree of bio-oil conversion ($\Delta Y_{bio-oil}$). (c) and (d) HHVs of products from reforming of bio-oil from torrefaction at T_{TR} = 300 °C.

Figures 2-16c and d display the HHV of the char from the torrefaction at T_{TR} = 300 °C and combustible gas and bio-oil from the torrefaction and pyrolytic reforming as functions of T_{PYR}.

The calculation was performed after correcting their yields in the same way and with the same reason as that for the torrefaction. The properties of bio-oil used in calculating Q_{PYR} are shown in **Table 2-5.** The HHVs of the bio-oil and gas decreased and increased with T_{PYR}, as easily expected from their yields. It was noted that the total HHV of the products, *i.e.,* those of the char, bio-oil, and gas was equivalent to that of the feedstock. The combined torrefaction and *in-situ* pyrolytic reforming thus gave gross chemical energy recovery of around 100%.

Table 2-5 Properties of bio-oils and heat required for pyrolytic reforming.

	T_{PYR}, °C (cedar)						T_{PYR}, °C (w-cedar)					
	500	550	600	650	700	800	500	550	600	650	700	800
Properties of bio-oils												
H/C atomic ratio	1.55	1.69	1.81	1.53	1.71	1.31	1.48	1.51	1.42	1.39	1.27	0.97
O/C atomic ratio	0.63	0.59	0.56	0.55	0.26	0.24	0.60	0.56	0.58	0.45	0.35	0.37
standard enthalpy of formation $\Delta H_f°_{bio\text{-}oil}$, kJ/mol-C [a]	−119	−115	−112	−101	−54	−36	−108	−102	−103	−77	−55	−49
$R_{\Delta H,bio\text{-}oil}$ [b]	0.76	0.78	0.79	0.74	0.73	0.64	0.74	0.73	0.72	0.69	0.65	0.60
Heat required for pyrolytic reforming												
MJ/kg-daf-biomass	0.4	0.5	0.6	0.8	1.0	1.2	0.3	0.4	0.5	0.6	0.7	0.9
%-HHV-daf-biomass	2.0	2.5	3.3	4.1	4.9	5.8	1.4	1.8	2.4	3.1	3.7	4.6
Properties of bio-oils from GC/MS-detectable compounds												
H/C atomic ratio	1.65	1.70	1.67	1.56	1.31	0.89	1.64	1.67	1.66	1.51	1.22	0.88
O/C atomic ratio	0.80	0.85	0.68	0.58	0.40	0.02	0.81	0.83	0.69	0.52	0.31	0.01
standard enthalpy of formation $\Delta H_f°_{bio\text{-}oil}$, kJ/mol-C [a]	−160	−175	−132	−107	−64	12	−163	−169	−134	−93	−46	13
$R_{\Delta H,bio\text{-}oil}$ [b]	0.82	0.85	0.79	0.75	0.67	0.49	0.82	0.84	0.79	0.73	0.64	0.49

a) $\Delta H_f°_{char}$ and $\Delta H_f°_{bio\text{-}oil}$ were calculated according to Yang *et al*. b) $R_{\Delta H,bio\text{-}oil}$ is an essential parameter for calculating the enthalpy of bio-oil vapor as a function of temperature, and is a function of H/C and O/C ratios of the bio-oil.

2.4 Conclusions

This study has investigated the chemical and thermal characteristics of torrefaction and *in-situ* vapor-phase pyrolytic reforming of the volatiles, and demonstrated the followings within the ranges of experimental conditions.

(1) Q_{TR} and Q_{PYR} were within the ranges of 1.0–4.0%-HHV at T_{TR} = 250–350 °C and 1.4–5.8%-HHV at T_{PYR} = 500–800 °C, respectively. Q_{PYR} increased in semi-linear function of T_{PYR} while non-linearly with the bio-oil conversion into gas. The torrefaction of the w-cedar required more Q_{TR} than that of the cedar, which was attributed largely to the lower standard enthalpy of formation of the w-cedar. On the other hand, the torrefaction gave more bio-oil from the cedar than the w-cedar at T_{TR} = 300 °C, and therefore needed more Q_{PYR}.

(2) For both the torrefaction and pyrolytic reforming, the total chemical energies of the products were almost equivalent to that of the feedstock. This trend was arisen from weakly endothermic natures of the torrefaction and reforming. The chemical energies of char and bio-oil from torrefaction decreased and increased monotonously with T_{TR}, respectively, and became near equivalent to each other at T_{TR} = 350 °C. The reforming converted the chemical energy of bio-oil to that of combustible gases, which was represented by those of CO and CH_4, C_2H_4, and H_2. The lower calorific value of gas from the torrefaction, 5–7 MJ/Nm^3-dry, was greatly increased to 17–18 MJ/Nm^3-dry by the reforming at $T_{PYR} \geq$ 700–800 °C.

(3) The pyrolytic reforming converted at most 90 wt% of the bio-oil from the torrefaction at T_{PY} = 300 °C. into gas. The reforming at T_{PYR} = 700 or 800 °C converted acids, sugars, furans, ketones, aldehydes, esters, and alcohols completely, leaving phenols. Only the yield of aromatic hydrocarbons increased as T_{PYR} increased. The fraction of the GC-detectable lighter

components in the bio-oil did not increase by the reforming. In other words, selective removal of the heavier components was difficult only by the vapor-phase reforming.

2.5 References

[1] G.W. Huber, S. Iborra, A. Corma, Synthesis of transportation fuels from biomass: Chemistry, catalysts, and engineering, Chem. Rev. 106 (2006) 4044-4098.

[2] A. Corma, S. Iborra, A. Velty, Chemical routes for the transformation of biomass into chemicals, Chem. Rev. 107 (2007) 2411-2502.

[3] M.J.C. van der Stelt, H. Gerhauser, J.H.A. Kiel, K.J. Ptasinski, Biomass upgrading by torrefaction for the production of biofuels: A review, Biomass Bioenergy 35 (2011) 3748-3762.

[4] M.N. Cahyanti, T. Doddapaneni, T. Kikas, Biomass torrefaction: An overview on process parameters, economic and environmental aspects and recent advancements, Bioresour. Technol. 301 (2020) 122737.

[5] A. Zheng, Z. Zhao, S. Chang, Z. Huang, X. Wang, F. He, H. Li, Effect of torrefaction on structure and fast pyrolysis behavior of corncobs, Bioresour. Technol. 128 (2013) 370-377.

[6] S. Kudo, J. Okada, S. Ikeda, T. Yoshida, S. Asano, J.-i. Hayashi, Improvement of pelletability of woody biomass by torrefaction under pressurized steam, Energy Fuels 33 (2019) 11253-11262.

[7] S. Neupane, S. Adhikari, Z. Wang, A.J. Ragauskas, Y. Pu, Effect of torrefaction on biomass structure and hydrocarbon production from fast pyrolysis, Green Chem. 17 (2015) 2406-2417.

[8] S. Konsomboon, J.-M. Commandré, S. Fukuda, Torrefaction of various biomass feedstocks and its impact on the reduction of tar produced during pyrolysis, Energy Fuels 33 (2019) 3257-3266.

[9] S. Ren, H. Lei, L. Wang, Q. Bu, S. Chen, J. Wu, J. Julson, R. Ruan, The effects of torrefaction on compositions of bio-oil and syngas from biomass pyrolysis by microwave heating, Bioresour. Technol. 135 (2013) 659-664.

[10] R.J.M. Westerhof, D.W.F. Brilman, M. Garcia-Perez, Z. Wang, S.R.G. Oudenhoven, S.R.A. Kersten, Stepwise fast pyrolysis of pine wood, Energy Fuels 26 (2012) 7263-7273.

[11] S.-S. Liaw, Z. Wang, P. Ndegwa, C. Frear, S. Ha, C.-Z. Li, M. Garcia-Perez, Effect of pyrolysis temperature on the yield and properties of bio-oils obtained from the auger pyrolysis of Douglas Fir wood, J. Anal. Appl. Pyrolysis 93 (2012) 52-62.

[12] P. Nanou, M.C. Carbo, J.H.A. Kiel, Detailed mapping of the mass and energy balance of a continuous biomass torrefaction plant, Biomass Bioenergy 89 (2016) 67-77.

[13] L. Kumar, A.A. Koukoulas, S. Mani, J. Satyavolu, Integrating torrefaction in the wood pellet industry: A critical review, Energy Fuels 31 (2016) 37-54.

[14] S. Zhang, Y. Su, K. Ding, S. Zhu, H. Zhang, X. Liu, Y. Xiong, Effect of inorganic species on torrefaction process and product properties of rice husk, Bioresour. Technol. 265 (2018) 450-455.

[15] S. Chang, Z. Zhao, A. Zheng, F. He, Z. Huang, H. Li, Characterization of products from torrefaction of sprucewood and bagasse in an auger Reactor, Energy Fuels 26 (2012) 7009-7017.

[16] J. Huang, Y. Qiao, Z. Wang, H. Liu, B. Wang, Y. Yu, Valorization of food waste via torrefaction: Effect of food waste type on the characteristics of torrefaction products, Energy Fuels 34 (2020) 6041-6051.

[17] S. Zhang, Q. Dong, L. Zhang, Y. Xiong, Effects of water washing and torrefaction on the pyrolysis behavior and kinetics of rice husk through TGA and Py-GC/MS, Bioresour. Technol. 199 (2016) 352-361.

[18] S.-S. Liaw, C. Frear, W. Lei, S. Zhang, M. Garcia-Perez, Anaerobic digestion of C1–C4 light oxygenated organic compounds derived from the torrefaction of lignocellulosic materials, Fuel Process. Technol. 131 (2015) 150-158.

[19] T. Doddapaneni, R. Praveenkumar, H. Tolvanen, M.R.T. Palmroth, J. Konttinen, J. Rintala, Anaerobic batch conversion of pine wood torrefaction condensate, Bioresour. Technol. 225 (2017) 299-307.

[20] T.R.K.C. Doddapaneni, R. Jain, R. Praveenkumar, J. Rintala, H. Romar, J. Konttinen, Adsorption of furfural from torrefaction condensate using torrefied biomass, Chem. Eng. J. 334 (2018) 558-568.

[21] L. Santamaria, G. Lopez, E. Fernandez, M. Cortazar, A. Arregi, M. Olazar, J. Bilbao, Progress on catalyst development for the steam reforming of biomass and waste plastics pyrolysis volatiles: A review, Energy Fuels 35 (2021) 17051-17084.

[22] G. Guan, M. Kaewpanha, X. Hao, A. Abudula, Catalytic steam reforming of biomass tar: Prospects and challenges, Renewable Sustainable Energy Rev. 58 (2016) 450-461.

[23] S.B. Saleh, B.B. Hansen, P.A. Jensen, K. Dam-Johansen, Influence of biomass chemical properties on torrefaction characteristics, Energy Fuels 27 (2013) 7541-7548.

[24] L. Deng, T. Zhang, D. Che, Effect of water washing on fuel properties, pyrolysis and combustion characteristics, and ash fusibility of biomass, Fuel Process. Technol. 106 (2013) 712-720.

[25] T. Okuno, N. Sonoyama, J.-i. Hayashi, C.-Z. Li, C. Sathe, T. Chiba, Primary release of alkali and alkaline earth metallic species during the pyrolysis of pulverized biomass, Energy Fuels 19 (2005) 2164-2171.

[26] Karnowo, Z.F. Zahara, S. Kudo, K. Norinaga, J.-i. Hayashi, Leaching of alkali and alkaline earth metallic species from rice husk with bio-oil from its pyrolysis, Energy Fuels 28 (2014) 6459-6466.

[27] H. Yang, S. Kudo, H.-P. Kuo, K. Norinaga, A. Mori, O. Mašek, J.-i. Hayashi, Estimation of enthalpy of bio-oil vapor and heat required for pyrolysis of biomass, Energy Fuels 27 (2013) 2675-2686.

[28] S. Kudo, Y. Hachiyama, Y. Takashima, J. Tahara, S. Idesh, K. Norinaga, J.-i. Hayashi, Catalytic hydrothermal reforming of lignin in aqueous alkaline medium, Energy Fuels 28 (2013) 76-85.

[29] L. Shi, S. Yu, F.-C. Wang, J. Wang, Pyrolytic characteristics of rice straw and its constituents catalyzed by internal alkali and alkali earth metals, Fuel 96 (2012) 586-594.

[30] K. Zeng, X. He, H. Yang, X. Wang, H. Chen, The effect of combined pretreatments on the pyrolysis of corn stalk, Bioresour. Technol. 281 (2019) 309-317.

[31] D. Chen, A. Gao, K. Cen, J. Zhang, X. Cao, Z. Ma, Investigation of biomass torrefaction based on three major components: Hemicellulose, cellulose, and lignin, Energy Convers. Manage. 169 (2018) 228-237.

[32] D. Mourant, Z. Wang, M. He, X.S. Wang, M. Garcia-Perez, K. Ling, C.-Z. Li, Mallee wood fast pyrolysis: Effects of alkali and alkaline earth metallic species on the yield and composition of bio-oil, Fuel 90 (2011) 2915-2922.

[33] P.R. Patwardhan, R.C. Brown, B.H. Shanks, Product distribution from the fast pyrolysis of hemicellulose, ChemSusChem 4 (2011) 636-643.

[34] P.R. Patwardhan, D.L. Dalluge, B.H. Shanks, R.C. Brown, Distinguishing primary and secondary reactions of cellulose pyrolysis, Bioresour. Technol. 102 (2011) 5265-5269.

[35] Y. Le Brech, T. Ghislain, S. Leclerc, M. Bouroukba, L. Delmotte, N. Brosse, C. Snape, P. Chaimbault, A. Dufour, Effect of potassium on the mechanisms of biomass pyrolysis studied using complementary analytical techniques, ChemSusChem 9 (2016) 863-872.

[36] P.R. Patwardhan, J.A. Satrio, R.C. Brown, B.H. Shanks, Product distribution from fast pyrolysis of glucose-based carbohydrates, J. Anal. Appl. Pyrolysis 86 (2009) 323-330.

[37] S. Wang, B. Ru, H. Lin, Z. Luo, Degradation mechanism of monosaccharides and xylan under pyrolytic conditions with theoretic modeling on the energy profiles, Bioresour. Technol. 143 (2013) 378-383.

[38] Y.S. Choi, P.A. Johnston, R.C. Brown, B.H. Shanks, K.-H. Lee, Detailed characterization of red oak-derived pyrolysis oil: Integrated use of GC, HPLC, IC, GPC and Karl-Fischer, J. Anal. Appl. Pyrolysis 110 (2014) 147-154.

[39] X. Zhou, W. Li, R. Mabon, L.J. Broadbelt, A mechanistic model of fast pyrolysis of hemicellulose, Energy Environ. Sci. 11 (2018) 1240-1260.

[40] Y. Yu, Y.W. Chua, H. Wu, Characterization of pyrolytic sugars in bio-oil produced from biomass fast pyrolysis, Energy Fuels 30 (2016) 4145-4149.

[41] D.E. Daugaard, R.C. Brown, Enthalpy for pyrolysis for several types of biomass, Energy Fuels 17 (2003) 934-939.

[42] J.R. Galdámez, L. García, R. Bilbao, Hydrogen production by steam reforming of bio-oil using coprecipitated Ni−Al catalysts. Acetic acid as a model compound., Energy Fuels 19 (2005) 1133-1142.

[43] M.C. Ramos, A.I. Navascués, L. García, R. Bilbao, Hydrogen production by catalytic steam reforming of acetol, a model compound of bio-oil, Ind. Eng. Chem. Res. 46 (2007) 2399-2406.

[44] S. Guo, H. Liang, D. Che, H. Liu, B. Sun, Quantitative study of the pyrolysis of levoglucosan to generate small molecular gases, RSC Adv. 9 (2019) 18791-18802.

[45] F. Valentini, V. Kozell, C. Petrucci, A. Marrocchi, Y. Gu, D. Gelman, L. Vaccaro, Formic acid, a biomass-derived source of energy and hydrogen for biomass upgrading, Energy Environ. Sci. 12 (2019) 2646-2664.

[46] A. Fukutome, H. Kawamoto, S. Saka, Processes forming gas, tar, and coke in cellulose gasification from gas-phase reactions of levoglucosan as Intermediate, ChemSusChem 8 (2015) 2240-2249.

[47] N. Akiya, P.E. Savage, Role of water in formic acid decomposition, AIChE J. 44 (1998) 405-415.

[48] C. Cavallotti, M. Pelucchi, A. Frassoldati, Analysis of acetic acid gas phase reactivity: Rate constant estimation and kinetic simulations, Proc. Combust. Inst. 37 (2019) 539-546.

[49] P.R. Patwardhan, R.C. Brown, B.H. Shanks, Understanding the fast pyrolysis of lignin, ChemSusChem 4 (2011) 1629-1636.

[50] K.B. A. B. Lovell, I. Glassman, The gas phase pyrolysis of phenol, Int. J. Chem. Kinet. 21 (1989) 547-560.

[51] M.L. J.A. Mulholl, D.H. Kim, Pyrolytic growth of polycyclic aromatic hydrocarbons by cyclopentadienyl moieties, Proc. Combust. Inst. 28 (2000) 2593-2599.

Chapter 3 Staged Pyrolytic Conversion of Acid-Loaded Woody Biomass for Production of High-Strength Coke and Valorization of Volatiles

3.1 Introduction

A shortage of fossil fuels and increasing environmental pollution associated with their excessive use have stimulated the global search for alternative and sustainable sources of energy, chemicals, and materials [1,2]. Lignocellulosic biomass, as a readily available neutral carbon source, is considered to be one of the most promising alternatives to fossil fuels [3,4]. Pyrolysis is a technology used to thermochemically convert lignocellulosic biomass into some products. Depending on the target product, pyrolysis is often referred to by different names: torrefaction, fast pyrolysis, and carbonization for upgraded solid fuel, bio-oil, and carbon material production, respectively. These pyrolysis-based pathways involve thermal depolymerization of cellulose, hemicellulose and lignin with the product being liquid (bio-oil) rich in light oxygenates, anhydrosugars and phenols as well as char and non-condensable gas. The tuning of reaction conditions, such as temperature and heating rate, enables controlling the product distribution of char, bio-oil, and gas, but the natural advantage of the different chemical structures of cellulose, hemicellulose, and lignin as feedstock for corresponding chemicals is generally lost during the pyrolysis unless special techniques, such as catalysis, are employed.

Likewise, biomass is an attractive resource for the iron and steel-making industry since it is one of the most energy-intensive industries [5]. Coal-derived coke used in blast furnaces for

reducing iron ore generates 1.6 to 3.1 tons of CO_2 per ton of crude steel production, resulting in the generation of 7% of global anthropogenic CO_2 emissions [6,7]. Biomass-derived char had been used for ancient iron smelting as a reductant [8]. The coke used in modern iron-making is required to have significant mechanical strength to provide space for the generated gas to travel to the top of the blast furnaces. Because biomass char is generally fragile, the majority of research has used it as an additive in coal blends [9-11]. The partial replacement of coal by biomass directly contributes to the reduction of CO_2 emissions, but the contribution is limited because its addition at high ratios significantly decreases the fluidity of coal [10]. The present authors have studied coke production from low-rank coals through a sequence of hot pelletization and carbonization [12-14]. Pelletization at around 100–200 °C induced thermomechanical plasticization and macromolecular relaxation, resulting in the formation of highly dense coal pellets. Coalescence of the coal particles, accompanied by volumetric shrinkage, during the carbonization produced a high-strength coke. The coke had a higher strength than conventional coke prepared from caking coals, although the strength was affected by several factors. The application of this technology to biomass successfully resulted in the preparation of strong cokes from bamboo, larch, and mallee [15]. It was notable that hydrothermal pretreatment greatly enhanced the strength, indicating a crucial role of physicochemical structure and composition of biomass components. This suggested that torrefaction, a low-temperature pyrolysis process (200–350 °C) for upgrading biomass, may also regulate and generate the optimal properties as a pretreatment.

A drawback of biomass as a coke feedstock is its low yield due to its high content of volatiles. Like conventional coke production, the valorization of volatiles generated during carbonization without negatively affecting the properties of coke is vital from an economic viewpoint. Anhydrosugars, including levoglucosan (LGA) and levoglucosenone (LGO), are valuable

chemical platforms potentially available from cellulose pyrolysis [16-19]. Furans from hemicellulose and phenols from lignin are also potential chemicals [20-22]. However, the pyrolysis liquid product is generally a multi-component mixture of organics, and it is difficult to enrich it with certain compounds. This is due to the inherent alkali and alkaline metallic species (AAEMs) in biomass, which tend to promote homolytic fission of pyranose and furanose rings during pyrolysis, significantly enhancing the formation of unwanted light oxygenates [23,24]. Moreover, pelletization can cause a decrease in yields of desired volatile products because primary volatiles are prone to decomposition or repolymerization over pyrolyzing biomass or char through their chemical interactions, which is physically promoted by pelletization [25]. While, noticeable pyrolysis of three components occurs at difference temperature ranges, although there is overlapping [26,27]. Therefore, it may be feasible to hypothesize that some of the hemicellulose and cellulose must be converted into desired products during pyrolysis at torrefaction-level temperatures before pelletization with a suitable pretreatment in order to separately pyrolyze those components.

Recent studies have demonstrated that mineral acids, such as H_2SO_4, loaded over biomass not only effectively passivate AEEMs but also act as acidic catalysts to decrease the onset temperature of biomass components and enhance the production of the target chemicals [28-31]. With pretreatment by the acids, pure hemicellulose and cellulose are almost completely decomposed at 320 °C and 390 °C, respectively [20,21]. With the employment of acid loading in the above-mentioned low-temperature pyrolysis pretreatment, we herein propose a way to achieve the co-production of valuable platform chemicals and high-strength metallurgical coke from biomass (**Figure 3-1**). The process involves two-step pyrolysis at torrefaction and carbonization temperatures. In the first step, the torrefaction of acid-loaded biomass particles enables the release

of desired anhydrosugars from a portion of hemicellulose and cellulose while maintaining or even optimizing the properties of the remaining components. After water-washing, the residual solid is pelletized and then carbonized to produce the coke. Because the solid is rich in lignin, the pellet carbonization is also expected to selectively produce phenols. The objective of this multistage design strategy is to maximize carbon conversion into directional products. In this work, the performance of the proposed process is investigated with a particular focus on the product yield and quality through a comparison of unloaded, H_2SO_4-loaded, and H_3PO_4-loaded woody biomass as the feedstock.

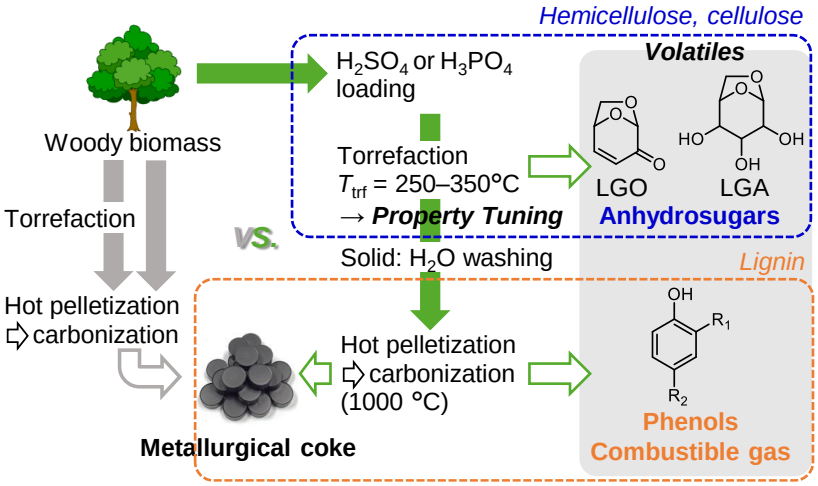

Figure 3-1 A schematic description of staged conversion of woody biomass to valuable chemicals and metallurgical coke.

3.2. Experimental section

3.2.1 Feedstock biomass and acid loading

Japanese cedar (CD) wood chips were collected at Oita prefecture, Japan. CD is the most forested wood and, therefore, is considered to be a major feedstock for biomass industry in Japan.

The chips were crushed and sieved to sizes ranging from 2.0 to 4.0 mm and then dried at 105 °C for 12 h before the experiments were conducted. H_2SO_4 or H_3PO_4 was loaded over CD at different ratios. 5 g of CD was added to 20 mL of deionized water containing the prescribed mass of acid, and the mixture was sonicated for 2 h at room temperature to ensure uniform mixing. The slurry was dried at 70 °C in an oven for 48 h and further at 105 °C to obtain the acid-loaded CD [28]. No apparent mass loss was observed during the pretreatment process. The thus-prepared H_2SO_4-loaded and H_3PO_4-loaded CDs are, hereafter, denoted by *y*-SA and *y*-PA, respectively, where *y* represents the content of loaded acid (0.5, 0.7, 1.0, 2.0, and 5.0 wt% on a CD mass basis).

3.2.2 Torrefaction

The first step of pyrolysis, torrefaction, of raw and acid-loaded CD was carried out in a tubular reactor shown in **Figure 3-2**. The reactor was heated to the torrefaction temperature (T_{trf}) of 250, 280, 300, 320, 350, or 500 °C in advance under N_2 (purity >99.9999 vol.%). 1.0 g of sample wrapped in a stainless-steel wire mesh (mesh size: 106 μm) was quickly inserted into the reactor and left at the desired temperature for 40 min. The volatiles' residence time in the hot zone was controlled at 1 s by adjusting the flow rate of N_2. The torrefaction volatiles entered a series of condensers consisting of an aerosol filter and −70 °C cold traps. The condensed volatiles were recovered as the liquid product and dissolved by acetone for the composition analysis. The non-condensable gas product was collected in a downstream gas bag. The yields of liquid and solid products were determined from their mass. The solid produced from CD and acid-loaded CD at different T_{trf} are denoted by CD-T_{trf}, *y*-SA-T_{trf}, and *y*-PA-T_{trf}, respectively.

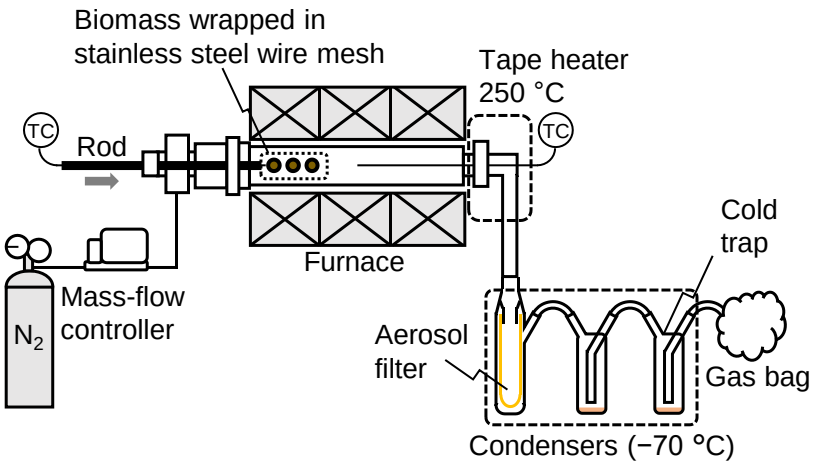

Figure 3-2 Schematic of apparatus for torrefaction experiment.

3.2.3 Hot pelletization and carbonization

The solid products from acid-loaded samples were washed with deionized water to remove excess acid and as many AAEMs as possible until the pH of filtrate was neutral. After drying, the solid was pulverized to sizes below 106 μm with a crusher (Osaka Chemical, WB-1) and used for the pelletization. 1.0 g of the solid sample was placed in a cylindrical mold with φ14 mm, heated to 200 ºC and left unpressed for 30 min, and then pelletized at a compressive force of 128 MPa for 8 min. After pressure release and cooling, the pellet was heated to 1000 ºC at 5 ºC/min with a holding time of 10 min under 300 mL/min N_2 in a quartz tube for carbonization. The carbonization reactor was also equipped with condensers for the recovery of liquid products and a gasbag. Before and after the carbonization, the dimensions and mass of the sample were measured. The mechanical strength of produced coke was measured on a tester (Shimadzu, EZ-L), for which details have been given in our previous works [12,13,15]. The strength is represented by tensile strength (*TS*) so as to avoid the influence of the sample dimensions. More than 4 samples were prepared and analyzed for each experimental condition, and the average is presented as the result.

3.2.4 Product analysis

The concentrations of components in non-condensable gas were quantified with an Agilent 490 Micro gas Chromatograph (GC). The chemical compounds in liquid products were identified by gas chromatography-mass spectrometry (GC-MS) on a PerkinElmer Clarus SQ 8, equipped with a GL Sciences TC-1701 column, according to reported methods [16]. The concentration of most compounds was determined by the analysis with a gas chromatogram-flame ionization detector (GC-FID: Shimadzu, GC-2030) operated with the column and conditions that were identical to those used in GC-MS analysis. The analysis used 39 types of standard chemicals or chemicals having similar structures and functionalities for the quantification. Separately, the concentration of organic acids, LGA, and LGO was analyzed by high-performance liquid chromatography on a Shimadzu Prominence series system equipped with a photodiode array and refractive index detectors. A BioRad Aminex 87H column with a guard column was used for the compound separation. The column compartment was maintained at 35 °C. 5 mmol/L of H_2SO_4 aqueous solution was used as the mobile phase. The analysis of LGA was carried out using double Shodex sugar SP0810 columns (80 °C) with water as a mobile phase and liquid product diluted with water after the removal of acetone by a rotary evaporator. The presented yields of components in liquid products were all based on the dry mass of CD.

The solid-state ^{13}C dipolar decoupling magic angle spinning nuclear magnetic resonance (^{13}C NMR) spectra were obtained with a JEOL ECA 400 spectrometer. The spectral deconvolution was performed to interpret fractions of carbon moieties with a Peakfit software employing the multiplicative Gaussian/Lorentzian function [12,32], where the carbon chemical shift referred to the method reported by Brech *et al.* [33]. Fracture surfaces of cokes were polished and observed by a Keyence VE-9800 scanning electron microscope (SEM). The components in CD and

pyrolyzed CDs were analyzed by the two-step acid hydrolysis method [34]. The hydrolysis residue is presented as acid-insoluble solid (AIS-Solid) because of the difficulty in distinguishing acid-insoluble lignin from char-like solid for the torrefied samples. The contents of C, H, and O in solid samples were analyzed with a PerkinElmer 2400 Series II CHN elemental analyzer. **Table 3-1** shows the elemental composition of selected samples. The contents of other elements including S and P were analyzed with the sample after ashing on a Malvern Panalytical Epsilon 1.

Table 3-1 Elemental composition of CD, CD-T_{trf}, 0.7-SA-T_{trf}, and 1.0-PA-T_{trf}.

	Composition (wt%-d.a.f.)			
	C	H	N	O[a]
Raw CD	49.3	6.1	0.49	44.1
CD-250	53.1	6.1	0.28	40.5
CD-280	55.4	5.7	0.32	38.6
CD-300	60.9	5.3	0.37	33.4
CD-320	70.7	4.9	0.40	24.0
CD-350	71.9	4.2	0.45	23.5
0.7-SA-250	54.1	5.8	0.10	40.0
0.7-SA-280	56.4	5.7	0.13	37.7
0.7-SA-300	59.6	5.4	0.15	34.8
0.7-SA-320	67.4	4.8	0.19	27.6
0.7-SA-350	73.0	4.4	0.18	22.4
1.0-PA-250	52.1	6.0	0.09	41.8
1.0-PA-280	55.0	5.8	0.10	39.1
1.0-PA-300	59.9	5.4	0.10	34.6
1.0-PA-320	68.2	4.8	0.15	26.8
1.0-PA-350	71.4	4.4	0.17	24.0

[a] Calculated by 100 – C, H, and N contents.

Thermogravimetric analysis (TGA) of CD and acid-loaded CDs were performed in a Hitachi High-Tech Science STA 7200. 5 mg of the sample was heated to 900 °C at 10 °C/min under N_2 of 100 mL/min. The mass decrease curve was presented by $1 - X$ (X: mass-based conversion) and transformed to the DTG (= dX/dt) profile. The CO_2 gasification reactivity of coke was also

analyzed by TGA. The coke samples fractured during the strength measurement (about 5 mg) was heated to 900 °C under a flow of 700 mL/min N_2. After confirming the stable mass, the gas was switched to 50 % CO_2/N_2 (700 mL/min) to initiate the gasification [35]. The conversion ($1 - X$) is presented on a dry and ash free basis (d.a.f.).

3.3 Results and discussion

3.3.1. Torrefaction

Figure 3-3 presents typical GC-MS chromatograms of liquid products from torrefaction of CD and the acid-loaded samples at 320 °C (see **Table 3-2** for the detailed composition and yields). The results show the remarkable influence of acid loading. When CD was torrefied without acid, the liquid product was dominated by light oxygenates such as acids, ketones, and furans. The yields of anhydrosugars, which could be formed from the depolymerization of cellulose and hemicellulose, were negligible despite the temperature being sufficient for inducing their pyrolysis. This was because of the strong ring fragmentation side reactions catalyzed by AAEMs [29,36]. Comparatively, adding either H_2SO_4 or H_3PO_4, as expected, reduced the catalytic effects of AAEMs through forming inactive metal salts, thus skewing towards the directional depolymerization of cellulose and hemicellulose into more anhydrosugars, LGA, its dehydrated product LGO, and small amounts of 1,4:3,6-dianhydro-α-D-glucopyranose, and 1,6-anhydro-α-D-galactofuranose.

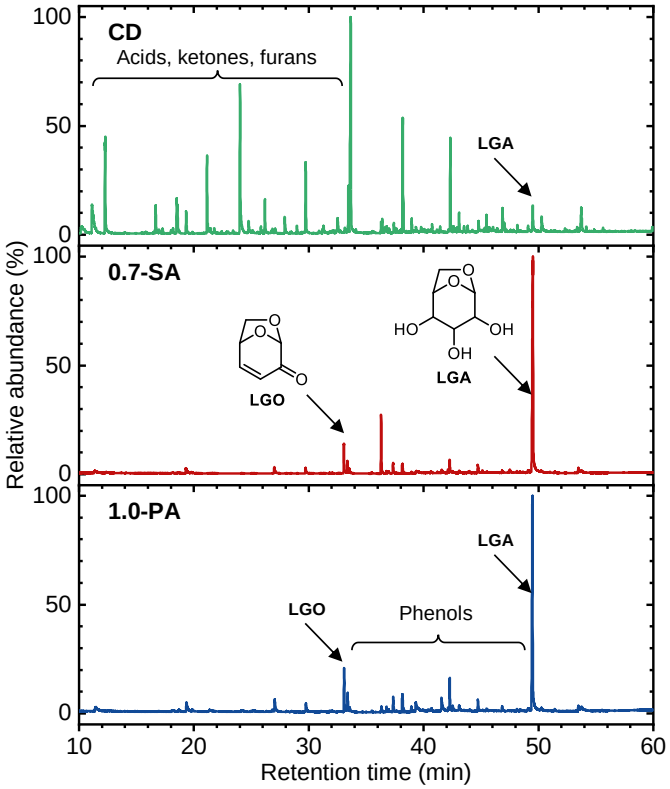

Figure 3-3 GC/MS chromatograms of liquid products from torrefaction of selected samples at 320 °C.

The influence of the amount of acid loaded on the composition and the yield of liquid product from the torrefaction at 320 °C is shown in **Figure 3-4**. With an increase in the amount of acid loading, the yields of total anhydrosugars increased and then decreased. The highest LGA yields of 9.5 and 6.9 wt% were obtained from 0.7-SA and 1.0-PA, respectively. Considering the significantly lower tendency for hemicellulose to release C6 anhydrosugars [24,37], cellulose is thought to be the main source of LGA. Taking the content in CD (37.7 wt%) into account, the cellulose-based LGA yields were calculated to be 25.3 and 18.2 wt%, respectively. LGA yields from cellulose greatly depend on the reaction conditions including feedstock, and the reported yields vary from a few percent to over 70% [18]. The high yields are generally observed in the

analytical flash pyrolysis of pure cellulose. In our previous work [16] using a drop tube reactor for fast pyrolysis of microcrystalline cellulose, the yield of LGA was 22.6%. Therefore, the yields obtained in the present work are reasonable and strongly support the fact that AAEM passivation effectively inhibits the occurrence of catalyzed ring-opening reactions. The catalytic passivation also mitigates the formation of inter- or intra-molecules cross-linking, causing the preferential breakage of glycosidic bonds to enhance the yield of anhydrosugars [28,38]. The excess acids enhanced dehydration of cellulose and LGA to promote the formation of char and LGO at the expense of undesirably lowering the total anhydrosugars yield. H_3PO_4 was more prone to this chemical event than H_2SO_4 probably due to its slower catalysis [39] and the ability to penetrate cellulose fibrils [31]. As a result, H_2SO_4 showed a better ability to selectively produce anhydrosugars, LGA in particular, than H_3PO_4.

Table 3-2 Yields of components in liquid products from torrefaction at 320 °C.

		y-SA					*y*-PA			
Yield (wt%-CD)	Raw CD	0.5-SA	0.7-SA	1.0-SA	2.0-SA	5.0-SA	0.7-PA	1.0-PA	2.0-PA	5.0-PA
Furans	**2.044**	**2.574**	**2.526**	**2.008**	**1.657**	**1.725**	**2.399**	**2.604**	**1.842**	**1.527**
furan	0.008	0.015	0.020	0.035	0.046	0.072	0.008	0.014	0.034	0.043
2-methylfuran	0.020	0.022	0.023	0.030	0.029	0.056	0.021	0.023	0.036	0.051
furfural	0.135	0.361	0.438	0.602	0.722	1.123	0.257	0.404	0.494	0.663
2-furanmethanol	0.706	0.575	0.147	0.032	0.023	0.039	0.889	0.241	0.024	0.027
2-acetylfuran	0.028	-	-	0.016	0.022	0.027	-	-	0.021	0.025
5-methyl furfural	0.038	0.074	0.074	0.073	0.067	0.074	0.051	0.069	0.078	0.101
2(5H)-furanone	0.394	0.128	0.058	0.039	0.036	0.037	0.232	0.076	0.045	0.042
methyl furan-3-carboxylate	-	0.056	0.063	0.068	0.066	0.061	-	0.057	0.112	0.110
5-hydroxymethylfurfural	0.071	1.343	1.703	1.113	0.646	0.236	0.941	1.720	0.998	0.465
other furans	0.644	-	-	-	-	-	-	-	-	-
Ketones	**2.497**	**0.912**	**0.393**	**0.269**	**0.205**	**0.077**	**1.401**	**0.416**	**0.108**	**0.101**
acetol	1.626	0.527	0.209	0.157	0.102	-	0.726	0.211	-	-
2-methyl-2-cyclopenten-1-one	0.017	0.009	0.005	-	-	-	0.015	0.007	0.006	0.010
4-cyclopentene-1,3-dione	0.010	0.044	0.022	0.021	0.026	0.024	0.054	0.020	0.018	0.024
2-hydroxycyclopent-2-en-1-one	0.595	0.269	0.107	0.056	0.044	0.034	0.525	0.133	0.047	0.035
3-methylcyclopentane-1,2-dione	0.068	0.063	0.050	0.035	0.033	0.019	0.081	0.045	0.037	0.032
other ketones	0.181	-	-	-	-	-	-	-	-	-
Phenols	**0.872**	**2.384**	**1.989**	**1.645**	**1.371**	**0.982**	**2.637**	**1.594**	**1.738**	**1.500**
phenol	0.041	0.010	0.011	0.011	0.011	0.011	0.018	0.009	0.013	0.015
guaiacol	0.198	0.323	0.322	0.255	0.189	0.127	0.315	0.220	0.180	0.143
p-cresol	0.008	0.095	-	0.006	-	-	0.171	0.030	0.023	0.020
2-methoxy-4-methylphenol	-	0.330	0.271	0.214	0.201	0.145	0.295	0.182	0.200	0.131
4-ethylguaiacol	0.028	0.039	0.034	0.026	0.026	-	0.039	0.026	0.019	0.018
4-vinylguaiacol	0.111	0.369	0.268	0.166	0.104	0.052	0.404	0.227	0.208	0.116
eugenol	-	0.084	0.061	0.047	0.039	0.031	0.094	0.059	0.053	0.042
isoeugenol	0.113	0.395	0.250	0.131	0.070	0.034	0.463	0.289	0.190	0.075
vanillin	0.035	0.099	0.097	0.091	0.093	0.079	0.104	0.092	0.093	0.081
dihydroeugenol	0.045	0.146	0.228	0.337	0.376	0.322	0.119	0.127	0.371	0.541

acetovanillone	0.038	0.043	0.051	0.051	0.042	0.031	0.063	0.052	0.046	0.032
guaiacylacetone	0.046	0.069	0.067	0.076	0.082	0.088	0.078	0.063	0.109	0.135
coniferyl alcohol	0.025	0.056	0.061	0.059	0.046	0.036	0.052	0.037	0.046	0.039
vanillyl ethyl ether	-	0.083	0.074	0.070	0.051	0.026	0.097	0.061	0.082	0.059
4-Hydroxy-2-methoxycinnamaldehyde	-	0.243	0.194	0.105	0.041	-	0.325	0.120	0.105	0.053
other phenols	0.184	-	-	-	-	-	-	-	-	-
Acids	**5.636**	**3.082**	**1.205**	**0.761**	**0.827**	**1.068**	**4.825**	**1.454**	**0.470**	**0.713**
formic acid	4.120	2.791	0.965	0.482	0.464	0.569	4.421	1.098	0.160	0.232
acetic acid	1.516	0.291	0.240	0.279	0.363	0.499	0.404	0.356	0.310	0.481
Sugars	**0.560**	**7.494**	**12.094**	**12.246**	**9.618**	**6.202**	**4.625**	**10.333**	**9.494**	**7.565**
2,3-anhydro-d-mannosan	0.019	0.016	0.052	0.049	0.041	0.018	0.014	0.025	0.033	0.017
3,4-anhydro-d-galactosan	-	0.053	0.072	0.070	0.065	0.027	0.040	0.053	0.069	0.039
1,4:3,6-dianhydro-α-d-glucopyranose	0.058	0.099	0.218	0.424	0.505	0.456	0.088	0.136	0.356	0.401
levoglucosenone	-	1.859	2.098	2.738	3.268	4.041	1.884	3.203	3.452	5.524
levoglucosan	0.454	5.410	9.533	8.802	5.646	1.635	2.576	6.857	5.496	1.558
1,6-anhydro-α-d-galactofuranose	-	0.057	0.121	0.163	0.093	0.025	0.023	0.059	0.088	0.026
DL-arabinose	0.029	-	-	-	-	-	-	-	-	-
Others	0.716	0.254	0.161	0.265	0.270	0.351	0.187	0.166	0.214	0.340

The yields of all category components (acids, furans, ketones, and phenols) except anhydrosugars decreased with an increase in the amount of acid loaded. As shown in **Figure 3-4**, the non-condensable gas was dominated by CO and CO_2, and their yields also decreased with the acid loading amount, followed by slight increases at high loadings. These results were closely related to AAEM passivation and the resulting enhancement or weakening of a series of reactions caused by higher acid loading, such as secondary dehydration, polymerization/oligomerization, decarboxylation/decarbonylation, and ring cleavage reactions [40,41]. The solid product yield also declined by the acid loading (from 0 to 0.5 wt%) and then rose sharply. The first decrease of solid product yield demonstrates that the acid-loading inactivates AAEMs having the ability to promote the formation of cross-linking. The acid worked not only for the AAEM passivation but also for the promotion of dehydration and cross-linking at the high loadings.

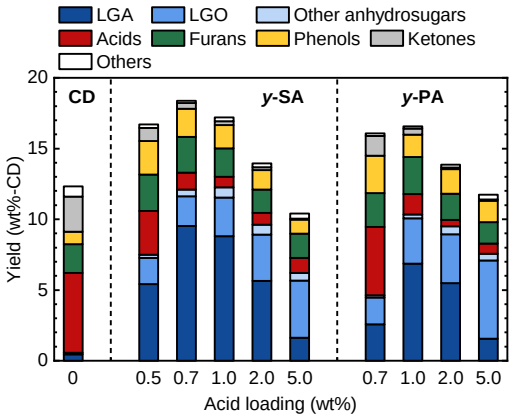

Figure 3-4 Influence of acid loading amount on composition and yield of liquid product from torrefaction at 320 °C.

Table 3-3 Yields of components in liquid products from torrefaction of 0.7-SA and 1.0-PA at different temperatures.

	0.7-SA: T_{trf} (°C) =						1.0-PA: T_{trf} (°C) =					
Yield (wt%-CD)	250	280	300	320	350	500	250	280	300	320	350	500
Furans	**0.185**	**0.607**	**1.399**	**2.526**	**2.602**	**2.325**	**0.152**	**0.674**	**1.503**	**2.604**	**2.532**	**1.936**
furan	0.002	0.011	0.012	0.020	0.035	0.051	-	-	0.005	0.014	0.017	0.028
2-methylfuran	0.007	0.002	0.009	0.023	0.047	0.067	-	0.001	0.009	0.023	0.037	0.048
furfural	0.082	0.121	0.287	0.438	0.483	0.551	0.054	0.128	0.276	0.404	0.362	0.372
2-furanmethanol	-	0.020	0.052	0.147	0.137	0.066	0.004	0.062	0.147	0.241	0.272	0.120
5-methyl furfural	-	0.040	0.040	0.074	0.092	0.122	-	0.022	0.043	0.069	0.081	0.098
2(5H)-furanone	-	0.020	0.032	0.058	0.069	0.083	-	0.031	0.047	0.076	0.095	0.106
methyl furan-3-carboxylate	-	0.025	0.046	0.063	0.060	0.108	-	0.022	0.034	0.057	0.055	0.035
5-hydroxymethylfurfural	0.094	0.368	0.921	1.703	1.679	1.277	0.094	0.408	0.942	1.720	1.613	1.129
Ketones	**-**	**0.023**	**0.146**	**0.393**	**0.527**	**0.957**	**-**	**0.118**	**0.212**	**0.416**	**0.566**	**0.945**
acetol	-	-	0.085	0.209	0.281	0.618	-	0.083	0.127	0.211	0.276	0.540
2-methyl-2-cyclopenten-1-one	-	-	-	0.005	0.009	0.031	-	-	-	0.007	0.015	0.045
4-cyclopentene-1,3-dione	-	-	-	0.022	0.030	0.027	-	-	-	0.020	0.029	0.039
2-hydroxycyclopent-2-en-1-one	-	0.015	0.043	0.107	0.128	0.161	-	0.026	0.063	0.133	0.167	0.199
3-methylcyclopentane-1,2-dione	-	0.008	0.018	0.050	0.079	0.120	-	0.009	0.022	0.045	0.079	0.122
Phenols	**0.303**	**0.886**	**1.404**	**1.989**	**2.638**	**2.362**	**0.209**	**0.675**	**1.135**	**1.594**	**2.145**	**1.924**
phenol	0.002	0.002	0.006	0.011	0.023	0.079	0.002	0.002	0.004	0.010	0.014	0.062
guaiacol	0.017	0.064	0.162	0.322	0.480	0.387	0.010	0.039	0.101	0.220	0.319	0.332
p-cresol	-	-	-	-	0.024	0.036	-	0.006	0.017	0.030	0.038	0.040
2-methoxy-4-methylphenol		0.052	0.126	0.271	0.534	0.517	0.007	0.035	0.090	0.182	0.395	0.087
4-ethylguaiacol	-	-	0.013	0.034	0.063	0.100	-	0.012	0.015	0.026	0.049	0.090
4-vinylguaiacol	0.026	0.092	0.173	0.268	0.369	0.344	0.018	0.073	0.147	0.227	0.331	0.342
eugenol	-	0.029	0.047	0.061	0.071	0.027	0.009	0.029	0.048	0.059	0.075	0.029
isoeugenol	0.036	0.125	0.202	0.250	0.271	0.222	0.026	0.133	0.229	0.289	0.338	0.317
vanillin	0.031	0.055	0.075	0.097	0.114	0.121	0.032	0.059	0.076	0.092	0.098	0.127
dihydroeugenol	0.034	0.106	0.179	0.228	0.240	0.197	0.015	0.048	0.089	0.127	0.130	0.122
acetovanillone	0.032	0.044	0.048	0.051	0.050	0.037	0.011	0.026	0.041	0.052	0.062	0.081
guaiacylacetone	0.017	0.030	0.049	0.067	0.077	0.069	0.011	0.027	0.045	0.063	0.077	0.079
coniferyl alcohol	0.012	0.031	0.048	0.061	0.065	0.059	0.009	0.020	0.029	0.037	0.042	0.053

vanillyl ethyl ether	0.023	0.056	0.064	0.074	0.080	0.061	-	0.033	0.053	0.060	0.065	0.061
4-hydroxy-2-methoxycinnamaldehyde	0.073	0.200	0.212	0.194	0.177	0.106	0.059	0.133	0.153	0.120	0.112	0.102
Acids	**0.108**	**0.370**	**0.690**	**1.205**	**1.335**	**1.475**	**-**	**0.721**	**1.266**	**1.876**	**1.958**	**2.077**
formic acid	-	0.250	0.503	0.965	1.039	0.938	-	0.441	0.866	1.206	1.237	1.149
acetic acid	0.108	0.120	0.187	0.240	0.296	0.537	-	0.280	0.400	0.670	0.721	0.928
Sugars	**0.716**	**3.719**	**8.232**	**12.094**	**11.522**	**9.839**	**0.368**	**1.523**	**4.256**	**10.333**	**8.633**	**6.871**
2,3-anhydro-d-mannosan	-	0.005	0.022	0.052	0.062	0.041	0.006	0.008	0.011	0.025	0.041	0.038
3,4-anhydro-d-galactosan	-	0.019	0.044	0.072	0.083	0.065	0.007	0.014	0.027	0.053	0.060	0.050
1,4:3,6-dianhydro-α-d-glucopyranose	0.027	0.094	0.170	0.218	0.236	0.194	0.004	0.033	0.072	0.136	0.150	0.126
levoglucosenone	0.194	0.998	1.683	2.098	1.883	1.692	0.201	0.867	1.652	3.203	2.394	1.513
levoglucosan	0.495	2.558	6.215	9.533	9.148	7.755	0.150	0.601	2.467	6.857	5.937	5.100
1,6-anhydro-α-d-galactofuranose	-	0.045	0.098	0.121	0.110	0.092	-	-	0.027	0.059	0.051	0.044
Others	0.009	0.077	0.118	0.161	0.299	0.378	0.021	0.059	0.097	0.166	0.205	0.383

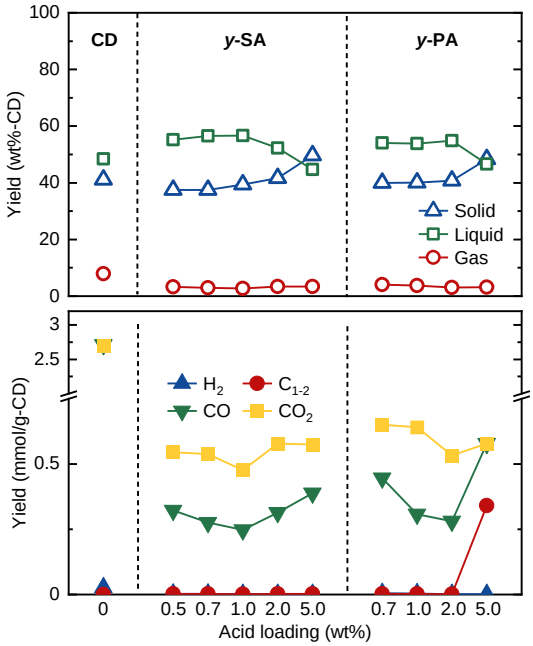

Figure 3-5 Influence of acid loading amount on product distribution and yields of non-condensable gas from torrefaction at 320 °C.

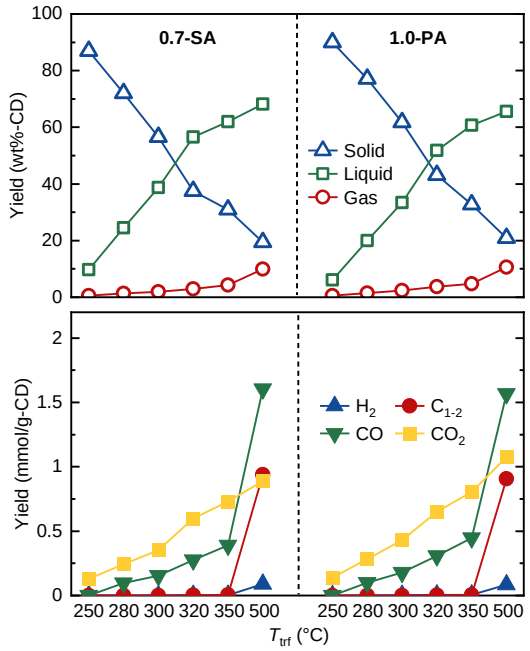

Figure 3-6 Influence of T_{trf} on product distribution and yields of non-condensable gas from 0.7-SA and 1.0-PA.

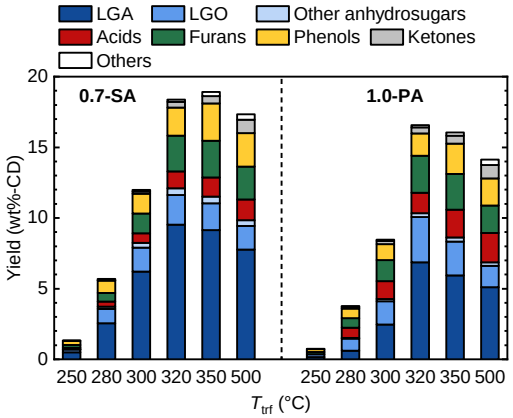

Figure 3-7 Influence of T_{trf} on composition and yield of liquid product from 0.7-SA and 1.0-PA.

The best acid loadings of 0.7-SA and 1.0-PA for producing anhydrosugars corresponded to 0.071 mmol-H_2SO_4/g-CD and 0.102 mmol-H_3PO_4/g-CD, respectively. Those amounts were less than the total content of inherent AAEMs in CD (K 0.048 mmol/g-CD and Ca 0.072 mmol/g-CD, calculated from **Table 3-4,** while they seemed to be sufficient for deactivating them. To further evaluate the feasibility of optimizing the anhydrosugars yield, the effects of temperature on the distribution of torrefaction products were investigated for 0.7-SA and 1.0-PA (**Figures 3-6 and 3-7**). Increasing temperatures led to the increase in non-condensable gas, especially CO and CO_2, and liquid product yields, accompanied by a decrease in solid product yield as a result of the enhanced decomposition. An interesting observation was that the decrease in solid yield was remarkable in the narrow range of 250–350 °C, compared to 350–500 °C, indicating the completion of cellulose and hemicellulose pyrolysis below 350 °C. The most noteworthy was that the yields of LGA and total anhydrosugars showed the maximum at 320–350 °C. The LGA yields of 9.5 wt% and 6.9 wt% from 0.7-SA and 1.0-PA, respectively, at 320 °C were higher than those at 500 °C. This trend well suggested that temperatures of 320–350 °C were sufficient for the acids to work as AAEM passivators and to show catalysis toward glycosidic cleavage. Moreover, high

temperatures like 500 °C caused the decomposition of LGA in the gas phase, even within a short time. Indeed, a degradation of more than 10% of gaseous LGA to smaller molecules at 500 °C in 1.2 s was reported by Fukutome et al. [42]. The result, in other words, suggests that this anhydrosugar production step does not need high temperatures that can cause excess alternation of the lignocellulose structure. The significant change in lignocellulosic structure is unfavorable for the preparation of strong coke in the subsequent step.

Table 3-4 Ash content and composition in selected samples.

	Coke from						
	Raw CD	Raw CD	CD-280	0.7-SA-320	0.7-SA-350	1.0-PA-280	1.0-PA-320
Ash content (wt%-sample)							
	0.92	2.40	2.51	2.84	3.30	3.38	3.94
Ash composition (wt%)							
SiO_2	16.4	17.6	17.1	10.5	7.1	6.7	10.3
P_2O_5	0.0	0.0	0.0	0.0	0.0	37.7	36.0
SO_3	4.0	3.7	3.8	16.2	27.3	0.0	0.4
K_2O	24.9	20.3	20.5	36.3	37.1	26.9	24.4
CaO	43.9	48.5	50.4	24.0	24.1	22.6	17.8
Fe_2O_3	8.9	8.0	6.7	11.1	3.6	5.0	9.4
Others	1.6	1.8	1.5	1.8	0.9	1.1	1.7
Content (mmol/g-sample)							
SiO_2	0.025	0.070	0.072	0.050	0.039	0.038	0.067
P_2O_5	0.000	0.000	0.000	0.000	0.000	0.090	0.100
SO_3	0.005	0.011	0.012	0.057	0.112	0.000	0.002
K_2O	0.024	0.052	0.055	0.109	0.130	0.096	0.102
CaO	0.072	0.207	0.226	0.121	0.142	0.136	0.125
Fe_2O_3	0.005	0.012	0.011	0.020	0.007	0.011	0.023
Content (wt%-sample)							
Si	0.07	0.20	0.20	0.14	0.11	0.11	0.19
P	0.00	0.00	0.00	0.00	0.00	0.55	0.62
S	0.01	0.04	0.04	0.18	0.36	0.00	0.01
K	0.19	0.40	0.43	0.85	1.01	0.75	0.80
Ca	0.29	0.83	0.91	0.49	0.57	0.55	0.50
Fe	0.06	0.13	0.12	0.22	0.08	0.12	0.26
Removal during conversion to coke (%)							
S				84.4	67.7		

P					47.6	49.4
K						
Ca	36.2	39.2	12.9	–[a]	–[a]	–[a]
Fe	13.4	15.2	67.4	59.7	43.7	55.2
	30.0	44.5	25.7	70.5	38.4	–[a]

[a] Calculated to be negative values (in the rage between –8.5% and –12.8%) probably because of analytical accuracy, indicating small changes in its presence during the conversion.

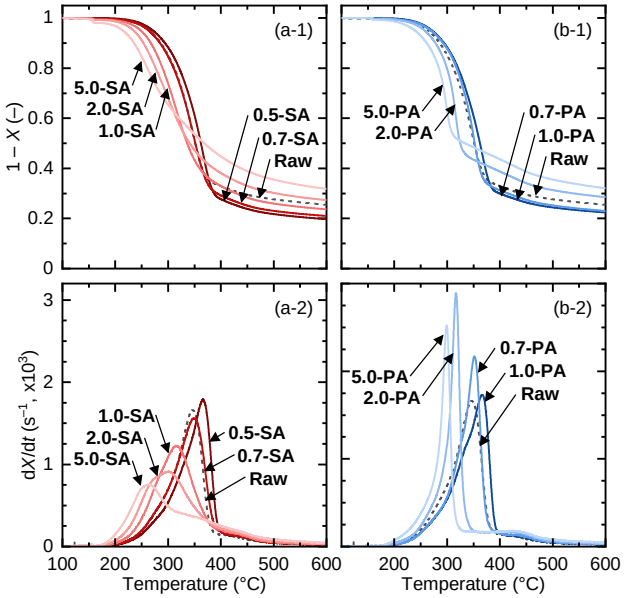

Figure 3-8 TGA of CD, *y*-SA, and *y*-PA.

TGA further intuitively revealed the influence of acid on CD pyrolysis, as depicted in **Figure 3-8**. The pyrolysis curves were almost unchanged by the acid loadings below 0.5–0.7 wt% and 0.7–1.0 wt% for H_2SO_4 and H_3PO_4, respectively, with the peak temperatures similar to or rather higher than that of CD in d*X*/dt profiles. In these acid loading ranges, the catalysis of acids was not apparent from TGA, while the result indicated that acid loadings brought out the inherent cellulose nature for releasing LGA by suppressing the catalysis of AAEMs. Above these critical-loading amounts, the acids worked for catalyzing depolymerization and dehydration, lowering the onset pyrolysis temperature and enhancing char yield. The sharper peaks in d*X*/dt profiles of *y*-PA,

compared to those of *y*-SA, may support deeper penetration of H_3PO_4 into cellulose fibrils, although its benefit was not found in anhydrosugars yield. It should be noted that completion of a noticeable decrease in the mass of TGA required a temperature of around 400 °C. This temperature was, however, not important in the above torrefaction experiment because it involved 40 min of holding time at T_{trf}.

3.3.2. Coke strength

Based on the above findings, 0.7-SA-T_{trf} and 1.0-PA-T_{trf} were chosen as feedstock for coke preparation. The torrefied CDs were washed by water, pulverized, pelletized at 200 °C, and then carbonized at 1000 °C. Characteristics of coke, the *TS* in particular, were analyzed and compared. The analysis of volatile products from carbonization of the pellet is presented in the next section.

The *TS* of coke prepared by their pelletization and carbonization is shown and compared to that from CD-T_{trf} in **Figure 3-9**. The coke prepared from raw CD without torrefaction showed a *TS* of 9.0 MPa. This strength is higher than that generally found in conventional coke from caking coal (2–6 MPa) [43].However, a higher strength is strongly preferred for this type of coke derived from low-rank carbon resources, such as lignite and biomass, because they are rich in micropores, as shown in **Table 3-5** for the present samples. The pores can be enlarged by gasification during the use in blast furnaces and cause a quicker deterioration in strength. Therefore, the initial strength should be as high as possible [12]. **Figure 3-9** showed that the strength could be increased by staged conversion, even without acid loading. The torrefaction at 300 °C, interpolated before the pelletization, doubled the strength of coke, being 18.4 MPa. This was unexpected because it has been generally known that torrefaction of feedstock reduces the strength of the biomass pellet [44-46]. In our study [46], the pellet strength from a hardwood was reduced from 4.6 MPa to 1.3 MPa

by the feedstock torrefaction at 250 °C. The reason was explained by the thermal degradation of lignin working as a binder or the formation of hemicellulose-derived char during torrefaction. This trend was also confirmed in this study when analyzing the strength of the pellet before carbonization (**Figure 3-10**), although a small increase was observed for CD-250 and -280. This implied that the enhancement of coke strength occurred mainly during the carbonization.

Table 3-5 Specific surface area (S_{CO2}) and pore volume (V_{CO2}), analyzed with CO_2 ad/desorption at 273K, of selected coke samples.

	Coke from							
	Raw CD	CD-280	CD-350	0.7-SA-250	0.7-SA-320	0.7-SA-350	1.0-PA-320	1.0-PA-350
S_{CO2} (m^2/g)	682	674	700	715	718	738	719	731
V_{CO2} (cm^3/g)	0.181	0.178	0.184	0.186	0.190	0.197	0.188	0.193

* CO_2 ad/desorption isotherms obtained at 273 K was analyzed by non-localized density functional theory. The analysis gave S_{CO2} and V_{CO2} within the range of pore width of 0.35–1.5 nm.

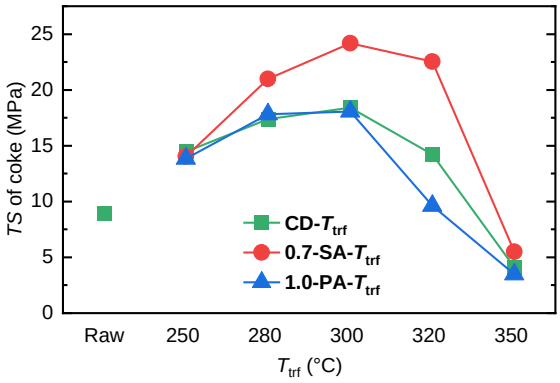

Figure 3-9 *TS* of coke prepared from 0.7-SA-T_{trf}, 1.0-PA-T_{trf}, and CD- T_{trf}.

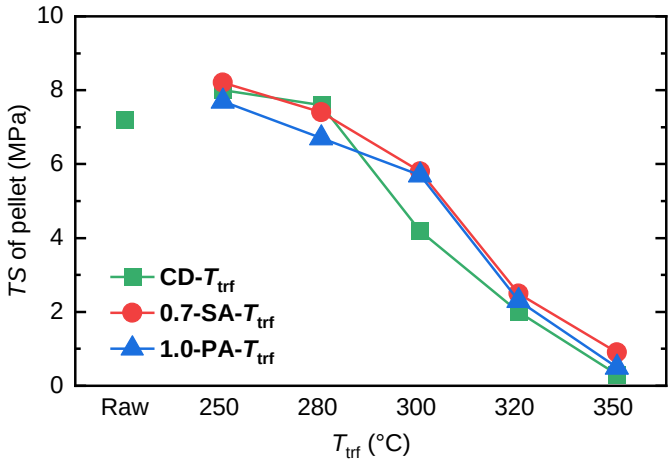

Figure 3-10 *TS* of pellet prepared from CD-T_{trf}, 0.7-SA-T_{trf}, and 1.0-PA-T_{trf} (before carbonization).

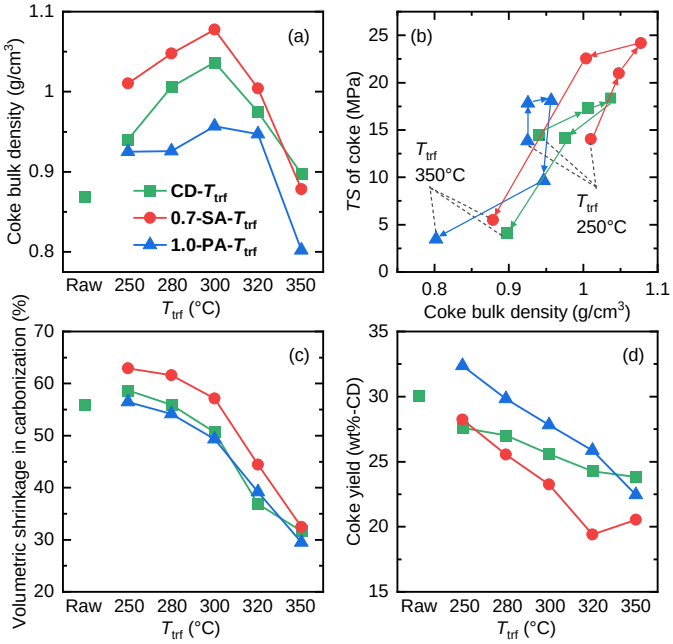

Figure 3-11 Characterization of carbonization and resulting coke from CD-T_{trf}, 0.7-SA-T_{trf}, and 1.0-PA-T_{trf}.

The reaction and its products were analyzed in more detail to better understand the mechanisms behind the development of strength. As shown in **Figure 3-11 a and b**, the *TS* of coke was closely related to its bulk density. This was accounted for by the fact that cracks and pores in formed coke could be the origin of fractures under mechanical pressure [12]. The microscopic observation of the fracture surface of coke with SEM (**Figure 3-12**) broadly supported this relationship, where the weaker cokes showed large pores (CD) or coarse surfaces (CD-350), compared to CD-300. The large pores were derived from vessels inherent in CD. The torrefaction could alter the physical properties of biomass, which caused the deformation and closing of void spaces in vessels during hot pelletization and further enhancement of coalescence between particles during carbonization, resulting in the improved bulk density and strength of coke. The excess T_{trf} produced more char-like repolymerization product in the solid that could not be densified during pelletization and carbonization. In fact, the volumetric shrinkage of pellet during carbonization decreased with T_{trf} and showed a large drop from 300 °C to 320 °C (**Figure 3-11c**). The component analysis also showed that CD-320 and -350 °C were dominated by AIS-Solid (**Table 3-6**). In **Figure 3-11d**, CD-T_{trf} showed lower coke yields than raw CD. This was inevitable as a result of the torrefaction of CD in the state of small particles with fast heating rate for effectively releasing the volatiles. More details for the influence of torrefaction on the coke from acid-unloaded CD will be available soon from our different work [47].

Table 3-6 Chemical composition of CD, CD-T_{trf}, 0.7-SA-T_{trf}, and 1.0-PA-T_{trf}.

	Composition (wt%-d.a.f.)			
	Cellulose	Hemicellulose	AS-Lig[a]	AIS-Solid[b]
Raw CD	37.7	14.0	38.1[c]	
CD-250	34.6	15.7	2.8	39.5

CD-280	31.4	8.0	2.9	50.7
CD-300	25.0	4.2	2.5	68.8
CD-320	6.1	2.8	1.1	91.0
CD-350	0.6	-	0.2	100.2
0.7-SA-250	35.5	12.8	3.4	39.4
0.7-SA-280	32.3	7.8	2.8	48.8
0.7-SA-300	26.4	4.2	2.4	60.7
0.7-SA-320	4.4	2.7	0.6	94.0
0.7-SA-350	1.3	-	0.1	100.1
1.0-PA-250	33.3	14.3	2.6	42.4
1.0-PA-280	32.0	7.5	2.8	49.6
1.0-PA-300	22.0	4.0	2.3	67.3
1.0-PA-320	3.1	2.6	0.4	93.1
1.0-PA-350	1.3	-	0.2	100.4

[a] Acid-soluble lignin. [b] Acid-insoluble solid including lignin and char-like material. [c] Total of acid-insoluble and -soluble lignin.

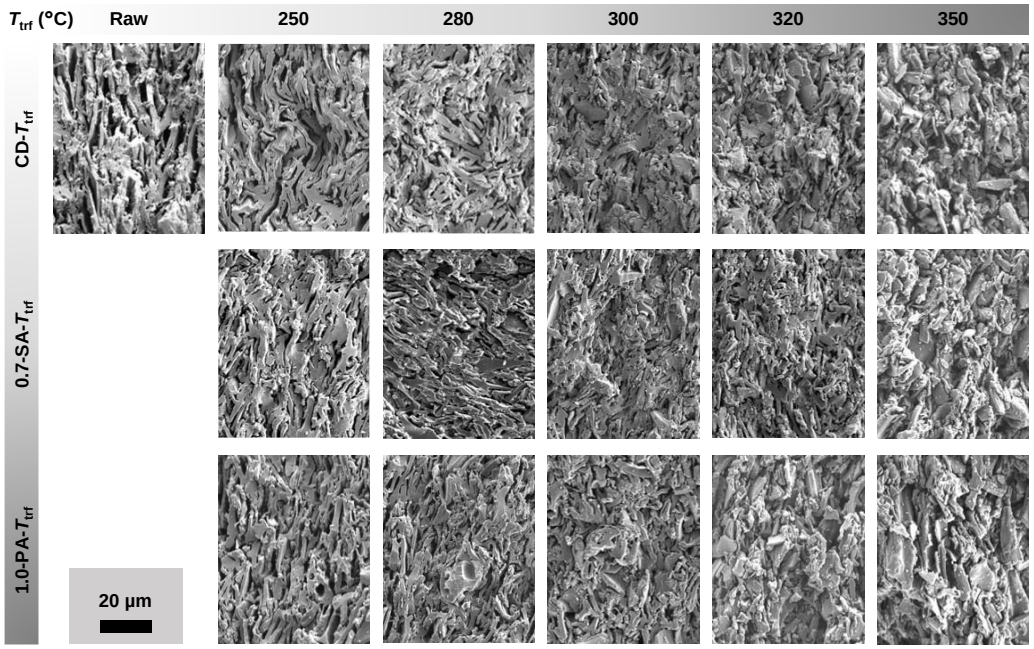

Figure 3-12 SEM images of fracture surface of coke prepared from CD-T_{trf}, 0.7-SA-T_{trf}, and 1.0-PA-T_{trf}.

In comparison with the raw CD and CD-T_{trf}, of notable significance in **Figure 3-11** was that the *TS* of cokes from acid-loaded CDs, 0.7-SA-T_{trf} and 1.0-PA-T_{trf}, similarly showed an increase

and decrease with T_{trf}. The result supports the above explanation of this trend for CD-T_{trf} because the presence of pores and char-like substrate in feedstock critically affects coke strength regardless of acid loading. More importantly, the cokes from 0.7-SA-T_{trf} rather had a higher strength than those from CD-T_{trf}. The strength reached 24.2 MPa and 22.5 MPa with 0.7-SA-300 and -320, respectively. The T_{trf} of 320 °C agrees with the temperature maximizing anhydrosugars yields during the torrefaction. The loading of H_2SO_4, thus, contributed to an improvement of not only anhydrosugars production but also coke strength.

Table 3-7 Carbon fraction of moieties, analyzed with ^{13}C solid-state NRM, in raw CD and solid products from torrefaction at 300 °C.

Component (%-C)	Raw	CD-300	0.7-SA-300	1.0-PA-300
Carbohydrate carbons				
C_1	11.0	9.2	10.0	9.8
C_2, C_3, C_5	22.3	14.1	14.6	12.8
C_4	6.8	3.15	4.3	3.7
C_6	15.5	7.3	8.4	7.2
Lignin carbons (methoxyl, aromatic carbons linked to oxygen)				
Methoxyl	10.6	9.2	9.8	10.1
G_4/G_3, S_3/S_5 nonetherified	3.0	8.9	8.4	9.2
S_3/S_5 etherified	2.6	3.3	3.1	3.2
Other carbons				
Aliphatic	10.2	12.2	10.3	11.2
Aromatic	15.9	30.7	27.8	30.9
Carbonyl, acetate	2.0	1.9	3.4	1.9

Assignment was performed according to a method reported by Le Brech et al. (*Carbon* **2016**, 108, 165-177) as follows: carbohydrates C_1 (105, 104−96); carbohydrates C_2, C_3, C_5 (74); carbohydrates C_4 (88.5, 84); carbohydrates C_6 (64); methoxyl groups (56.2); lignin G_4/G_3, S_3/S_5 nonetherified (150−144); lignin S_3/S_5 etherified (154−152); aliphatics (10-50); aromatics (141−120, 116−110, 108−106); carbonyls, acetates (>154).

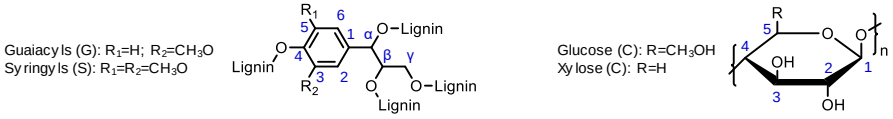

Such an enhancement of coke strength should be attributed to the fact that a proper amount of H_2SO_4 inhibited the catalysis of AAEMs toward the pyrolysis of carbohydrates including cellulose. The coke substrate is derived mainly from lignin, having the lowest volatiles content of the three components. This, in turn, means that carbohydrates contribute to the volumetric shrinkage of pellets during carbonization. ^{13}C Solid-state NMR analysis of 0.7-SA-300 (**Figure 3-13**) revealed the richness in carbohydrates, compared to that in CD-300 and 1.0-PA-300. The component analysis (**Table 3-6**) also showed the highest cellulose content in 0.7-SA-T_{trf}, although the differences were not noticeable. TGA of the solid products from the torrefaction confirmed the lowest char yields from 0.7-SA-T_{trf} at all the T_{trf} (**Figure 3-14**). As a result of the relative richness in cellulose, 0.7-SA-T_{trf} were shrunk and densified at the highest degree during the carbonization (**Figure 3-11** (c)) to be converted to the strongest coke. The other potential factors causing the enhancement of coke strength with H_2SO_4 loading were the alteration of lignin properties, such as thermoplasticity, during the torrefaction and lower char-like solid content in the solid product. The former is unlikely to be the main factor because the influence of AAEMs at their content in CD and the present temperature range of T_{trf} on lignin pyrolysis is insignificant [48,49]. The low char-like solid content in 0.7-SA-T_{trf} was related to the richness in carbohydrates and, indeed, demonstrated by the carbon distribution in **Figure 3-13**, where it showed lower f_a content, compared to CD-300 and 1.0-PA-300. The discussed mechanisms of strength development in 0.7-SA-T_{trf} indicated the importance of the amount of H_2SO_4 loaded. As expected, *TS* of coke from *y*-SA-300 decreased significantly from 24.2 MPa (0.7 wt%) to 11.4–12.4 MPa by the increase in loading to 2.0 and 5.0 wt% (**Figure 3-15**). As such, an appropriate H_2SO_4 loading amount and T_{trf} during torrefaction regulated the composition of CD so it could be converted to a strong coke.

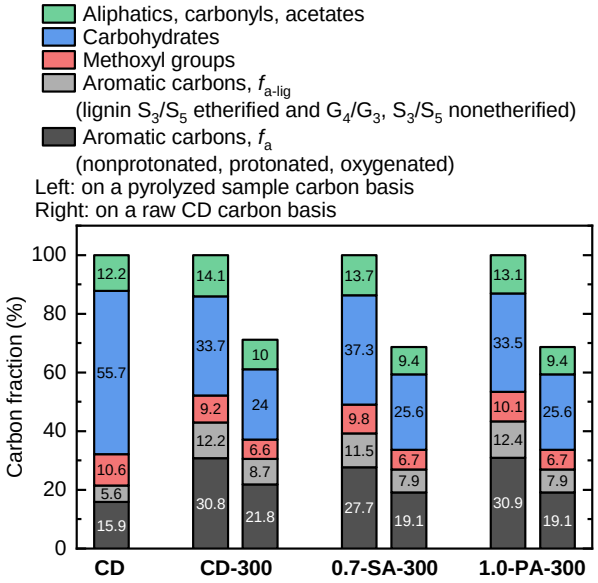

Figure 3-13 Carbon fraction of moieties in raw CD and the solid products from the torrefaction at 300 °C.

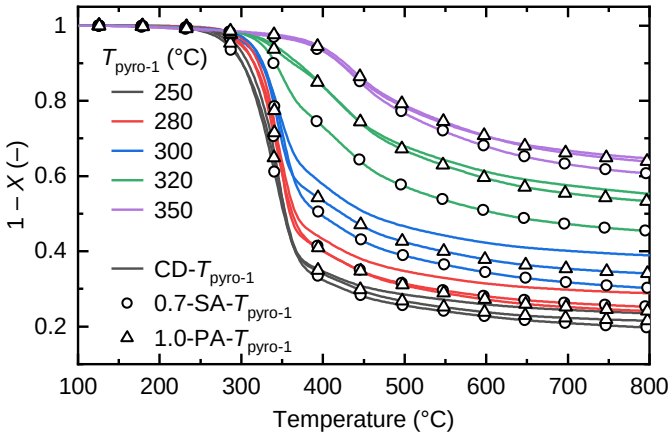

Figure 3-14 TGA of CD-T_{trf}, 0.7-SA-T_{trf}, and 1.0-PA-T_{trf} under N_2.

In contrast, the loading of H_3PO_4 did not improve or even slightly decreased the *TS* of coke despite its ability to promote the release of anhydrosugars during torrefaction, like H_2SO_4. The result could be explained by the better penetration of H_3PO_4 into cellulose to cause harder dehydration and charring. As shown in **Figure 3-13**, the contents of carbohydrates and aromatic

carbons in 1.0-PA-300 were almost the same as those in CD-300, regardless of the activity of H_3PO_4 toward AAEM passivation. Alternatively, the catalysis of H_3PO_4 resulted in an important advantage: the highest coke yields were obtained from 1.0-PA-T_{trf} (**Figure 3-11** (d)). The loading of H_3PO_4 was, thus, effective for addressing the problem of lignocellulose as the coke feedstock. Also considering that the *TS* of cokes from 1.0-PA-T_{trf} of $T_{trf} \leq 300$ °C was much higher than that from raw CD, H_3PO_4 was likely an option for the additive.

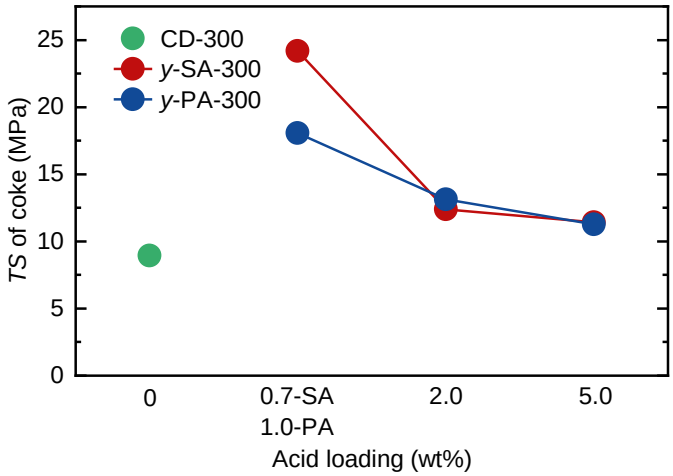

Figure 3-15 *TS* of coke prepared from CD-300, *y*-SA-300, and *y*-PA-300.

3.4 Distribution of products from pellet carbonization

Figure 3-16 shows the yields of products from carbonization of 0.7-SA-T_{trf} and 1.0-PA-T_{trf} on a CD-mass basis. All yields of solid, liquid, and gas products decreased with T_{trf}. Different from torrefaction, the product distribution was hardly affected by acid loading and its type, except for the solid (coke) yield from 1.0-PA-T_{trf} (**Table 3-8**). Meanwhile, the yield of gas was distinct, ranging from 6.1 to 18.4%. It was composed mainly of combustible molecules, H_2, CO, and C_{1-2} hydrocarbons with H_2 as a major component. For example, the gas composition from 0.7-SA-320

was $H_2/CO/CO_2/C_{1-2}$ = 50.4/26.1/12.6/10.9 mol%. Hence, the gas is also a valuable product of carbonization.

Table 3-8 Product yields during pellet carbonization on a torrefied sample mass basis.

	Yield (wt%-sample)			Yield (mmol/g-sample)			
	Solid (coke)	Liquid	Gas	H_2	CO	CO_2	C_{1-2}[a]
CD-250	31.3	49.7	17.0	4.4	1.8	2.1	1.0
CD-280	36.2	44.4	17.4	4.5	2.0	2.0	1.1
CD-300	44.2	36.0	17.4	5.8	2.2	1.7	1.4
CD-320	59.0	23.1	16.9	7.6	2.3	1.3	1.8
CD-350	67.0	16.2	16.7	8.5	2.4	1.2	1.8
0.7-SA-250	30.2	51.9	16.8	3.7	2.4	1.8	1.0
0.7-SA-280	33.0	48.5	16.3	4.0	2.4	1.6	1.1
0.7-SA-300	38.3	41.6	17.4	4.9	2.6	1.6	1.2
0.7-SA-320	48.1	32.2	18.6	6.0	3.1	1.5	1.3
0.7-SA-350	61.7	18.7	18.2	7.2	3.4	1.0	1.9
1.0-PA-250	32.4	46.5	18.4	4.3	2.9	1.7	1.0
1.0-PA-280	34.8	45.1	17.7	4.3	2.9	1.5	1.1
1.0-PA-300	40.6	39.5	17.9	4.9	3.1	1.4	1.3
1.0-PA-320	54.3	24.1	18.6	6.4	3.5	1.0	1.6
1.0-PA-350	61.7	18.5	18.7	7.4	3.8	0.8	1.9

[a] C_{1-2} hydrocarbons; methane, ethane, and ethylene.

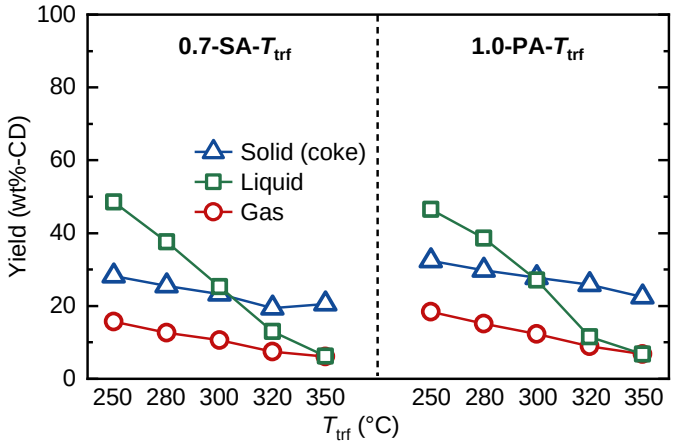

Figure 3-16 Influence of T_{trf} on distribution of products from carbonization of 0.7-SA-T_{trf} and 1.0-PA-T_{trf}.

Typical GC-MS chromatograms of liquid products are provided in **Figure 3-17.** It was apparent that the majority of compounds were lignin-derived phenol monomers. The yields of categorized compound groups are summarized in **Figure 3-18**. The total yields accounted only for a portion of liquid product yields (14.3–20.1 wt%). This was because the liquid product contained water and heavy molecules that could not be detected by GC-MS. The heavy portion would have potential applications or be cracked into smaller molecules by reforming, which was outside the scope of this work. The total yield of GC-MS-detectable compounds remarkably decreased with T_{trf} due to the enhanced degradation of biomass components, including lignin, during torrefaction. A notable difference between raw and acid-loaded CDs was that cellulose- and hemicellulose-derivatives were mainly anhydrosugars and furans for the acid-loaded CD, but ketones were dominant from CD-T_{trf}. This also arose from the AAEMs passivation during torrefaction. The analysis also confirmed that phenols were always dominant products. Fractions of phenols among detected compounds were 35.9–49.4 wt% and 41.0–65.0 wt% for the carbonization of acid-loaded CDs with T_{trf} of 300 °C and 320 °C, where anhydrosugars production and coke strength were maximized. The high selectivity was brought about by the enrichment of lignin during the torrefaction, in other words, the staged conversion.

It was unlikely that acid loading affected the phenols' formation through the AAEM passivation, as seen from the similar yields and compositions among CD-T_{trf}, 0.7-SA-T_{trf}, and 1.0-PA-T_{trf}. The acid catalysis was also unlikely to occur because the samples were washed by water before pelletization, although the removal was not thorough as discussed later. Among the lignin-derived phenols, guaiacols, such as guaiacol and 4-alkylguaiacols, were the most abundant, accounting for 43.9–84.8 wt%. This was derived from the structural characteristics of softwood lignin rich in guaiacyl nuclei.

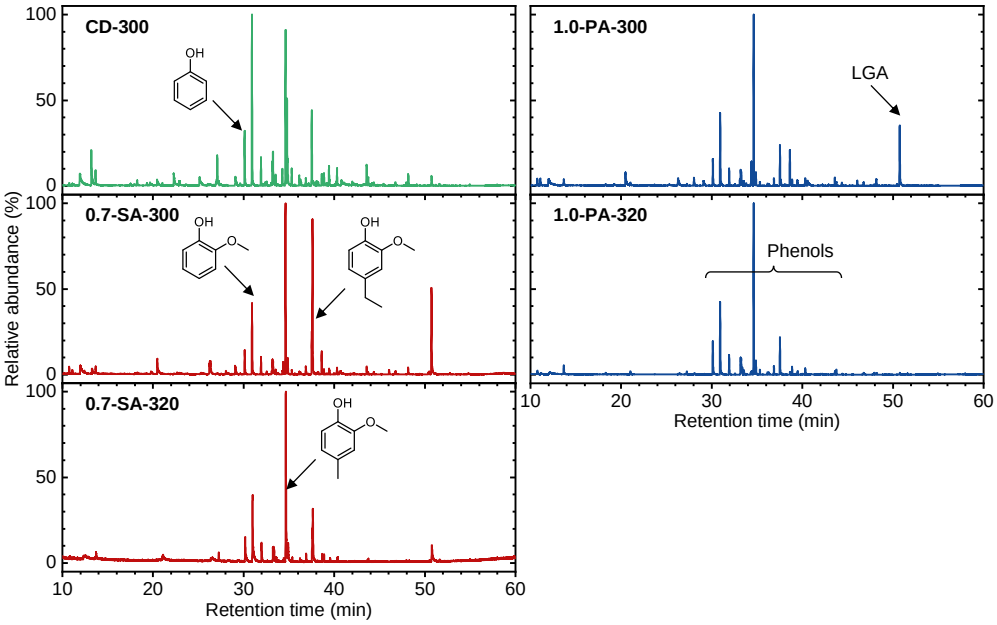

Figure 3-17 GC/MS chromatograms of liquid products from carbonization of pellets.

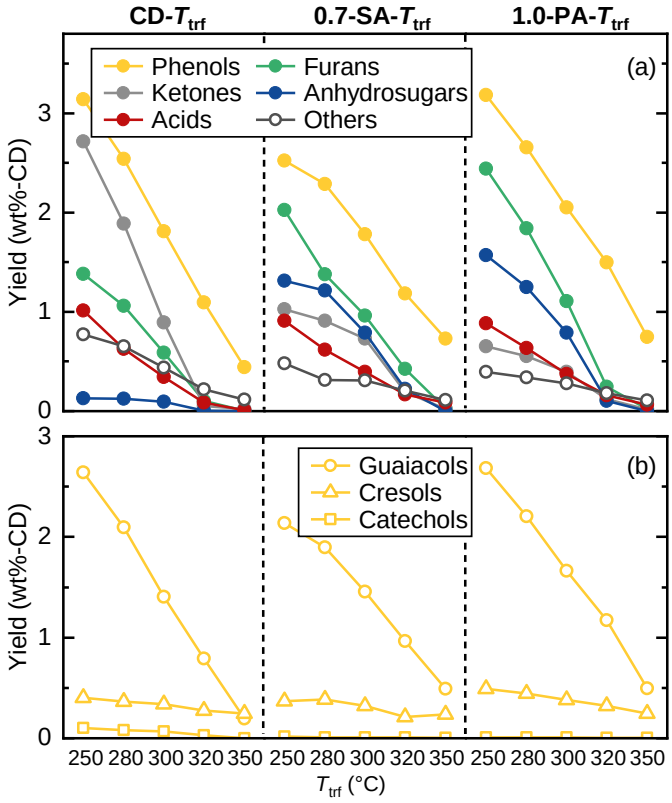

Figure 3-18 Yields of compounds identified by GC analyses from the pellet carbonization.

Table 3-9 Yields of components in liquid products from carbonization of pellets.

	CD-T_{trf}: T_{trf} (°C) =					0.7-SA-T_{trf}: T_{trf} (°C) =					1.0-PA-T_{trf}: T_{trf} (°C) =				
Yield (wt%-CD)	250	280	300	320	350	250	280	300	320	350	250	280	300	320	350
Furans	**1.382**	**1.058**	**0.589**	**0.105**	**0.005**	**2.023**	**1.376**	**0.960**	**0.425**	**0.026**	**2.439**	**1.840**	**1.108**	**0.244**	**0.022**
furan	0.049	0.044	0.027	0.013	0.002	0.118	0.054	0.068	0.036	0.004	0.115	0.089	0.066	0.025	0.002
2,3-dihydrofuran	0.034	0.032	0.015	0.002	-	-	-	-	-	-	-	-	-	-	-
2-methylfuran	0.129	0.117	0.080	0.026	0.003	0.195	0.109	0.124	0.068	0.010	0.202	0.176	0.140	0.061	0.009
2,5-dimethyl-furan	0.012	0.011	0.014	0.007	-	0.057	0.030	0.033	0.016	0.012	0.070	0.059	0.042	0.019	0.011
furfural	0.199	0.158	0.105	0.022	-	0.727	0.378	0.234	0.086	-	0.721	0.432	0.249	0.046	-
2-furanmethanol	0.770	0.546	0.258	0.017	-	0.109	0.044	0.043	0.046	-	0.067	0.058	0.045	0.029	-
5-methyl furfural	-	-	-	-	-	0.159	0.163	0.121	0.041	-	0.141	0.122	0.087	0.014	-
2-acetylfuran	0.037	0.022	0.016	0.002	-	-	-	-	-	-	-	-	-	-	-
2(5H)-furanone	0.095	0.075	0.043	0.007	-	0.049	0.033	0.025	0.014	-	0.048	0.040	0.025	0.011	-
3,5-dimethyl-2(5H)-furanone	0.026	0.024	0.016	0.003	-	-	-	-	-	-	-	-	-	-	-
5-hydroxymethylfurfural	0.031	0.029	0.015	0.006	-	0.609	0.565	0.312	0.118	-	1.075	0.864	0.454	0.039	-
Ketones	**2.713**	**1.886**	**0.893**	**0.052**	**0.023**	**1.025**	**0.907**	**0.728**	**0.192**	**0.023**	**0.650**	**0.551**	**0.395**	**0.119**	**0.018**
2,3-butanedione	0.467	0.299	0.162	0.012	-	0.274	0.166	0.153	0.023	-	0.202	0.156	0.101	0.025	-
2-butanone	0.040	0.031	0.025	0.017	0.008	0.051	0.025	0.029	0.018	0.013	0.064	0.050	0.040	0.023	0.009
3-methyl-3-buten-2-one	0.005	-	0.002	-	-	0.006	0.011	0.011	-	-	0.044	0.034	0.023	0.001	-
acetol	1.521	1.050	0.453	-	-	0.274	0.321	0.218	-	-	-	-	-	-	-
cyclopentanone	0.008	0.003	-	-	-	-	-	-	-	-	-	-	-	-	-
succindialdehyde	0.247	0.163	0.050	0.006	0.004	-	-	-	-	-	-	-	-	-	-
2-hydroxycyclopent-2-en-1-one	0.148	0.113	0.063	-	-	0.012	0.030	0.021	0.005	-	0.030	0.027	0.018	-	-
2-oxobutyl acetate	-	-	-	-	-	0.164	0.126	0.121	0.078	-	0.079	0.078	0.059	0.040	-
2-methyl-2-cyclopentene-1-one	-	-	-	-	-	0.011	0.013	0.008	-	-	0.008	0.008	0.005	-	-
3-methylcyclopentane-1,2-dione	0.245	0.200	0.120	0.017	0.011	0.233	0.215	0.167	0.068	0.010	0.223	0.198	0.149	0.030	0.009
3-ethyl-2-hydroxy-2-cyclopenten-1-one	0.015	0.013	0.006	-	-	-	-	-	-	-	-	-	-	-	-
delta-valerolactone	0.017	0.014	0.012	-	-	-	-	-	-	-	-	-	-	-	-
Phenols	**3.140**	**2.540**	**1.812**	**1.094**	**0.440**	**2.521**	**2.288**	**1.781**	**1.185**	**0.728**	**3.182**	**2.655**	**2.049**	**1.498**	**0.746**
Cresols	**0.401**	**0.363**	**0.338**	**0.275**	**0.247**	**0.368**	**0.383**	**0.321**	**0.213**	**0.235**	**0.491**	**0.444**	**0.379**	**0.323**	**0.246**
phenol	0.129	0.122	0.113	0.098	0.075	0.098	0.088	0.083	0.067	0.067	0.119	0.108	0.101	0.105	0.079
o-cresol	0.049	0.047	0.045	0.041	0.034	0.046	0.046	0.043	0.034	0.037	0.058	0.052	0.048	0.046	0.039
3,4-dimethylphenol	0.067	0.050	0.042	0.023	0.042	0.081	0.062	0.052	0.037	0.036	0.062	0.056	0.051	0.047	0.036
p-cresol	0.070	0.062	0.061	0.048	0.028	0.045	0.083	0.066	0.019	0.041	0.087	0.083	0.074	0.059	0.041
m-cresol	0.071	0.068	0.065	0.055	0.047	0.046	0.047	0.044	0.036	0.036	0.064	0.056	0.055	0.048	0.035

2,3,5-Trimethylphenol	-	-	-	-	0.005	0.016	0.027	0.012	0.009	0.006	0.066	0.063	0.034	0.008	0.006
4-ethylphenol	0.015	0.014	0.012	0.010	0.012	0.019	0.011	0.010	0.006	0.006	0.014	0.012	0.011	0.005	0.005
4-hydroxy-3-propyl-benzoic acid	-	-	-	-	0.004	0.017	0.019	0.011	0.005	0.006	0.021	0.014	0.005	0.005	0.005
Guaiacols	**2.639**	**2.096**	**1.406**	**0.791**	**0.193**	**2.138**	**1.897**	**1.454**	**0.963**	**0.489**	**2.683**	**2.204**	**1.663**	**1.171**	**0.497**
guaiacol	0.692	0.613	0.477	0.315	0.094	0.474	0.384	0.342	0.258	0.163	0.520	0.462	0.395	0.309	0.157
3-methylguaiacol	0.178	0.152	0.074	0.054	0.027	0.027	0.034	0.030	0.025	0.021	0.036	0.031	0.030	0.031	0.020
creosol	0.495	0.447	0.355	0.216	0.049	0.694	0.644	0.564	0.373	0.216	0.826	0.718	0.652	0.496	0.219
4-ethvlguaiacol	0.296	0.254	0.181	0.104	0.019	0.174	0.169	0.143	0.089	0.050	0.213	0.189	0.162	0.126	0.049
4-vinylguaiacol	0.234	0.153	0.078	0.018	-	0.107	0.076	0.063	0.046	0.009	0.139	0.107	0.067	0.041	0.010
eugenol	0.050	0.029	0.013	0.024	-	0.074	0.044	0.023	0.012	0.004	0.079	0.058	0.029	0.009	0.003
dihydroeugenol	0.056	0.046	0.034	0.001	0.004	0.089	0.111	0.056	0.022	0.007	0.200	0.133	0.068	0.026	0.008
isoeugenol	0.294	0.168	0.077	0.032	-	0.189	0.137	0.078	0.048	0.019	0.255	0.175	0.092	0.054	0.031
vanillin	0.054	0.038	0.022	0.005	-	0.061	0.088	0.041	0.027	-	0.095	0.066	0.036	0.022	-
methyl vanillate	0.059	0.046	0.022	0.006	-	0.067	0.067	0.036	0.027	-	0.080	0.072	0.041	0.026	-
guaiacylacetone	0.154	0.113	0.057	0.012	-	0.133	0.104	0.056	0.023	-	0.198	0.151	0.074	0.021	-
4-(1-hydroxyallyl)-2-methoxyphenol	0.017	0.007	0.005	0.004	-	0.049	0.039	0.022	0.013	-	0.042	0.042	0.017	0.010	-
eugenol	0.060	0.030	0.011	-	-	-	-	-	-	-	-	-	-	-	-
Catechols	**0.100**	**0.082**	**0.067**	**0.029**	**-**	**0.015**	**0.007**	**0.006**	**0.009**	**0.004**	**0.009**	**0.007**	**0.007**	**0.005**	**0.003**
catechol	0.014	0.012	0.010	0.005	-	0.015	0.007	0.006	0.009	0.004	0.009	0.007	0.007	0.005	0.003
resorcinol	0.032	0.028	0.027	0.009	-	-	-	-	-	-	-	-	-	-	-
orcinol	0.054	0.042	0.030	0.015	-	-	-	-	-	-	-	-	-	-	-
Acids	**1.013**	**0.625**	**0.342**	**0.085**	**0.010**	**0.911**	**0.618**	**0.395**	**0.166**	**0.085**	**0.882**	**0.633**	**0.374**	**0.161**	**0.066**
acetic acid	1.013	0.625	0.342	0.085	0.010	0.911	0.618	0.395	0.166	0.085	0.882	0.633	0.374	0.161	0.066
Sugars	**0.129**	**0.126**	**0.094**	**0.006**	**-**	**1.314**	**1.215**	**0.789**	**0.225**	**-**	**1.571**	**1.249**	**0.789**	**0.103**	**-**
1,4:3,6-dianhydro-α-d-glucopyranose	0.025	0.024	0.026	0.006	-	0.197	0.151	0.089	0.037	-	0.244	0.196	0.142	0.014	-
levoglucosenone	-	-	-	-	-	0.194	0.125	0.085	0.052	-	0.292	0.209	0.148	0.048	-
levoglucosan	0.104	0.102	0.068	-	-	0.923	0.939	0.615	0.136	-	1.035	0.844	0.499	0.041	-
Others	0.772	0.653	0.436	0.221	0.117	0.478	0.315	0.307	0.207	0.113	0.394	0.338	0.280	0.181	0.109

3.5 Discussion

The staged conversion of CD loaded with H_2SO_4 or H_3PO_4 at an amount equal to or slightly less than that of inherent AAEMs enabled the selective and separate production of anhysrosugars, phenols, and combustible gas with the coke. The strength of coke was improved by torrefaction and particularly by H_2SO_4-loading. The anhydrosugars yield and coke strength suggested 300–320 °C was the optimal T_{trf}. Under the best conditions, the yields of anhydrosugars/phenols/gas/coke were 12.1/1.2/19.4/13.0 wt% from 0.7-SA and 10.3/1.5/25.9/11.5 wt% from 1.0-PA, valorizing 45.7 wt% and 49.2 wt% of CD, respectively. The *TS* of coke was 22.5 MPa (from 0.7-SA) and 9.6 MPa (from 1.0-PA), which was higher than that directly produced from CD (9.0 MPa). Torrefaction also benefits the pulverization of feedstock with low energy [50]. The use of coarse particles for the torrefaction, followed by fine pulverization before pelletization, as performed in this study, would be practical.

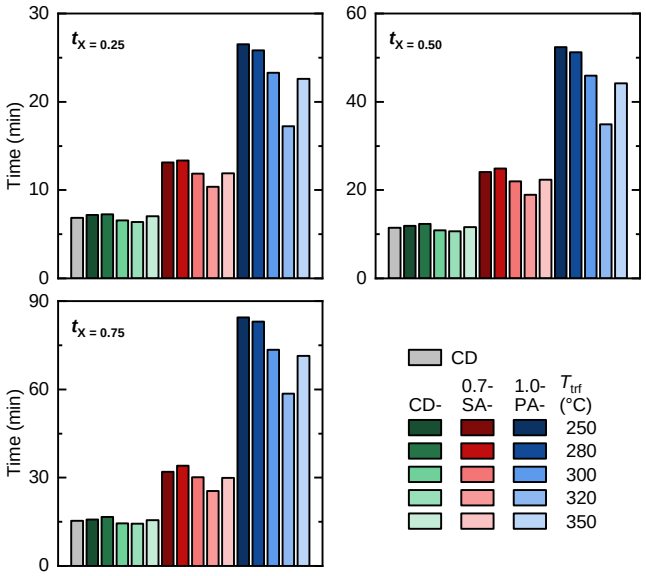

Figure 3-19 Time required to achieve coke conversion (X) of 0.25, 0.50, and 0.75 during CO_2 gasification at 900 °C.

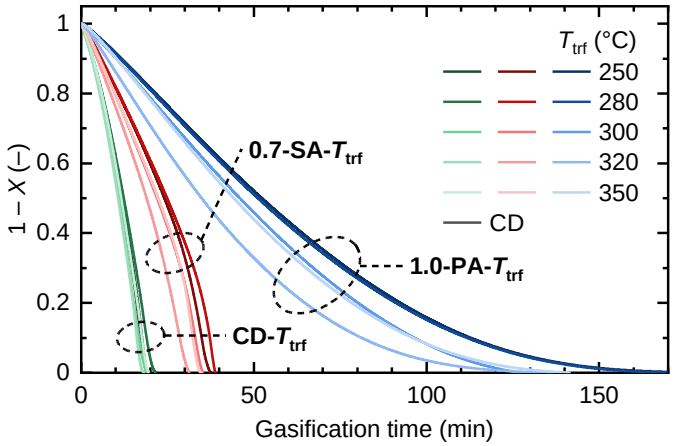

Figure 3-20 Gasification of cokes from CD-T_{trf}, 0.7-SA-T_{trf}, and 1.0-PA-T_{trf} at 900 °C under 50% CO_2/N_2.

One may be concerned with the loading of S and P because these elements have a deleterious impact on iron products. Technologies for thoroughly removing S and P during the steel-making process have already been established, but their removal requires commensurate energy usage and cost. According to Japanese Industrial Standards, the content of S in coke should be below 0.8 wt%, and the P content is recommended to be below 0.02 wt% [51]. The loadings of 0.7 wt% H_2SO_4 and 1.0 wt% H_3PO_4 could result in a content of over 1 wt% in coke if S and P were stable during the conversion sequence. As seen in **Table 3-4** for selected cokes derived from 0.7-SA-T_{trf}, the S content (0.18–0.36 wt%) satisfied this criterion because its large portion was volatilized during the sequence of torrefaction and pyrolysis or washed off by water before pelletization. The S removal was 67.7–84.4%. A portion of P was also removed (47.6–49.4%) during the conversion; however, the contents in coke (0.55–0.62 wt%) were well above the recommended value. Because coal scarcely contains P [51], the limitation of very low content poses a limited problem for coke-

making in general. Accordingly, the external loading of P over the coke precursor would be a critical problem in this regard.

Another concern about biomass-derived coke can be its high reactivity with CO_2 and H_2O, i.e., gasification reactivity, during its use in a blast furnace. The high reactivity is derived mainly from the catalysis of AAEMs. In our opinion, the high reactivity is not a significant issue if the coke retains its strength because the blast furnace is operated by consuming only a portion of the carbon in coke. In fact, some iron-making companies seek to improve coke reactivity by externally adding catalytic metals for more efficient blast furnace operation [52,53]. Nevertheless, reactivity analysis is worthwhile for understanding the influence of torrefaction and acid loading. Because the acid loading, in particular, deactivated the catalysis of AAEMs toward the pyrolysis of carbohydrates, the reactivity of cokes from acid-loaded CDs could be suppressed. The analysis results are shown in **Figure 3-19**. As anticipated, the cokes from 0.7-SA-T_{trf}, and 1.0-PA-T_{trf} needed roughly 2 times and 4 times longer gasification times to achieve the same conversion compared to those from raw CD and CD-T_{trf}, respectively. The reactivity was less influenced by the torrefaction temperature. This meant that the activity and number of catalytic metals were reduced during the conversion to coke. The reactivity was, however, still very high as compared to the reactivity of conventional coke; the gasification of coke from a caking coal under the same condition showed $t_{X = 0.50}$ of about 300 min [35]. A dramatic decrease in the reactivity was also possible in this study with the thorough removal of AAEMs by washing CD in a high concentration (3 mol/L) HCl aqueous solution, followed by pelletization and carbonization, as shown in **Figure 3-21**. It should be noted that the staged conversion of this acid-washed CD would produce volatile products similar to those from acid-loaded CDs, and low-reactivity strong coke. However, acid-washing requires a volume of highly acidic water to sufficiently remove the AAEMs and simultaneously produces the same

volume of waste stream, which was considered to be impractical. This was why acid loading was employed in this study. Coming back to the reactivity of cokes from 0.7-SA-T_{trf}, and 1.0-PA-T_{trf}, the high reactivity was caused by the catalytic metals. More than half of Ca was removed during the conversion to coke, but a non-negligible amount of AAEMs as well as Fe was left in the coke (**Table 3-4**). The metals were deactivated for anhydrosugars production during torrefaction, while they were likely active during gasification.

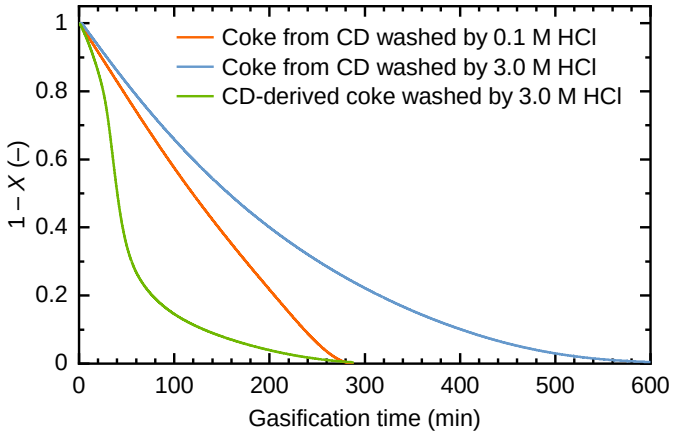

Figure 3-21 Gasification of CD-derived cokes at 900 °C under 50% CO_2/N_2. Acid washing was carried out before or after the coke making with HCl aqueous solution at 60 °C for 24 h, followed by water washing.

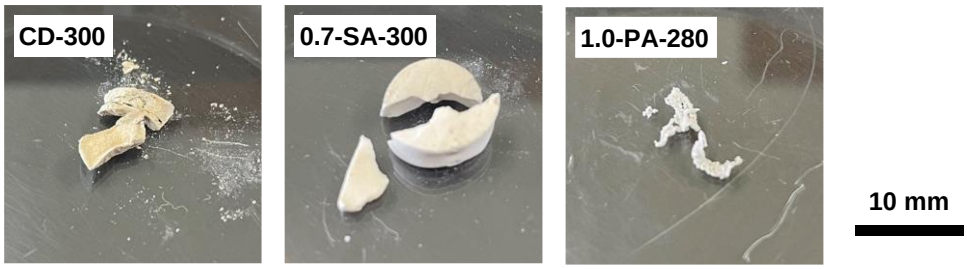

Figure 3-22 Appearance of ash obtained by ashing of fractured coke. 0.7-SA-T_{trf}-derived ash retained the dimensions of coke, 1.0-PA-T_{trf}-derived ash was melted and agglomerated during ashing, and CD-T_{trf}-derived ash showed an intermediate appearance, as a general trend.

3.6 Conclusions

The staged conversion of acid-loaded biomass was proposed as an efficient strategy for simultaneously producing high-strength coke and valorizing volatiles as valuable chemicals such as anhydrosugars and phenols. The influence of acid loading, its type and amount, and T_{trf} on product yields and quality was investigated using CD as the feedstock. The experimental results revealed its performance as follows:

(1) The loading of H_2SO_4 and H_3PO_4 worked for AAEM passivation and dramatically increased anhydrosugars yield, mainly consisting of LGA and LGO, during torrefaction. The highest anhydrosugars yields achieved by 0.7-SA and 1.0-PA were 12.1 and 10.3 wt%, respectively. The conversion of cellulose in CD to LGA reached 25.3 wt% and 18.2 wt%, respectively. Having a molar amount of loaded-acid equal to or slightly less than that of AAEMs in CD and T_{trf} of 300–320 °C was essential for achieving high anhydrosugars yields.

(2) In comparison with the direct pelletization and carbonization of CD, the staged conversion enabled the formation of higher-strength coke because torrefaction improved the deformation and densification of CD during pelletization. More importantly, H_2SO_4 loading and torrefaction under conditions suitable for maximizing the anhydrosugars yield improved the components composition of CD so that it could be greatly shrunk and densified during pelletization and carbonization. The resulting coke had a much higher strength (24.2 MPa) than that of coke prepared directly from CD (9.0 MPa). H_3PO_4 was less effective than H_2SO_4 for enhancing coke strength because it was prone to increasing the content of char-like solid during torrefaction, which inhibits densification during pelletization. An advantage of H_3PO_4 loading was the ability to increase coke yield.

(3) The enrichment in lignin during torrefaction helped in the selective production of phenols, guaiacols in particular, during carbonization, although the yield was low, in the range of 0.7 to 3.2

wt%-CD. The carbonization also produced non-condensable gas rich in combustible and useful components such as H_2 at a yield of up to 18.4 wt%-CD.

(4) Under the best conditions obtained in this work, CD was valorized as anhydrosugars, phenols, gas, and strong coke at total yields of 45.7 and 49.2 wt% by staged conversion using H_2SO_4 and H_3PO_4, respectively. The loading of H_3PO_4 could be a problem regarding the P content in coke when being used in furnaces. The S content in coke from H_2SO_4-loaded CD was satisfactorily low. The catalysis of AAEMs for pyrolysis of carbohydrates was deactivated during torrefaction, while it was highly active in the gasification of coke.

3.7 References

[1] J.R. Regalbuto, Cellulosic biofuels—got gasoline?, Science 325 (2009) 822-824.

[2] Q. Yang, H. Zhou, P. Bartocci, F. Fantozzi, O. Masek, F.A. Agblevor, Z. Wei, H. Yang, H. Chen, X. Lu, G. Chen, C. Zheng, C.P. Nielsen, M.B. McElroy, Prospective contributions of biomass pyrolysis to China's 2050 carbon reduction and renewable energy goals, Nat. Commun. 12 (2021) 1698.

[3] A. Corma, S. Iborra, A. Velty, Chemical routes for the transformation of biomass into chemicals, Chem. Rev. 107 (2007) 2411-2502.

[4] G.W. Huber, S. Iborra, A. Corma, Synthesis of transportation fuels from biomass: Chemistry, catalysts, and engineering, Chem. Rev. 106 (2006) 4044-4098.

[5] A. Hasanbeigi, M. Arens, L. Price, Alternative emerging ironmaking technologies for energy-efficiency and carbon dioxide emissions reduction: A technical review, Renewable Sustainable Energy Rev. 33 (2014) 645-658.

[6] S.J. Davis, N.S. Lewis, M. Shaner, S. Aggarwal, D. Arent, I.L. Azevedo, S.M. Benson, T. Bradley, J. Brouwer, Y.M. Chiang, C.T.M. Clack, A. Cohen, S. Doig, J. Edmonds, P. Fennell, C.B. Field, B. Hannegan, B.M. Hodge, M.I. Hoffert, E. Ingersoll, P. Jaramillo, K.S. Lackner, K.J. Mach, M. Mastrandrea, J. Ogden, P.F. Peterson, D.L. Sanchez, D. Sperling, J. Stagner, J.E. Trancik, C.J. Yang, K. Caldeira, Net-zero emissions energy systems, Science 360 (2018).

[7] L.J. Sonter, D.J. Barrett, C.J. Moran, B.S. Soares-Filho, Carbon emissions due to deforestation for the production of charcoal used in Brazil’s steel industry, Nat. Clim. Change 5 (2015) 359-363.

[8] P. Rousset, A. Caldeira-Pires, A. Sablowski, T. Rodrigues, LCA of eucalyptus wood charcoal briquettes, J. Cleaner Prod. 19 (2011) 1647-1653.

[9] M.W. Seo, H.M. Jeong, W.J. Lee, S.J. Yoon, H.W. Ra, Y.K. Kim, D. Lee, S.W. Han, S.D. Kim, J.G. Lee, S.M. Jeong, Carbonization characteristics of biomass/coking coal blends for the application of bio-coke, Chem. Eng. J. 394 (2020) 124943.

[10] R. Wei, L. Zhang, D. Cang, J. Li, X. Li, C.C. Xu, Current status and potential of biomass utilization in ferrous metallurgical industry, Renewable Sustainable Energy Rev. 68 (2017) 511-524.

[11] Y. Mochizuki, N. Tsubouchi, Preparation of pelletized coke by co-carbonization of caking coal and pyrolyzed char modified with tar produced during pyrolysis of woody biomass, Fuel Process. Technol. 193 (2019) 328-337.

[12] S. Kudo, A. Mori, G. Hayashi, T. Yoshida, N. Okuyama, K. Norinaga, J.-i. Hayashi, Characteristic properties of lignite to be converted to high-strength coke by hot briquetting and carbonization, Energy Fuels 32 (2017) 4364-4371.

[13] A. Mori, S. Kubo, S. Kudo, K. Norinaga, T. Kanai, H. Aoki, J.-i. Hayashi, Preparation of high-strength coke by carbonization of hot-briquetted Victorian brown coal, Energy Fuels 26 (2011) 296-301.

[14] M. Matoba, S. Kudo, A. Mori, K. Norinaga, K. Uchida, Y. Dohi, K. Uebo, J.-i. Hayashi, Production of high-strength cokes from non-/slightly caking coals. Part I: Effects of coal pretreatment and variables for briquetting and carbonization on coke properties, ISIJ Int. 59 (2019) 1440-1448.

[15] S. Kudo, A. Mori, R. Soejima, F. Murayama, Karnowo, S. Nomura, Y. Dohi, K. Norinaga, J.-i. Hayashi, Preparation of coke from hydrothermally treated biomass in sequence of hot briquetting and carbonization, ISIJ Int. 54 (2014) 2461-2469.

[16] S. Kudo, N. Goto, J. Sperry, K. Norinaga, J.-i. Hayashi, Production of levoglucosenone and dihydrolevoglucosenone by catalytic reforming of volatiles from cellulose pyrolysis using supported ionic liquid phase, ACS Sustainable Chem. Eng. 5 (2016) 1132-1140.

[17] S. Kudo, Z. Zhou, K. Norinaga, J.-i. Hayashi, Efficient levoglucosenone production by catalytic pyrolysis of cellulose mixed with ionic liquid, Green Chem. 13 (2011) 3306.

[18] S. Maduskar, V. Maliekkal, M. Neurock, P.J. Dauenhauer, On the yield of levoglucosan from cellulose pyrolysis, ACS Sustainable Chem. Eng. 6 (2018) 7017-7025.

[19] I. Itabaiana Junior, M. Avelar do Nascimento, R.O.M.A. de Souza, A. Dufour, R. Wojcieszak, Levoglucosan: a promising platform molecule?, Green Chem. 22 (2020) 5859-5880.

[20] H. Yang, R. Yan, H. Chen, D.H. Lee, C. Zheng, Characteristics of hemicellulose, cellulose and lignin pyrolysis, Fuel 86 (2007) 1781-1788.

[21] D. Chen, A. Gao, K. Cen, J. Zhang, X. Cao, Z. Ma, Investigation of biomass torrefaction based on three major components: Hemicellulose, cellulose, and lignin, Energy Convers. Manage. 169 (2018) 228-237.

[22] X. Zhou, W. Li, R. Mabon, L.J. Broadbelt, A mechanistic model of fast pyrolysis of hemicellulose, Energy Environ. Sci. 11 (2018) 1240-1260.

[23] P.R. Patwardhan, J.A. Satrio, R.C. Brown, B.H. Shanks, Influence of inorganic salts on the primary pyrolysis products of cellulose, Bioresour. Technol. 101 (2010) 4646-4655.

[24] P.R. Patwardhan, R.C. Brown, B.H. Shanks, Product distribution from the fast pyrolysis of hemicellulose, ChemSusChem 4 (2011) 636-643.

[25] N. Sonoyama, J.-i. Hayashi, Characterisation of coal and biomass based on kinetic parameter distributions for pyrolysis, Fuel 114 (2013) 206-215.

[26] J. Zhang, Y.S. Choi, C.G. Yoo, T.H. Kim, R.C. Brown, B.H. Shanks, Cellulose–hemicellulose and cellulose–lignin interactions during fast pyrolysis, ACS Sustainable Chem. Eng. 3 (2015) 293-301.

[27] P.J. de Wild, H.d. Uil, J.H. Reith, J.H.A. Kiel, H.J. Heeres, Biomass valorisation by staged degasification: A new pyrolysis-based thermochemical conversion option to produce value-added chemicals from lignocellulosic biomass, J. Anal. Appl. Pyrolysis 85 (2009) 124-133.

[28] F. Cao, S. Xia, X. Yang, C. Wang, Q. Wang, C. Cui, A. Zheng, Lowering the pyrolysis temperature of lignocellulosic biomass by H_2SO_4 loading for enhancing the production of platform chemicals, Chem. Eng. J. 385 (2020) 123809.

[29] N. Kuzhiyil, D. Dalluge, X. Bai, K.H. Kim, R.C. Brown, Pyrolytic sugars from cellulosic biomass, ChemSusChem 5 (2012) 2228-2236.

[30] B. Hu, Q. Lu, Y.-t. Wu, W.-l. Xie, M.-s. Cui, J. Liu, C.-q. Dong, Y.-p. Yang, Insight into the formation mechanism of levoglucosenone in phosphoric acid-catalyzed fast pyrolysis of cellulose, J. Energy Chem. 43 (2020) 78-89.

[31] G. Dobele, T. Dizhbite, G. Rossinskaja, G. Telysheva, D. Meier, S. Radtke, O. Faix, Pre-treatment of biomass with phosphoric acid prior to fast pyrolysis, J. Anal. Appl. Pyrolysis 68-69 (2003) 197-211.

[32] J. Liu, L. Luo, J. Ma, H. Zhang, X. Jiang, Chemical properties of superfine pulverized coal particles. 3. Nuclear magnetic resonance analysis of carbon structural features, Energy Fuels 30 (2016) 6321-6329.

[33] Y. Le Brech, J. Raya, L. Delmotte, N. Brosse, R. Gadiou, A. Dufour, Characterization of biomass char formation investigated by advanced solid state NMR, Carbon 108 (2016) 165-177.

[34] B.H. A. Sluiter, R. Ruiz, C. Scarlata, J. Sluiter, D. Templeton, and D. Crocker, Determination of structural carbohydrates and lignin in biomass, NREL/TP-510-42618, US National Renewable Energy Laboratory, (2008).

[35] Karnowo, S. Kudo, A. Mori, Z.F. Zahara, K. Norinaga, J.-i. Hayashi, Modification of reactivity and strength of formed coke from Victorian lignite by leaching of metallic species, ISIJ Int. 55 (2015) 765-774.

[36] P.R. Patwardhan, D.L. Dalluge, B.H. Shanks, R.C. Brown, Distinguishing primary and secondary reactions of cellulose pyrolysis, Bioresour. Technol. 102 (2011) 5265-5269.

[37] X. Yang, Y. Zhao, W. Li, R. Li, Y. Wu, Unveiling the pyrolysis mechanisms of hemicellulose: Experimental and theoretical studies, Energy Fuels 33 (2019) 4352-4360.

[38] S. Zhou, Y. Xue, J. Cai, C. Cui, Z. Ni, Z. Zhou, An understanding for improved biomass pyrolysis: Toward a systematic comparison of different acid pretreatments, Chem. Eng. J. 411 (2021) 128513.

[39] S.M. Shaik, P.N. Sharratt, R.B.H. Tan, Influence of selected mineral acids and alkalis on cellulose pyrolysis pathways and anhydrosaccharide formation, J. Anal. Appl. Pyrolysis 104 (2013) 234-242.

[40] S. Zhou, N.B. Osman, H. Li, A.G. McDonald, D. Mourant, C.-Z. Li, M. Garcia-Perez, Effect of sulfuric acid addition on the yield and composition of lignin derived oligomers obtained by the auger and fast pyrolysis of Douglas-fir wood, Fuel 103 (2013) 512-523.

[41] S. Zhou, D. Mourant, C. Lievens, Y. Wang, C.-Z. Li, M. Garcia-Perez, Effect of sulfuric acid concentration on the yield and properties of the bio-oils obtained from the auger and fast pyrolysis of Douglas Fir, Fuel 104 (2013) 536-546.

[42] A. Fukutome, H. Kawamoto, S. Saka, Processes forming gas, tar, and coke in cellulose gasification from gas-phase reactions of levoglucosan as Intermediate, ChemSusChem 8 (2015) 2240-2249.

[43] J.W. Patrick, A.E. Stacey, H.C. Wilkinson, The strength of industrial cokes: Part 2. Tensile strength of foundry cokes, Fuel 51 (1972) 174-179.

[44] Q.-V. Bach, Ø. Skreiberg, Upgrading biomass fuels via wet torrefaction: A review and comparison with dry torrefaction, Renewable Sustainable Energy Rev. 54 (2016) 665-677.

[45] P. Pradhan, S.M. Mahajani, A. Arora, Production and utilization of fuel pellets from biomass: A review, Fuel Process. Technol. 181 (2018) 215-232.

[46] S. Kudo, J. Okada, S. Ikeda, T. Yoshida, S. Asano, J.-i. Hayashi, Improvement of pelletability of woody biomass by torrefaction under pressurized steam, Energy Fuels 33 (2019) 11253-11262.

[47] A. Wibawa, U.P.M. Ashik, S. Kudo, S. Asano, Y. Dohi, T. Yamamoto, Y. Kimura, X. Gao, J.-i. Hayashi, Preparation of formed coke from biomass by sequenence of Torrefaction, binderless hot briquetting and carbonization, ISIJ Int. (in press).

[48] S. Wang, Z. Li, X. Bai, W. Yi, P. Fu, Influence of inherent hierarchical porous char with alkali and alkaline earth metallic species on lignin pyrolysis, Bioresour. Technol. 268 (2018) 323-331.

[49] D.L. Dalluge, K.H. Kim, R.C. Brown, The influence of alkali and alkaline earth metals on char and volatile aromatics from fast pyrolysis of lignin, J. Anal. Appl. Pyrolysis 127 (2017) 385-393.

[50] Q.-V. Bach, K.-Q. Tran, R.A. Khalil, Ø. Skreiberg, G. Seisenbaeva, Comparative assessment of wet torrefaction, Energy Fuels 27 (2013) 6743-6753.

[51] T. Miyagawa, Chemical properties of blast-furnace coke, Nenryo Kyokaishi 58 (1979) 940-953.

[52] S. Nomura, M. Naito, K. Yamaguchi, Post-reaction strength of catalyst-added highly reactive coke, ISIJ Int. 47 (2007) 831-839.

[53] T. Yamamoto, T. Sato, H. Fujimoto, T. Anyashiki, K. Fukada, M. Sato, K. Takeda, T. Ariyama, Reaction behavior of ferro coke and its evaluation in blast furnace, Tetsu-to-Hagane 97 (2011) 501-509.

Chapter 4 Steam Torrefaction of Biomass for Bio-oil Production

4.1 Introduction

The world is currently facing the challenge of shifting from reliance on fossil fuels to a sustainable supply of renewable energy. Biomass, especially lignocellulosic biomass, is a unique and renewable carbon-neutral resource that can be used to produce green fuels and high value-added chemicals through different technologies [1-3]. In addition to the main components of hemicellulose, cellulose and lignin, lignocellulosic biomass also contains a small amount of extracts rich in high value-added terpenes and polyphenols [4,5]. Each of these four components has varying degrees of resistance to chemical, thermal, and biodegradation. This often requires the use of different techniques to overcome the problems associated with the differences or heterogeneity in reactivity. Research efforts, however, have been focused exclusively on the conversion of hemicellulose, cellulose, and lignin [6-8], while ignoring the research on the extracts. Sustainable industrial development requires comprehensive development and utilization of biomass resources, even a small proportion of the extracts, to improve effectiveness, efficiency, and cost.

Steam treatment is one promising physicochemical method for extracting extracts and obtaining high value-added chemicals in them [5,9,10]. It can induce thermal degradation, hydrolysis and water solubilization of some fragrance constituents or solvent residues. In this method, biomass is treated with chemical-free and water-only media in a wide range of

temperatures and treatment times[11]. In addition, steam can be absorbed on the surface of char and in this way inhibit the adsorption of tar vapors on char surface. This also prevents the secondary cracking reactions in the gas phase and helps to maximize the yield of liquid products [12].

The stream treatment herein was employed to systematically study the effects of temperature and water/biomass mass ratio on the yield of high value-added products extracted from cedar. In addition, staged steam treatment was proposed for comparative studies to obtain highly selective product yields.

4.2 Experimental section

4.2.1 Materials

The as-received chipped Japanese cedar from Oita prefecture of Japan was ground and sieved to 2.0−4.0 mm for use as the feedstock in the steam treatment process. Alkaline lignin was used as the raw material for the comparative experiment. All samples were vacuum-dried at 80 °C for 24 h before use.

4.2.2 Steam treatment experiment

The experiments were performed in a self-made steam treatment reactor as shown in **Figure 4-1**. The reactor consists of a reaction tube for filling biomass samples, an oven for heating the reaction tube, steam and N_2 (purity >99.9999 vol.%) supply and mixing systems, and an extract recovery system. Briefly, the reactor filled with 8 g of sample was heated to the specified temperature of 130, 160, 190, 220, or 250 °C under N_2 of 10 mL/min until the steam-N_2 mixer and the reaction tube reached the same temperature. Then, the water was fed to the reactor with a

syringe pump for 2 h at a flow rate to ensure that water of 2, 5, 10, or 15 times the mass of the sample was supplied, respectively. The extract and steam entered a 0 °C recovery system to be collected. At the end of the run, after stopping the water supply and holding the temperature for 10 minutes, the was air-cooled to ambient temperature.

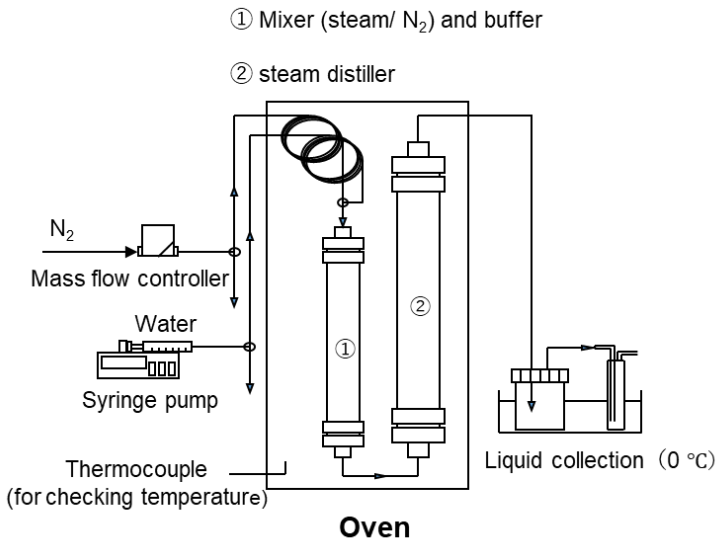

Figure 4-1 Steam/N_2 treatment system

For the investigation of the effect of steam treatment, the experiments were directly performed at 220 °C in N_2 of 10 mL/min. Furthermore, staged steam distillation was carried out at 130, 160, and 220 °C with an aim to more intuitively investigate the products at different temperatures and to improve the selectivity of specific compounds. Briefly, after the reaction at 130 °C, continue to raise the temperature to 160 °C for the reaction, and then to 220 °C, and recover the extracts were recovered separately.

The liquid phase consisting of the extracts and an aqueous were separated by dichloromethane and weighed by rotary evaporation to remove the solvent, and then mixed with a certain amount

of tetrahydrofuran (THF) for the component analysis. The yield of solid residues was obtained from the mass. As for gas and water yield was determined by overall material balance.

4.2.3 Product analysis

The chemical compounds in the extracts was analyzed by gas chromatography-mass spectrometry (GC-MS) on a PerkinElmer Clarus SQ 8, as reported elsewhere in detail [13]. The percentages of the identified major compounds were calculated from the total ion chromatogram peak area for semi-quantified analysis. The concentration of conifer aldehyde was determined by a gas chromatogram-flame ionization detector (GC-FID: Shimadzu, GC-2030). Both GC–MS and GC-FID were equipped with a GL Sciences TC-1701 column. Here, the yield of conifer aldehyde was defined based on biomass, and the selectivity was defined based on extracts. The two-step acid hydrolysis was used to quantify the amount of glucose, xylan, arabinose, galactose, mannose, and lignin in the solid residues, according to a report by the National Renewable Energy Laboratory (NREL) [14].

4.3 Results and discussion

4.3.1 Product yields

Figure 4-2 shows the effect of temperature on product yields of the solid residue and extract. The yield of solid residue decreased continuously with increasing temperature as a result of the enhanced degradation reactions, resulting in the continuous increase of the extract. The noteworthy was that the degradation rate of the sample was remarkable at over 220 °C, indicating that the thermal decomposition of hemicellulose and cellulose became significant under the low temperature steam. A similar trend was observed in terms of the correlation between temperature

and biomass component conversion, as shown in **Table 4-1**. With the increase in the extraction temperature, the cellulose and hemicellulose components in the solid residue dramatically decreased above 220 °C. This indicates that was hydrolyzed at a high temperature above 220 °C. This trend well suggested that the temperature of 220 °C was sufficient to obtain more extracts with the decomposition of smaller sugar components. Therefore, in this study, a temperature range from 130 to 220 °C was selected.

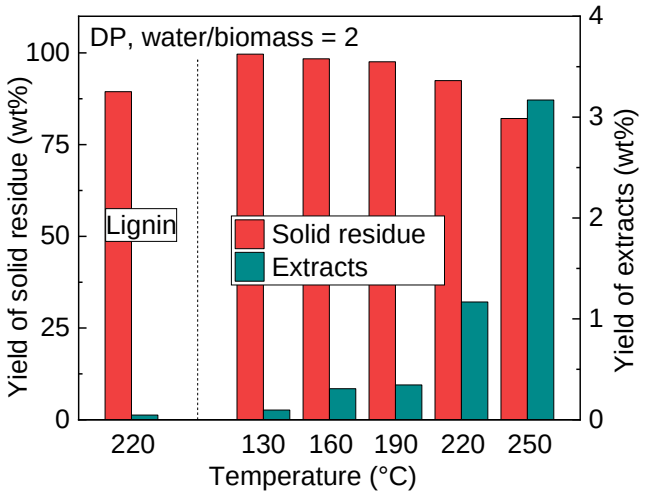

Figure 4-2 The effect of temperature on the degree of extraction.

Table 4-1 Chemical composition of samples before and after steam treatment.

	Yield (wt%-sample)					
	glucose	xylose	galactose	arabinose	mannose	lignin
raw	41.5	7.1	2.1	1.5	7.3	37.7
1-130-2	40.5	7.2	2.0	1.5	7.4	38.9
1-160-2	39.8	7.1	2.0	1.6	7.3	38.5
1-190-2	39.3	5.2	1.8	1.5	7.4	40.6
1-220-2	38.9	5.1	1.7	1.1	6.8	44.9
1-250-2	34.4	3.5	1.4	0.7	5.9	49.2
1-220-0	36.9	6.5	2.0	1.1	6.7	42.8
1-220-5	39.3	6.0	1.9	1.0	7.3	42.2
1-220-10	39.8	5.9	1.7	0.9	7.1	44.4
1-220-15	38.6	5.7	1.6	0.9	6.9	40.5

2-220-2	40.1	6.3	1.8	0.9	7.8	42.7
2-220-5	38.8	5.8	1.8	1.1	8.2	43.2
2-220-10	39.5	6.0	1.8	1.0	8.1	42.4
2-220-15	39.1	5.9	1.8	1.0	8.3	49.9

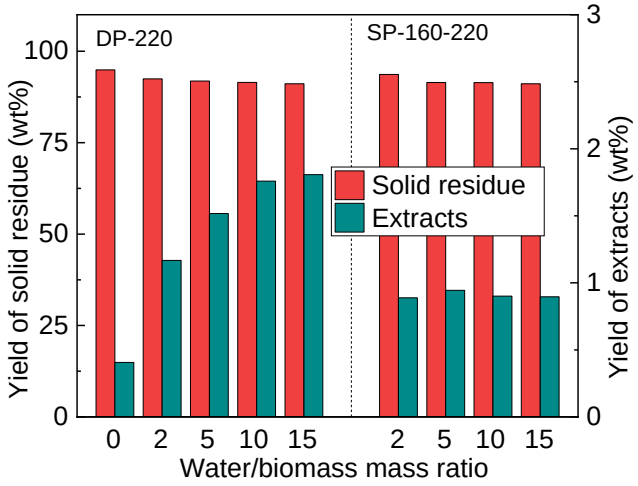

Figure 4-3 The effect of water/biomass mass ratio on the degree of extraction.

In comparison with an inert atmosphere, the steam treatment produced lower solid residue yields and higher extract yields, as shown in **Figure 4-3**. These results are closely related to the permeability of steam and enhanced desorption, distillation, and accelerated transport of the produced volatiles, and thus facilitated thermal degradation of biomass samples. In addition, unlike N_2 which was only used as a carrier, steam can also act as a reactant to stabilize the radicals obtained from the thermal decomposition of samples and inhibit the polycondensation reactions to form less solid residues [12]. This is well illustrated by the fact that higher solid residue with less cellulose content was obtained under N_2 atmosphere. However, the higher liquid-to-solid ratio promoted the thermal degradation of biomass, resulting in lower solid yields. This result can be explained by the higher steam concentration promoting the reaction. The staged steam treatment

did not significantly increase or decrease the solid yields, but obtained lower extract yields, which can be expected.

4.3.2 Characterization of extracts

The typical GC−MS chromatograms of extracts from lignin and cedar are presented in **Figure 4-4**. The major substances found in the extracts was listed in **Table 4-2**. The composition of the extracts was significantly affected by temperature. The resulting compounds were dominated by terpenoids, especially agathadiol, totarol, and sclareol, at low temperatures (<160 °C). The proportion of these three components increased from 51.7 area% at 130 °C to 61.1 area% at 160 °C. It is generally believed that this is extracted from the natural components of biomass as is. However, the proportion decreased gradually with the increase of extraction temperature. This shows that terpenoids can be selectively extracted by steam treatment extraction below 160 °C.

As the steam treatment temperature continued to rise to 220 °C, more aromatic compounds are detected, especially coniferyl aldehyde, which is commonly used in perfumes and pharmaceutical/medical industries. Comparatively, under nitrogen atmosphere at 220 °C, the detected compounds were still dominated by terpenoids. This result well demonstrates that the presence of steam tended to promote the production of coniferyl aldehyde. When the temperature rises to 250 °C, the peak displayed was more complex, which was due to the decomposition of the main components of biomass. This also reflected that the temperature of the best extraction was 220 °C.

Table 4-2 Relative peak area (%) of compounds identified in extracts by GC/MS.

	Lignin	DP, water/biomass = 2					DP, T_p = 220°C				SP, 220°C			
	T_p (°C)	T_p (°C)					Water/biomass				Water/biomass			
Compounds	220	130	160	190	220	250	0	5	10	15	2	5	10	15
Ketones	**5.9**	**0.1**	**5.7**	**6.0**	**5.1**	**7.9**	**0.0**	**3.5**	**2.7**	**2.5**	**7.4**	**5.9**	**4.1**	**3.9**
2,3-butanedione	3.7	0.1	5.7	4.2	1.2	1.5	-	1.9	1.4	1.3	1.0	0.9	1.5	1.4
2,3-pentanedione	-	-	-	0.6	<0.1	0.2	-	0.3	0.1	0.1	0.1	0.6	0.1	0.1
acetol	-	-	-	-	1.4	1.9	-	0.3	0.2	0.2	2.8	1.4	0.8	0.8
acetoin	0.9	-	-	0.6	0.3	0.2	-	0.1	0.1	0.1	0.4	0.3	0.2	0.2
2-oxobutanol	-	-	-	0.2	0.5	0.6	-	0.2	0.1	0.1	0.7	0.5	0.3	0.3
acetol acetate	-	-	-	-	0.1	0.2	-	0.1	0.1	0.1	0.2	0.2	0.2	0.1
2-cyclopentene-1,4-dione	0.4	-	-	0.2	0.1	0.2	-	0.2	0.1	0.1	0.2	0.2	0.2	0.1
2-hydroxy-2-cyclopentenone	0.1	-	-	0.3	1.4	2.7	-	0.4	0.5	0.5	2.0	1.7	0.9	0.9
3,4-dimethylcyclopent-2-enone	0.8	-	-	-	-	0.5	-	-	-	-	-	-	-	-
Furans	**3.2**	**1.1**	**2.5**	**10.1**	**13.2**	**13.2**	**4.9**	**9.6**	**8.6**	**7.9**	**20.1**	**16.4**	**15.1**	**14.1**
furfural	0.4	0.7	1.0	3.8	3.0	2.4	<0.1	3.4	2.2	2.0	4.4	4.0	3.9	3.7
2-furanmethanol	0.1	0.2	0.9	4.4	6.7	7.0	3.5	4.2	4.3	4.0	11.0	8.4	8.1	7.6
acetylfuran	-	-	-	0.1	0.1	0.1	-	<0.1	<0.1	<0.1	0.1	0.1	<0.1	<0.1
5-methylfurfural	-	0.1	0.2	0.9	0.5	0.6	0.7	0.5	0.3	0.3	0.6	0.5	0.5	0.5
butyrolactone	1.6	0.1	0.2	0.2	0.3	0.5	0.4	0.2	0.2	0.2	0.4	0.3	0.3	0.3
2(5H)-furanone	-	0.1	0.2	0.6	1.0	1.4	0.2	0.7	0.7	0.6	1.4	1.3	1.1	0.9
methyl 3-furoate	1.1	-	-	-	0.2	0.2	-	0.1	0.2	0.1	-	0.3	0.2	0.1
4-methyl-2(5H)-furanone	-	-	-	-	<0.1	0.1	-	<0.1	<0.1	<0.1	0.1	0.1	0.1	0.1
(5S)-5-(hydroxymethyl)oxolan-2-one	-	-	-	-	0.3	0.1	-	0.1	0.1	0.1	0.4	0.3	0.1	0.1
5-acetyloxolan-2-one	-	-	-	-	0.1	0.1	-	<0.1	<0.1	<0.1	0.1	0.1	0.1	0.1
hydroxymethylfurfural	-	-	-	0.2	1.1	0.8	0.1	0.3	0.5	0.5	1.6	1.2	0.8	0.7
Phenols	**89.4**	**3.0**	**2.4**	**9.6**	**27.5**	**33.9**	**9.6**	**31.0**	**34.6**	**39.8**	**32.5**	**35.7**	**38.8**	**42.4**
phenol	4.0	-	-	0.5	0.4	0.8	0.3	0.3	0.2	0.2	0.5	0.4	0.4	0.4
guaiacol	60.7	0.1	0.3	0.4	1.1	2.6	0.5	0.8	0.7	0.6	1.2	1.0	1.1	1.1

p-creosol	0.6	-	-	-	0.2	0.7	-	0.2	0.1	0.1	0.3	0.2	0.2	0.2
4-ethylguaiacol	1.9	0.1	0.1	0.1	-	0.1	-	-	-	-	-	-	-	-
4-vinylguaiacol	0.8	-	-	-	-	3.0	-	-	-	-	-	-	-	-
2-methoxy-3-allylphenol	0.2	-	-	-	-	0.7	-	-	-	-	-	-	-	-
syringol	0.2	-	-	-	-	-	1.3	-	-	-	-	-	-	-
isoeugenol	0.3	<0.1	0.4	-	0.8	3.2	0.3	0.7	0.7	0.6	0.9	0.7	0.8	0.8
vanillin	3.7	0.2	0.4	0.8	1.7	1.9	0.3	1.5	1.7	1.5	1.5	1.4	1.8	1.7
cerulignol	0.1	-	-	0.2	0.6	0.9	<0.1	0.7	0.6	0.5	0.6	0.7	0.7	0.7
4-t-butylcatechol	3.3	-	-	-	-	0.6	-	-	-	-	-	-	0.3	0.3
guaiacylacetone	1.2	2.6	1.2	3.5	5.6	4.7	4.3	6.3	5.9	5.4	5.8	5.8	4.4	4.2
coniferol	-	-	-	-	0.3	0.9	0.1	0.2	0.6	0.5	0.2	0.2	0.3	0.3
homovanillyl alcohol	0.7	-	-	-	-	-	-	-	-	-	-	-	-	-
vanillacetic acid	11.5	-	-	1.2	1.6	2.9	-	1.2	1.6	1.4	1.2	1.6	2.1	2.0
coniferyl aldehyde	-	-	-	2.8	15.2	10.8	2.5	19.2	22.6	28.7	20.3	23.6	26.6	30.9
Terpenoids	**0.0**	**93.7**	**88.4**	**72.1**	**51.2**	**39.1**	**84.7**	**53.0**	**51.7**	**47.6**	**35.9**	**38.0**	**36.6**	**34.4**
maltol	-	-	-	-	0.3	0.6	-	0.1	0.1	0.1	1.4	0.2	0.3	0.3
(-)-bete-elemene	-	-	-	-	0.1	0.7	0.7	0.1	0.1	0.1	0.1	0.1	0.1	0.1
cedr-8-ene	-	-	-	-	0.2	0.2	0.2	0.2	0.2	0.2	0.7	0.2	0.1	0.1
2-isopropenyl-4a,8-dimethyl-1,2,3,4,4a,5,6,7 octahydronaphthalene	-	-	-	0.4	0.8	0.5	0.9	0.8	0.7	0.7	1.1	0.9	0.6	0.5
α-muurolene	-	0.3	0.3	1.0	1.8	1.8	2.1	1.9	1.7	1.6	2.5	2.3	1.9	1.8
δ-cadinene	-	0.8	0.4	0.8	0.8	0.6	-	0.9	0.8	0.8	1.1	1.0	0.8	0.8
isoledene	-	-	-	0.1	0.2	0.3	0.2	0.2	0.2	0.2	0.3	0.2	0.2	0.2
1,2,3,4,4a,7-hexahydro-1,6-dimethyl-4-(1-methylethyl)-naphthalene	-	0.2	0.2	0.6	0.5	0.4	0.8	0.6	0.6	0.5	0.7	0.6	0.6	0.6
valencen	-	-			0.1		0.1	0.1	0.1	0.1	0.1	0.1	0.1	0.1
calamenene	-	1.2	0.9	1.5	1.8	1.4	2.3	1.9	1.9	1.7	2.4	2.1	2.2	2.0
isolongifolene, 4,5,9,10-dehydro-	-	0.8	0.9	0.6	0.5	0.3	0.7	0.4	0.5	0.3	0.5	0.5	0.5	0.3
α-calacorene	-	2.1	0.8	1.4	1.0	0.6	1.6	1.1	1.0	0.9	1.4	1.0	0.9	0.8
3,4-dehydroionene	-	0.5	0.2	-	-	-	-	-	-	-	-	-	-	-
elemol	-	1.1	0.4	0.6	0.6	0.6	0.9	0.6	0.6	0.5	0.5	0.5	0.4	0.4
γ-elemene	-	0.4	0.2	0.3	0.3	0.3	0.3	0.3	0.3	0.4	0.3	0.3	0.3	0.4

2,5,8-trimethyltetralin	-	-	-	0.1	-	-	0.1	-	0.1	0.1	0.2	0.1	0.1	0.1
naphthalene, 1,2,3,4,6,8a-hexahydro-1-isopropyl-4,7-dimethyl-	-	4.0	1.7	-	2.8	1.8	2.9	2.4	2.4	2.2	2.1	1.9	1.6	1.5
γ-eudesmol	-	0.7	0.3	0.6	0.7	0.7	0.9	0.8	0.7	0.7	0.8	0.8	0.8	0.7
T-muurolol	-	0.8	0.2	-	-	0.4	-	-	-	-	-	-	-	-
torreyol	-	1.3	0.4	1.2	1.2	0.7	0.9	0.9	0.9	0.9	1.2	0.9	0.9	0.9
α-cadinol	-	0.4	0.1	0.3	0.3	0.2	0.4	-	0.3	0.3	0.2	0.3	0.2	0.2
juniper camphor	-	1.5	0.5	0.7	-	0.5	0.5	-	-	-	-	-	-	-
apo-12-lycopenal	-	3.4	0.9	2.2	1.9	1.1	2.5	2.2	1.9	1.8	1.9	2.0	2.1	2.0
isophyllocladen	-	3.5	2.0	2.2	2.4	2.1	4.0	2.6	3.0	2.8	1.8	2.3	2.9	2.7
1-oxaspiro[2.5]octane, 5,5-dimethyl-4-(3-methyl-1,3-butadienyl)-	-	2.1	0.7	1.6	2.0	-	2.5	2.2	2.2	2.0	2.0	2.0	2.4	2.3
atiserene	-	0.8	0.4	-	-	0.7	-	-	-	-	-	-	-	-
1,5-cyclooctadiene, 3,4,7,8-tetrakis(1-methylethylidene)-	-	3.3	3.1	3.5	2.0	1.2	4.5	1.8	1.7	1.6	1.3	1.4	1.2	0.9
cembrene	-	-	-	0.3	0.2	0.2	0.3	0.3	0.3	0.3	0.2	0.3	0.2	0.2
ethyl cholate	-	0.9	-	0.7	0.4	-	0.4	0.4	0.4	0.4	0.2	0.3	0.3	0.5
o-methylpodocarpinol	-	1.4	0.4	-	-	1.1	-	-	-	-	-	-	-	-
androstan-17-one, 3-ethyl-3-hydroxy-, (5α)-	-	1.9	1.2	2.2	1.1	0.6	1.0	1.2	1.1	1.0	0.8	0.9	0.8	0.7
phyllocladene	-	9.5	3.9	-	-	0.5	-	-	-	-	-	-	-	-
17-oxoandrosta-5,7-dien-3-yl acetate	-	1.8	1.3	-	-	-	-	-	-	-	-	-	-	-
biformen	-	23.5	27.4	21.3	12.2	8.4	26.6	14.6	14.3	13.2	4.3	8.1	7.1	6.7
androsta-5,7-diene, 4,4-dimethyl-	-	4.4	3.2	-	-	1.5	-	-	-	-	-	-	-	-
totarol	-	18.7	29.8	23.4	11.7	6.3	21.7	11.1	10.7	9.8	4.1	4.7	4.9	4.6
14-isopropylpodocarpa-8,11,13-triene-7,13-diol	-	2.2	6.6	4.6	3.1	2.7	4.5	3.3	3.0	2.7	1.6	2.0	2.0	1.9
Others	**1.5**	**2.1**	**0.9**	**2.1**	**3.1**	**5.9**	**0.7**	**2.9**	**2.3**	**2.2**	**4.1**	**4.0**	**5.4**	**5.2**

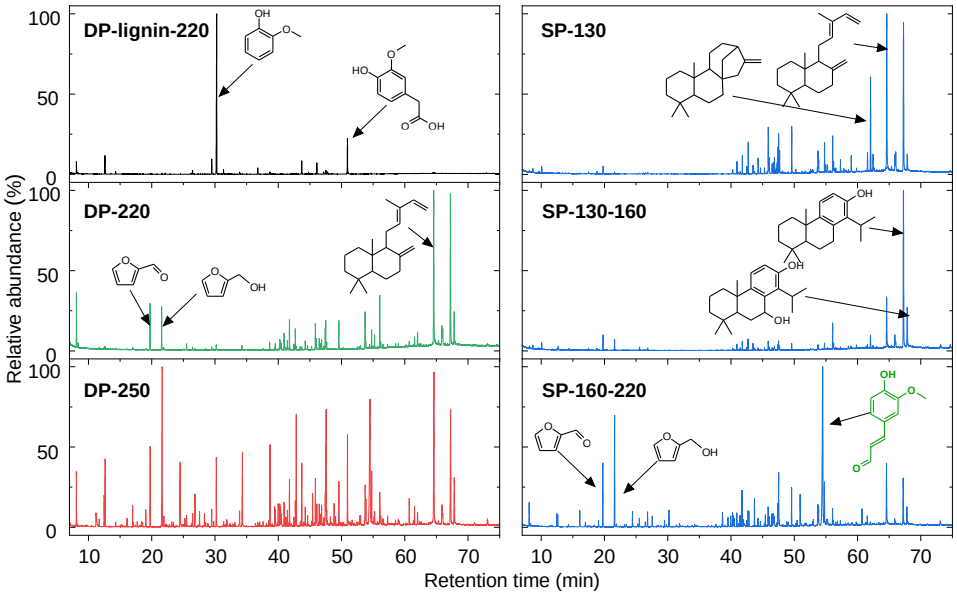

Figure 4-4 GC-MS chromatograms of extracts from selected samples.

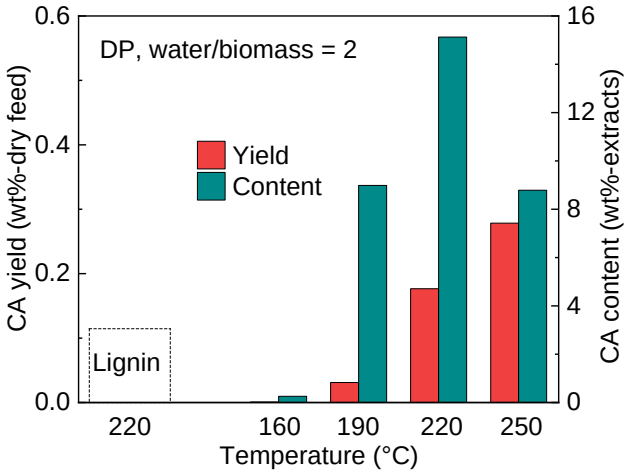

Figure 4-5 The effect of temperature on the yield of coniferyl aldehyde.

In order to estimate the influence of steam on coniferyl aldehyde production and its formation mechanism, quantitative analysis was carried out. As shown in **Figure 4-5**, it is noted that the coniferyl aldehyde yield increased substantially as temperature increased, while its selectivity

increased and then decreased. The highest coniferyl aldehyde yield of 0.28 wt% and selectivity of 15.13 wt% were obtained from 250 °C and 220 °C, respectively. This was mainly due to the decomposition of other components of biomass at higher temperatures to generate more extracts, as shown in Figure 3, the yield extracts was increased by a factor of 1.7.

An interesting observation compared to lignin was that almost no coniferyl aldehyde was produced at the same temperature despite the accelerated degradation of lignin leading to lower solids yields. As shown by the GC-MS chromatograms of lignin extracts in **Figure 4-4**, no obvious peak of coniferyl aldehyde was found. Therefore, it can be inferred that coniferyl aldehyde was not derived from lignin, but from the binding site of lignin and hemicellulose.

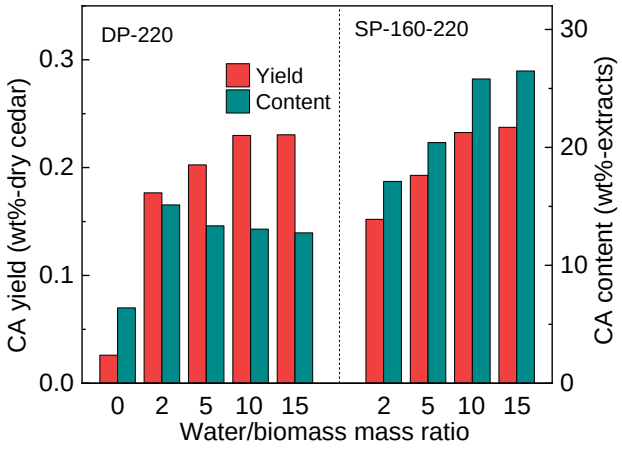

Figure 4-6 The effect of water/biomass mass ratio on the yield of coniferyl aldehyde.

The influence of water/biomass mass ratio on the yield and selectivity of coniferyl aldehyde at 220 °C is shown in **Figure 4-6**. The yield of coniferyl aldehyde increased while its selectivity gradually decreased as the liquid-to-solid ratio increased. as the liquid-to-solid ratio increased. It was clear that the higher liquid-to-solid ratio promoted the production of more extracts while promoting the production of coniferyl aldehyde. More importantly, a noteworthy result was that

the yield of coniferyl aldehyde was only 0.03 wt% under nitrogen atmosphere at 220 °C, which was much smaller than those of steam treatment. Such an enhancement can be attributed to the promoting effect of steam. These results further provide better evidence that coniferyl aldehyde does not exist in biomass as a free component, but is generated by the decomposition of biomass after contact with steam.

Compared with direct extraction, as expected, staged extraction significantly improved the selectivity of coniferyl aldehyde, especially at higher liquid-to-solid ratios, and their selectivities were as high as 17.12-23.7 wt%, although it did not improve or even slightly decreased the yield of coniferyl aldehyde. The results can be explained by the higher liquid-to-solid ratio preferentially extracting more extracts at low temperature.

4.4 Conclusions

The staged steam treatment extraction was proposed to simultaneously produce high value-added terpenoids and coniferyl aldehyde. The influence of temperature and biomass-to-water ratio on the yield and selectivity of coniferyl aldehyde was investigated. The formation of coniferyl aldehyde mainly comes from the binding site of lignin and hemicellulose, not from lignin. The presence of steam treatment can promote the production of coniferyl aldehyde, especially at higher water-to-biomass ratio. The staged steam treatment can further improve of coniferyl aldehyde selectivity without affecting its yield. Most importantly, the staged steam treatment can be achieved coniferyl aldehyde at 220 °C while extracting natural components terpenoids directly below 160 °C. Combined with chapter 3, steam treatment extraction can be carried out before the staged pyrolytic conversion of acid-loaded biomass to simultaneously obtain terpenoids and

coniferyl aldehyde, further optimizing staged conversion progress, which provides the possibility to develop its potential utilization.

4.5 References

[1] R.A. Sheldon, Green and sustainable manufacture of chemicals from biomass: state of the art, Green Chem. 16 (2014) 950-963.

[2] M. Wang, R. Dewil, K. Maniatis, J. Wheeldon, T. Tan, J. Baeyens, Y. Fang, Biomass-derived aviation fuels: Challenges and perspective, Prog. Energy Combust. Sci. 74 (2019) 31-49.

[3] A. Corma, S. Iborra, A. Velty, Chemical routes for the transformation of biomass into chemicals, Chem. Rev. 107 (2007) 2411-2502.

[4] C. Turek, F.C. Stintzing, Stability of Essential Oils: A Review, Comprehensive Reviews in Food Science and Food Safety 12 (2013) 40-53.

[5] C.S. Tavares, A. Martins, M.L. Faleiro, M.G. Miguel, L.C. Duarte, J.A. Gameiro, L.B. Roseiro, A.C. Figueiredo, Bioproducts from forest biomass: Essential oils and hydrolates from wastes of Cupressus lusitanica Mill. and Cistus ladanifer L, Ind. Crops Prod. 144 (2020) 112034.

[6] Y. Luo, Z. Li, X. Li, X. Liu, J. Fan, J.H. Clark, C. Hu, The production of furfural directly from hemicellulose in lignocellulosic biomass: A review, Catalysis Today 319 (2019) 14-24.

[7] C. Chio, M. Sain, W. Qin, Lignin utilization: A review of lignin depolymerization from various aspects, Renewable Sustainable Energy Rev. 107 (2019) 232-249.

[8] K. Liu, H. Du, T. Zheng, H. Liu, M. Zhang, R. Zhang, H. Li, H. Xie, X. Zhang, M. Ma, C. Si, Recent advances in cellulose and its derivatives for oilfield applications, Carbohydrate polymers 259 (2021) 117740.

[9] X. Zhang, H. Gao, L. Zhang, D. Liu, X. Ye, Extraction of essential oil from discarded tobacco leaves by solvent extraction and steam distillation, and identification of its chemical composition, Ind. Crops Prod. 39 (2012) 162-169.

[10] P. Masango, Cleaner production of essential oils by steam distillation, J. Cleaner Prod. 13 (2005) 833-839.

[11] R. Zhu, V. Yadama, Effects of hot water extraction pretreatment on physicochemical changes of Douglas fir, Biomass Bioenergy 90 (2016) 78-89.

[12] A. EPütün, E. Apaydin, E. Pütün, Bio-oil production from pyrolysis and steam pyrolysis of soybean-cake: product yields and composition, Energy 27 (2002) 703-713.

[13] S. Kudo, Y. Hachiyama, Y. Takashima, J. Tahara, S. Idesh, K. Norinaga, J.-i. Hayashi, Catalytic hydrothermal reforming of lignin in aqueous alkaline medium, Energy Fuels 28 (2013) 76-85.

[14] A. Sluiter, B. Hames, R. Ruiz, C. Scarlata, J. Sluiter, D. Templeton, D. Crocker, Determination of structural carbohydrates and lignin in biomass: Laboratory Analytical Procedure (LAP), (2008).

Chapter 5 General Conclusions

Chapter 2: Torrefaction of Japanese cedar (TR) and *in-situ* pyrolytic reforming of volatile matter (PYR) in vapor-phase showed that Q_{TR} was influenced by T_{TR} and also removal of water-extractable alkali and alkaline-earth metallic species, but within a range of 1.0–4.0% of the cedar HHV. The yield of bio-oil from TR increased with increasing T_{TR} up to around 40 wt%-daf while its chemical energy on the HHV basis became near equivalent to that of char. PYR decomposed 90% of the bio-oil at T_{PYR} = 800 °C producing CO/H_2–rich gas with LHV of 18 MJ/Nm^3-dry. Q_{PYR} was a semi-linear function of T_{PYR} and in a range of 1.4–5.8% of the cedar HHV for T_{TR} = 300 °C. The total chemical energy of the products was almost equivalent to that of the cedar regardless of T_{TR} or T_{PYR}. It was thus demonstrated that both TR and TR–PYR successfully conserved the chemical energy of the biomass, widely varying product distribution and composition, with relatively small heat requirements. Detailed analysis of bio-oils showed that PYR was not necessarily effective in either a significant increase in the yields of specific compounds or eliminating heavier components.

Chapter 3: Staged pyrolysis conversion of acid-loaded woody biomass showed the loading of H_2SO_4 or H_3PO_4 at an amount equal to or slightly less than that of metals inherent in the wood, having catalysis for promoting the formation of valueless light oxygenates from carbohydrates, was effective for passivating those metals and drastically improving the anhydrosugars yield in torrefaction at 300–320 °C. The total yield of anhydrosugars from wood and the yield of levoglucosan, a dominant anhydrosugar, from cellulose in the wood reached 12.1 wt% and 25.3 wt%, respectively. It was noteworthy that torrefaction altered the composition of components in

wood and positively influenced the strength of coke prepared by pelletization and carbonization. In particular, torrefaction in the presence of H_2SO_4 led to a remarkable densification of pellets during carbonization. The resulting in a coke strength (tensile strength) of up to 24.2 MPa, which was much higher than that of coke directly pelletized and carbonized from wood (9.0 MPa). Moreover, the lignin-enriched torrefied wood selectively produced phenols and combustible gas with H_2 as the major component in the carbonization. Under the most optimal conditions examined in this work, 45.7 wt% of the wood was converted into the desired products with the remainder being water, heavy condensable volatiles, whilst the yield of light oxygenates was greatly reduced.

Chapter 4: Steam treatment torrefaction of biomass showed that the formation of coniferyl aldehyde is mainly produced from the binding sites of lignin and hemicellulose, not lignin. Steam treatment can promote the production of coniferyl aldehyde. The staged steam treatment can further improve the selectivity of coniferyl aldehyde in the extracts, and directly extract the natural component terpenoids below 160 °C.

Acknowledgements

As the thesis is about to be completed, I would like to express my heartfelt thanks to those who have helped and guided me.

First of all, I would like to express my heartfelt thanks to my dedicated supervisor, Professor Jun-ichiro Hayashi, for his guidance, care, and help. I also sincerely thank Professor Shinji Kudo for his guidance and patience for my experiments, scientific papers, and thesis. At the same time, I would also like to express my sincere thanks to assistant Professor Shusaku Asano for his help and support in my study and life.

In addition, the successful completion of the paper is also inseparable from the help and support of other members of our laboratory. Also, I would like to thank the China Scholarship Council for its financial support, which was crucial to my studies in Japan.

Finally, I would like to thank my parents and family for their great support in my studies. It was their silent support and dedication that allowed me to complete my PhD studies without any worries!